NTNU – Trondheim
Norwegian University of
Science and Technology

Dynamic behaviour of synchronous machine during open conductor fault -

modeling, simulations and laboratory
experiments

Hans Olav Røste

Master of Science in Electric Power Engineering
Submission date: June 2015
Supervisor: Trond Toftevaag, ELKRAFT

Norwegian University of Science and Technology
Department of Electric Power Engineering

Problem description

NTE operates and is the owner of the regional power system network in Nord Trøndelag County in the middle on Norway. NTE owns Nedre Fiskumfoss Kraftverk (NFK) that is a hydro power plant with three generators; each rated 17 MVA, which experienced the uncontrolled speed oscillations that occurred at two separate events.

NTE experienced on two occasions in 2008 that the generators installed in NFK started to oscillate severely. The first occurrence of oscillations were caused by open conductor fault on the 66 kV line to Namsos. The second occurrence of oscillations happened during an unfavourable network configuration.

The task given is to study the occurrence of the open conductor fault, as that event had the most severe impact on the power system network. The actual open conductor fault occurred the 7th March 2008 in NTEs regional power system network. The fault occurred on the 66kV-line between NFK and Namsos.

The main research-question has been; why do the synchronous generators exhibit this poor damping during this kind of fault? The topic has been studied in two earlier Master-thesis works at NTNU.

To approach this question, the following study objectives is proposed:

- Study the previous work on this topic given in two earlier master theses.
- Review literature relevant to power system stability.
- Modelling and simulations by means of power system analysis tools, which includes:
    - Dynamic simulations
    - Modal analysis
    - Implementation of protective relays
- Possible measurements in laboratory if within timeframe.

The overall objective of this work is to obtain an understanding of the steady state and dynamic aspects of open conductor faults by review of the previous two master theses and by reviewing other relevant scientific materials.

The work should be supported by modelling and computer simulations with focus on open conductor faults and conducting laboratory experiments in order to obtain better knowledge about such fault events in the electrical power system.

Preface

This master thesis is the finishing work of the two years international master study program in electrical power engineering at the Norwegian University of Science and Technology spring 2015.

The topic of the master thesis deal with stability issues in Nedre Fiskumfoss Kraftverk that occurred following an open conductor fault the 7th of March 2008.

The master thesis report contains information which are subjected to confidentiality after § 6-3 in Forskrift om forebyggende sikkerhet og beredskap i energiforsyningen (Beredskaps-forskriften) and omitted from publication after Lov om rett til innsyn i dokument i offentleg verksemd (Offentlighetsloven) § 13. The content in question are placed in appendices, and do not come with the public publication.

During my studies and work on the master thesis there are several people I want to thank for their contributions:

I first want to thank my supervisor Trond Toftevaag for his many counselling advices, suggestions, queries and directions during my time working on the thesis.

I want to thank Henrik Kirkeby at SINTEF Energy Research for assisting with acquiring, extracting and guidance in configuring and use of measurement equipment in laboratory experiments.

The staff at NTNU Laboratory Service Office have been very helpful in assisting, guiding and configuring the laboratory experiments at NTNU laboratory facilities.

Trondheim June 2015

Hans Olav Røste

Sammendrag

Denne hovedoppgaven omhandler stabilitetsproblematikk i Nedre Fiskumfoss Kraftverk(NFK), som produserer elektrisk kraft i kraftnettet til Nord Trøndelag Elektrisitetsverk(NTE), som 7. mars 2008 opplevde hastighets- og effektpendlinger etter et fasebrudd. Det ble observert at aggregat G1NFISKUM ukontrollert varierte fra 0 til 100 % innen to sekunder i elektrisk produksjon etter fasebruddet.

Arbeidsomfanget består i hovedsak av litteraturstudier, simuleringer i dataverktøyet PowerFactory fra DIgSILENT og laboratorieeksperimenter for å studere dynamiske forløp ved fasebrudd. Kraftverket og kraftnettet studeres med bruk av dynamiske analyser, lineære analyser og laboratorieeksperimenter, der målsetning er å finne elementer som påvirket hastighets- og effektpendlingene i kraftverket som oppstod 7. mars 2008.

Kraftnettet er små signal stabilt i henhold til lineære analyser og egenverdi kalkulasjoner. Datasimuleringer viser at synkrongeneratoren i NFK viser at synkrongeneratoren i NFK opplever udempede pendlinger der oscillasjonsperiode er 1,2 sekunder under fasebruddet som skjedde 7. mars 2008.

Dynamiske simuleringer og lineære analyser vider at innstillingene på AVR og turbinregulator har negative innvirkning på systemstabilitet. Justeringer av parameterinnstillingene på regulatorene forbedret transiente respons.

Simuleringer av trefase kortslutninger og fasebrudd er utført for å sammenligne dempningsegenkaper. Resultatene viser en dempning på 0,77 % og 0,78 % for trefase kortslutning og fasebrudd når faktiske regulatorer er implementert. Resultatene ved simuleringer med modifiserte parameterinnstillinger i regulatorene viser en dempning på 2 % og 0,91 % for de samme feiltilfellene, noe som er en forbedring og markant forskjell i dempningsegenskaper ved trefase kortslutning og fasebrudd.

Spørsmålet på hvorfor simuleringsresultatene er forskjellige ved trefase kortslutning og fasebrudd er ikke funnet. Det spekuleres at uheldig lastflyt og feilsted kan påvirke den transiente responsen, men dette er ikke verifisert i simuleringene. De modifiserte parameter-innstillingene kan også gi et feilaktig bilde av generatorens dynamiske oppførsel.

Laboratorieeksperimenter ble utført for å studere fasebrudd og med ambisjon å gjengi forholdene i kraftnettet til NTE den 7. mars 2008 dersom det lot seg gjøre. Gjenskapelse av forholdene i kraftnettet lot deg ikke utføre, men resultatene fra laboratorieeksperimentene kan brukes til videre studier angående fasebrudd og pendlingsproblematikk.

Det konkluderes, basert på datasimuleringer og laboratorieeksperimenter at AVR og turbinregulator på aggregater i NFK ikke evnet å tilføre nok dempende moment, i kombinasjon med uheldig driftssituasjon i feiltidsrommet, som førte til kraftige pendlinger i kraftverket under fasebruddet, og tilslutt endte i systemkollaps.

Summary

The topic of this master thesis deal with stability issues in the hydro power plant Nedre Fiskumfoss Kraftverk (NFK) where speed and power oscillations occurred in the synchronous generators after an open conductor fault the 7th of March 2008. It was observed that G1NFISKUM generator output varied from 0 to 100 % within 2 seconds during the uncontrolled oscillations.

The scope of work consists of literature review, computer simulations and laboratory experiments in order to study dynamics of open conductor faults. The power plant and power system is studied by dynamic analysis with by means of linear analysis and laboratory experiments with aim to find the main factors that influence the uncontrolled power oscillations in NFK.

The linear analysis and eigenvalue calculations indicates that the network is small signal stable. However, the dynamic simulation of the Base Case network show that the network model experience underdamped oscillations, with an oscillation period of 1,2 seconds, like the open conductor fault that occurred the 7th of March 2008.

The dynamic simulation results and linear analysis show that the settings on the AVR and turbine governor have negative impact on system stability. Modifications on the parameter settings on the regulators improved transient response.

Simulations of symmetrical three-phase short circuit and open conductor fault is conducted to compare the damping properties. The results show that the damping ratio is 0,77 % and 0,78 % for symmetrical three-phase short circuit and open conductor fault, respectively, when the actual regulators are implemented. The results with modified regulators show damping ratio 2 % and 0,91 % for the same fault cases, which is an improvement and a significant difference in damping ratio during different fault cases.

The exact reason why simulation results show different transient response for symmetrical three-phase fault and open conductor fault with modified regulator settings are not found. It is speculated that unfavourable load flow conditions and fault location influence the transient response of the generators in NFK, but this is not verified through simulations. The modified parameter settings may give an incorrect response of the generators dynamic behaviour.

Laboratory experiments have been conducted to study the open conductor phenomena and to re-enact the open conductor fault event that happened the 7th March 2008. Although the laboratory test setup did not reproduce the properties of the real world network, the results provide basis for further stability studies regarding open conductor faults and oscillation problems.

Based on the simulations and laboratory experiments, the results indicates that the AVR and turbine governor in the generators in NFK were unable to provide sufficient damping torque, in combination with unfavourable load flow conditions at the time of the fault event, which led the power plant to experience severe oscillations during the open conductor fault, and eventually system collapse.

Table of content

Abbreviations, keywords and wordlist

AVR – Automatic Voltage Regulator

CB – Circuit Breaker

CT – Current Transformer

emf. – electromotive force

mmf. – magnetomotive force

NFK – Nedre Fiskumfoss Kraftverk

NTE – Nord Trøndelag Energiverk

NTNU – Norwegian University of Science and Technology

PSS – Power System Stabilizer

VT – Voltage Transformer

Vector notations in the report are shown $\vec{V}$, and phasor notations are shown $\underline{V}$.

The labelling and numbering of the nodes and components used in this report is not the actual names in the real network.

1 Introduction

1.1 Background

Open conductor faults occur from time to time in the power system. An open conductor fault in a regional power system caused unexpected large poorly damped rotor oscillations in the synchronous generators in a power station operated by NTE. This led to speed- and power oscillations in the connected generators at NFK, which after some time where disconnected from the grid.

NTE experienced 7th of March 2008 that the generators in NFK began to oscillate uncontrollably after an open conductor fault. It was observed that G1NFISKUM generator output varied from 0 to 100 % within 2 seconds during the uncontrolled oscillations.

The fault occurred on the 66kV-line between NFK and the transformerstation Namsos S. Appendix A shows the real world network topology at the time of fault event and where the fault location is indicated.

Figure 1 show the actual open conductor fault that occurred the 7th March 2008 in NTEs power system network. Figure 2 show the graphic presentation of the open conductor fault.

Figure 1: Figure 1: Photograph of the open conductor fault that caused power oscillations in NTEs network [1].

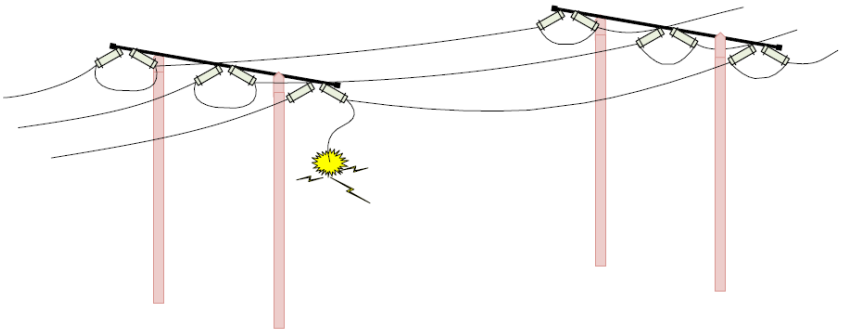

Figure 2: Figure 2: Schematic presentation of conductor fault [1].

1.2 Scope of work

The content of report deal with stability studies with aid of computer simulations for the power plant and power system network including controls, such as AVR and turbine governor. Laboratory experiments are conducted in order to study dynamics of open conductor faults.

The power system in question is the regional power system network of NTE, located in the county of Nord Trøndelag in the middle of Norway. The network consists of power generation and loads with external connection towards Statnett in Namsos.

The studied scenario is the case of open conductor fault that occurred in the network the 7th of March 2008. The whole power system network is modelled in PowerFactory from DIgSILENT and the fault event is simulated to study the response of the network.

The regulators parameter settings are studied in regards to their influence to network stability and damping properties.

Laboratory experiments are conducted in the laboratory facilities at NTNU, and measurement equipment are borrowed from Sintef Energy Research in order to study the dynamics of open conductor faults.

1.3 Previous studies

Two previous studies by K.Sjøholt [1] and S.Mabeta [2] have been written regarding the fault event that happened the 7th March 2008.

The report written by K.Sjøholt investigated the properties of the synchronous machine behaviour during an open conductor fault. The data on the network were provided from NTE, and simulations on a network model based on the real network were conducted in a power system analysis program. K.Sjøholt studied the rotor oscillations during an open conductor fault with different connection configurations, AVR and turbine regulator settings, with and without PSS, and literature on synchronous machine behaviour. Load flow analysis were conducted to replicate the actual operating condition prior to the open conductor fault. The open conductor fault caused the generators connected to the network to oscillate uncontrollably.

The conclusions from K.Sjøholts report state that different connection configurations and the settings on the regulators implemented on the simulation model change the damping on the generator. By implementing a PSS, the damping is improved. When implementing an out of step protection, power oscillations during open conductor faults can be detected and the faulty part can be disconnected from the network.

The proposed solution was to implement out of step protection, which can detect faults such as open conductor faults and prevent speed oscillations in the power system.

In the report written by S.Mabeta, the dynamic properties of open conductor faults in a power system, and the properties of open conductor faults were studied. The case of one- and two open conductors, and the impact on oscillations of synchronous machines were studied.

The conclusions S.Mabeta made was that open conductor faults may cause instability in a power system, and that the damping properties are influenced by open conductor faults.

1.4 Report content

The content in the report is consists of four main parts; theoretical background and mathematical descriptions, simulation model description and case description, simulation results and linear analysis, and laboratory experiments description and results.

Chapter 2 starts with a brief definition and classification of power system stability, followed by symmetrical components and open conductor faults. Theory and mathematical descriptions of the synchronous generator is presented, as it is important in the understanding regarding power system stability. Chapter 2 includes brief presentations of the turbine, turbine governor and AVR which are influencing the network stability and used in network modelling.

Chapter 3 describe the network topology, components and their functions, and limitations. The network model is verified by comparing load flow analysis with the actual measurements, followed by the case description.

Chapter 4 presents the simulation results and discussion, and linear analysis in PowerFactory is briefly presented, conducted and discussed.

Chapter 5 describe the laboratory setup, measurement configuration and limitations.

In Chapter 6 the laboratory results are presented and discussed, followed by chapter 7 and 8 where the laboratory experiments are done in simulations.

The discussion of results from simulations and experiments are presented in chapter 9.

Chapter 10 presents the conclusions, followed by chapter 11 that presents proposals for further works.

2 Theoretical background and mathematical descriptions

2.1 Power system stability

Power system stability is the ability of an electric power system, for a given initial operating condition, to regain a state of operating equilibrium after being subjected to a physical disturbance, with most system variables bounded so that practically the entire system remains intact [3].

Figure 3 show the overall picture of the power system stability problem, where the three main categories are; rotor angle stability, frequency stability and voltage stability [3]. As power systems are nonlinear, their stability depends on both the initial conditions and the size of a disturbance. Consequently, angle and voltage stability can be divided into small and large disturbance stability [4].

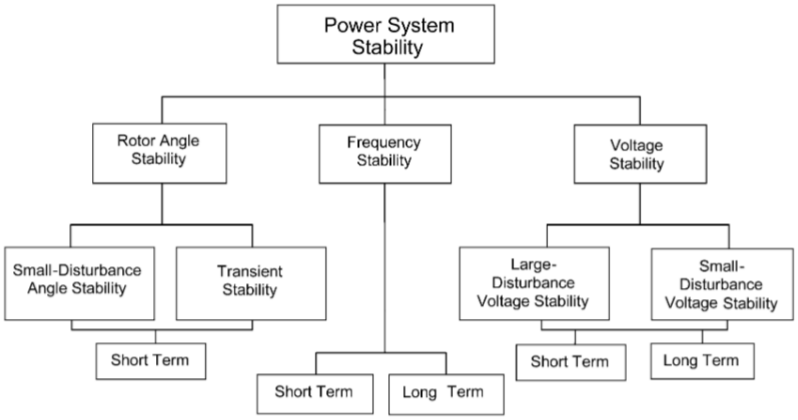

Figure 3: Power system stability [3].

2.2 Symmetrical components

Symmetrical components of voltages or currents are defined through a linear transformation of phase quantities. Let $\boldsymbol{X_p}$ be the phase quantities and $\boldsymbol{X_s}$ be their symmetrical components, where X may be voltages or currents. Thus

$$\boldsymbol{X_s} = \begin{bmatrix} X_0 \\ X_1 \\ X_2 \end{bmatrix} = \boldsymbol{S X_p} = \frac{1}{3}\begin{bmatrix} 1 & 1 & 1 \\ 1 & \sigma & \sigma^2 \\ 1 & \sigma^2 & \sigma \end{bmatrix}\begin{bmatrix} X_a \\ X_b \\ X_c \end{bmatrix} \tag{2.1}$$

The elements of $\boldsymbol{X_s}$ identified by the subscripts 0, 1, and 2 are known as the zero-, positive-, and negative-sequence components, respectively. The inverse of the matrix **S** is given by

$$\boldsymbol{S}^{-1} = 3\begin{bmatrix} 1 & 1 & 1 \\ 1 & \sigma & \sigma^2 \\ 1 & \sigma^2 & \sigma \end{bmatrix}^{-1} = \begin{bmatrix} 1 & 1 & 1 \\ 1 & \sigma^2 & \sigma \\ 1 & \sigma & \sigma^2 \end{bmatrix} \tag{2.2}$$

where $\sigma = \left(-0{,}5 + j\left(\sqrt{3}\right)/2\right)$ is a cube root of 1. ***S*** is a similarity transformation on impedance matrices of certain classes of three-phase power apparatus.

The impedance matrix (or admittance matrix) of a three-phase element $\boldsymbol{Z_p}$ transforms into a sequence impedance matrix $\boldsymbol{Z_s}$ in the symmetrical component frame of reference. The general transformation is

$$Z_s = SZ_pS^{-1} \tag{2.3}$$

2.3 Open conductor fault

Open-conductor fault conditions may occur by broken conductors or a deliberate single-phase switching operation. Such faults may involve the opening of one phase or two phases of a three phase circuit.

2.3.1 One open conductor

Figure 4 shows a three-phase system where phase a is open between p and p'.

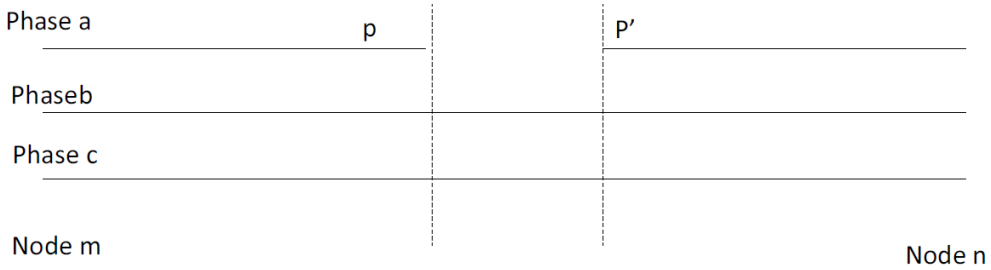

Figure 4: Schematic diagram showing a section of a three phase transmission line with an open conductor in line a between node p and p' [2].

From Figure 4, where phase a is disconnected and phase b and c are intact, the following assumptions can be made;

$$\mathrm{I_a} = 0, \qquad \mathrm{u_a} = \mathrm{u_b} = 0 \tag{2.4}$$

where I_a is the current flowing in conductor *a* after the fault and U_b and U_c are the series voltage drops between the points *p* and *p'*. Resolving these equations in to symmetrical components gives

$$\mathrm{u_{a1}} = \mathrm{u_{a2}} = \mathrm{u_{a0}} = \frac{1}{3}\mathrm{u_a} \tag{2.5}$$

$$\mathrm{I_{a1}} + \mathrm{I_{a2}} + \mathrm{I_{a0}} = \frac{1}{3}\mathrm{I_a} \tag{2.6}$$

The equations(2.5) and (2.6) give the connections shown in Figure 5 where the sequence networks are connected in parallel

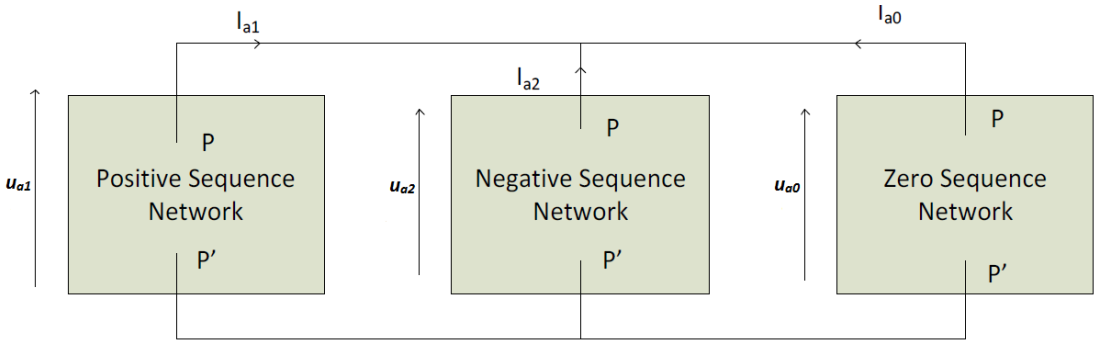

Figure 5: Connection of sequence networks to simulate one open conductor fault between p and p' [2].

2.3.2 *Two open conductors*

When two phases in a three-phase system are disconnected as shown in Figure 6, the following considerations are made;

$$u_a = 0, \qquad I_b = I_c = 0 \tag{2.7}$$

In terms of symmetrical components it become

$$\mathrm{u_{a1} + u_{a2} + u_{a0} = 0} \tag{2.8}$$

$$\mathrm{I_{a1} = I_{a2} = I_{a0} = \frac{1}{3} I_a} \tag{2.9}$$

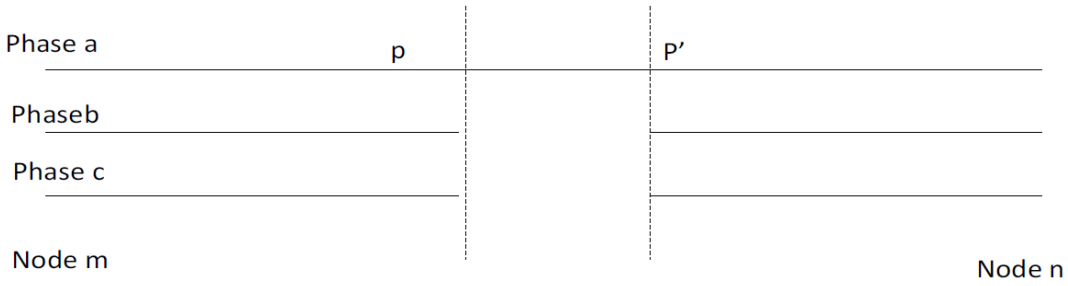

Figure 6: Schematic showing a section of a three phase system where phase b and c are disconnected between point p and p' [2].

The equations (2.8) and (2.9) give the connections shown in Figure 7 where the sequence networks are connected in series

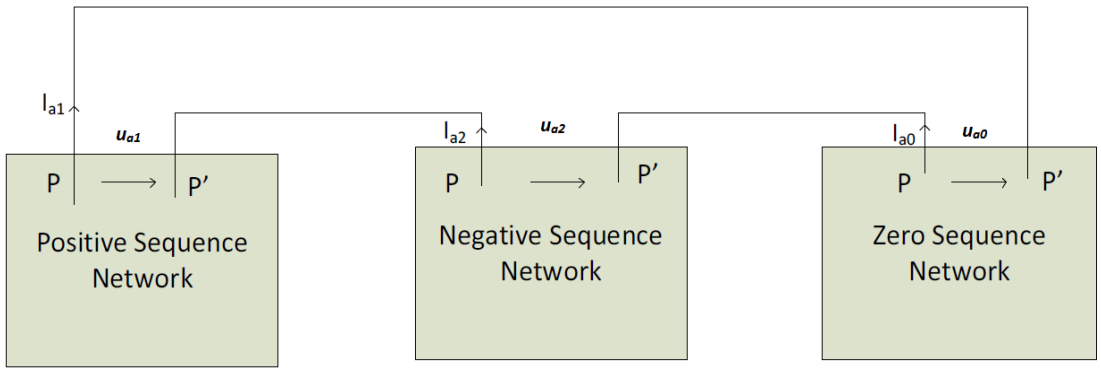

Figure 7: Connection of sequence networks of a system where phase b and c are disconnected between p and p' [2].

From Figure 6, where one phase is disconnected and the sequence networks are connected in parallel, therefore, even if the zero sequence circuit has infinite impedance, some power may be transferred from node m to n

In Figure 7, where two phases are disconnected, the sequence networks are connected in series, and thus, unless the zero sequence circuit have a finite impedance, no power may be transferred from node m to n.

2.4 Hydro turbines

Hydraulic turbines derive power from the force exerted by water as it falls from an upper to a lower reservoir. The vertical distance between the upper reservoir and the level of the turbine is called the head. The size of the head is used to classify hydroelectric power plants as high-head, medium-head and low-head plants, although there is no strict demarcation line [4].

Low and medium-head hydro-electric plant is built using reaction turbines such as the Francis turbine [4]. Because of the relatively LP head reaction, turbines typically use a large volume of water, require large water passages and operate at low speed. In operation, water enters the turbine from the intake passage or penstock through a spiral case, passes through the stay ring and the movable wicket gates onto the runner [4].

In high-head hydro-electric power plants, the Pelton-wheel impulse turbines are used [4]. In these turbines, the HP water is converted into high-velocity jets of water by a set of fixed nozzles. The high-velocity water jets hit on a set of bowl-shaped buckets attached around the periphery of the runner that turn back the water so the full effect of the water jet to the runner is affected. The size of the jet, and thus the power output of the turbine, is controlled by a needle in the centre of the nozzle. The governor controls the movement of the needle. A jet deflector is located just outside the nozzle tip to deflect the jet from the buckets in the event of sudden load reduction [4].

2.5 Synchronous machine

Synchronous machines are classified into two principal types - round-rotor machines, which have high rpm [4], and salient-pole machines, which have lower rpm [4]. Generators driven by steam turbines (turbogenerators) have cylindrical (round) rotors with slots in which distributed field windings are placed [5]. Generators driven by water wheels (hydraulic turbines/ hydro turbines) have laminated salient-pole rotors with concentrated field windings and, usually, a large number of poles. Some hydro powered generators are provided with amortisseur windings or damper windings; others are not [5].

2.5.1 Dq0 transformation

In the salient pole synchronous generator, the stator inductances are dependent on the position of the rotor [4] [5] [6]. To explain the behaviour of synchronous machines referred to stator quantities, the dq0 transformation is applied. Figure 8 show a synchronous machine

with the d-axis aligned with the rotor, and the q-axis aligned at an angle π/2 ahead of the d-axis.

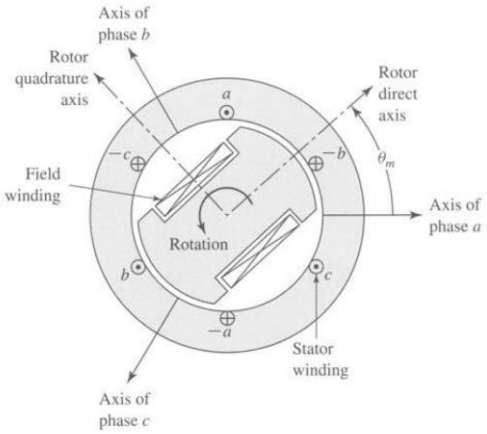

Figure 8: The synchronous machine [7].

The usefulness of this concept stems from the fact that although each of the stator phases sees a time varying inductance due to the saliency of the rotor, the transformed quantities rotate with the rotor and hence see constant magnetic paths [7]. Additional saliency effects are present under transient conditions due to the different conducting paths in the rotor [4], rendering the concept of the transformation all the more useful [7].

The dq0 transformation, is in [7], represented in terms of the electrical angle θ_{me}, where $\theta_{me} = \frac{polepairs}{2\,\theta_m}$, between the rotor direct axis and the stator phase a axis.

Letting S represent a stator quantity to be transformed (current, voltage, flux), the transformation in matrix form can be expressed

$$\begin{bmatrix} S_d \\ S_q \\ S_0 \end{bmatrix} = \frac{2}{3} \begin{bmatrix} \cos\theta_{me} & \cos\left(\theta_{me} - \frac{2\pi}{3}\right) & \cos\left(\theta_{me} + \frac{2\pi}{3}\right) \\ -\sin\theta_{me} & -\sin\left(\theta_{me} - \frac{2\pi}{3}\right) & -\sin\left(\theta_{me} + \frac{2\pi}{3}\right) \\ \frac{1}{2} & \frac{1}{2} & \frac{1}{2} \end{bmatrix} \begin{bmatrix} S_a \\ S_b \\ S_c \end{bmatrix}, \tag{2.10}$$

and the inverse transformation

$$\begin{bmatrix} S_a \\ S_b \\ S_c \end{bmatrix} = \begin{bmatrix} \cos\theta_{me} & -\sin\theta_{me} & 1 \\ \cos\left(\theta_{me} - \frac{2\pi}{3}\right) & -\sin\left(\theta_{me} - \frac{2\pi}{3}\right) & 1 \\ \cos\left(\theta_{me} + \frac{2\pi}{3}\right) & -\sin\left(\theta_{me} + \frac{2\pi}{3}\right) & 1 \end{bmatrix} \begin{bmatrix} S_d \\ S_q \\ S_0 \end{bmatrix}. \tag{2.11}$$

2.5.2 The generator on no load

When not generating any power, the armature current is zero. The DC field current i_f produces an mmf wave which is approximately sinusoidally distributed around the circumference of the stator [4]. The peak value of the mmf

$$F_f = N_f i_f \tag{2.12}$$

lies along the d axis and is determined by the effective number of field windings and field current [4].

The field winding mmf drives the excitation flux ϕ_f around the magnetic circuit. The flux path per pole is

$$\phi_f = \frac{F_f}{\Re} = \frac{N_f i_f}{\Re} \tag{2.13}$$

where $\Re$ is the reluctance of the path per pole [4]. As the reluctance of the path is iron is negligibly small compared with that in air, $\Re$ is approximately directly proportional to the width of the air gap [4].

As the rotor rotates at synchronous speed, the excitation flux rotates with it and produces a time varying flux linkage with each phase of the armature winding. Taking phase A as reference gives

$$\begin{aligned} \psi_{fA}(t) &= \psi_{fa}\cos\omega t = N_\phi \phi_f \cos\omega t = N_\phi \frac{N_f i_f}{\Re} = M_f i_f \cos\omega t \\ \psi_{fB}(t) &= M_f i_f \cos\left(\omega t - \frac{2\pi}{3}\right) \\ \psi_{fC}(t) &= M_f i_f \cos\left(\omega t + \frac{2\pi}{3}\right) \end{aligned} \tag{2.14}$$

where $\psi_{fa} = N_\phi \phi_f$ is the amplitude of the excitation flux linkage of an armature phase winding, $M_f = N_\phi N_f / \Re$ is the mutual inductance between the field and the armature winding, and $N_\phi = k_w N$ where *N* is the number of turns in series in each phase winding and k_w is the armature winding factor [4].

The time varying flux linkages induce an excitation emf in each of the phase windings gives

$$\begin{aligned} e_{fA} &= -\frac{d\psi_{fA}(t)}{dt} = \omega M_f i_f \sin\omega t \\ e_{fB} &= -\frac{d\psi_{fB}(t)}{dt} = \omega M_f i_f \sin\left(\omega t - \frac{2\pi}{3}\right) \\ e_{fC} &= -\frac{d\psi_{fC}(t)}{dt} = \omega M_f i_f \sin\left(\omega t + \frac{2\pi}{3}\right) \end{aligned} \tag{2.15}$$

At no load conditions these emfs represent the terminal voltage, the rms value is

$$E_f = \tfrac{1}{\sqrt{2}}\omega\psi_{fa} = \tfrac{1}{\sqrt{2}}\omega N_\phi \phi_f = \tfrac{1}{\sqrt{2}}\omega M_f i_f \cong 4.44\, f\, M_f i_f \text{ [4].} \tag{2.16}$$

2.5.3 Generator operating on load conditions

When an armature current flows in the phase windings of the stator, the terminal voltage will change and the current angle will shift due to the self- and mutual inductances, and

resistances in the stator and rotor [4]. The saliency of the rotor influence this [4] [6], and first the round rotor will be presented in this report.

The phase currents in respect to the reference flux linkage $\psi_{fA}(t)$ will have an angle λ, and may be expressed as

$$\begin{aligned} i_A &= I_m \cos(\omega t - \lambda) \\ i_B &= I_m \cos\left(\omega t - \lambda - \frac{2\pi}{3}\right) \\ i_C &= I_m \cos\left(\omega t - \lambda + \frac{2\pi}{3}\right) \end{aligned} \tag{2.17}$$

where I_m is the peak value of the armature current. Each of the phase currents produces a pulsating phase mmf per pole

$$\begin{aligned} F_A(t) &= N_a I_m \cos(\omega t - \lambda) \\ F_B(t) &= N_a I_m \cos\left(\omega t - \lambda - \frac{2\pi}{3}\right) \\ F_B(t) &= N_a I_m \cos\left(\omega t - \lambda + \frac{2\pi}{3}\right) \end{aligned} \tag{2.18}$$

where $N_a = (1/p)(4/\pi)\, N_\phi$ is the effective number of turns per phase pole and $N_\phi = k_w N$ [4].

In Machowski et al. [4], the resultant armature reaction mmf $\vec{F}_a$ is used as reference to represent the mmfs as space vector by adding the space operator $e^{j\theta}$to phase shift the phase vectors. The resulting armature mmf per pole $\vec{F}_a$ is expressed as

$$\vec{F}_a = \vec{F}_A + \vec{F}_B + \vec{F}_C = N_a I_A e^{j0} + N_a I_B e^{j2\pi/3} + N_a I_C e^{j4\pi/3} \tag{2.19}$$

and can be rearranged as

$$\vec{F}_a = 1.5\, N_a I_m e^{j(\omega t - \lambda)}. \tag{2.20}$$

$\vec{F}_a$ is a vector of constant magnitude which rotates in the complex plane with an angular velocity of ω. As ω is the rotational speed of the generator, the rotor and stator mmfs $\vec{F}_f$ and $\vec{F}_a$ are stationary with respect to each other. The relative spatial position of $\vec{F}_a$ with respect to $\vec{F}_f$ is determined by the angle λ. The two mmfs can be combined to give a resultant mmf $\vec{F}_r = \vec{F}_a + \vec{F}_f$ which drives the resultant air gap flux ϕ_r [4].

2.5.4 The salient pole machine

In a salient pole machine, the air gap varies circumferentially around the generator with the narrowest gap being along the d axis and the widest along the q axis. As mentioned in regards

to the dq0 transformation the inductance in the stator varies with the position of the rotor because of the reluctance variation between the d- and q-axis, where $\Re_{\mathrm{d}} < \Re_{\mathrm{q}}$.

As flux tends to take the path of least inductance, the flux vector $\psi_{fA}(t)$ in a salient pole machine is not in phase with the mmf vector $\vec{F}_f$ [4]. To solve this, the armature mmf $\vec{F}_a$ and current $\underline{I}$ are decomposed into d- and q-axis components [4]. Figure 9 illustrates this, where d-axis components are $\vec{F}_{ad}$ and $\underline{I}_d$, and q-axis components are $\vec{F}_{aq}$ and $\underline{I}_q$. The exitation mmf $\vec{F}_f$ is always alond the d-axis and does not need to be decomposed [4].

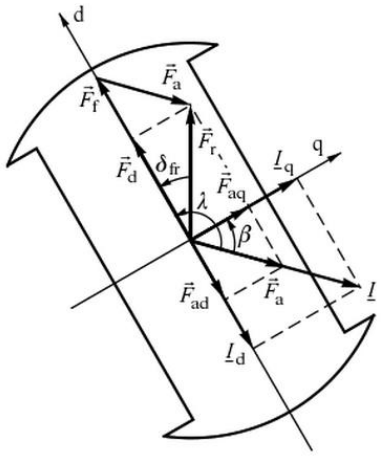

Figure 9: Currents and mmfs in d- and q components [4].

The resultant mmf $\vec{F}_r$ may then be expressed as

$$\vec{F}_r = \vec{F}_d + \vec{F}_q \tag{2.21}$$

where $\vec{F}_d = \vec{F}_f + \vec{F}_{ad}$ and $\vec{F}_q = \vec{F}_{aq}$. The current $\underline{I}$ may be expressed as

$$\underline{I} = \underline{I}_d + \underline{I}_q \tag{2.22}$$

The internal emf is expressed as

$$\underline{E}_f = \underline{V}_g + jX_d\underline{I}_d + j\underline{X}_q\underline{I}_q + RI \tag{2.23}$$

where $X_d = X_{ad} + X_l$ is the direct-axis synchronous reactance and $X_q = X_{aq} + X_l$ is the quadrature-axis synchronous reactance [4]. X_l is the leakage reactance and X_{ad} and X_{aq} is the d- and q-axis armature reactance. Figure 10 show the resulting phasor diagram.

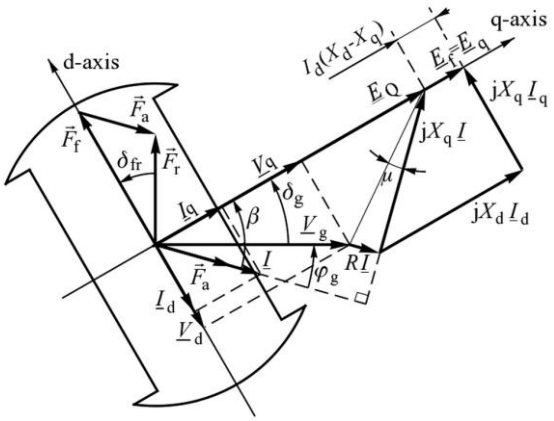

Figure 10: Phasor diagram of a salient pole machine [4].

Resolving the equation above into d- and q-components enables the equivalent circuit of the synchronous generator to be constructed.

On matrix form the equation can be expressed

$$\begin{bmatrix} E_d \\ E_q \end{bmatrix} = \begin{bmatrix} 0 \\ E_f \end{bmatrix} = \begin{bmatrix} V_{gd} \\ V_{gq} \end{bmatrix} + \begin{bmatrix} R & X_q \\ -X_d & R \end{bmatrix} \begin{bmatrix} I_d \\ I_q \end{bmatrix} \tag{2.44}$$

Figure 11 show the equivalent circuit for the salient pole machine with d- and q-axis.

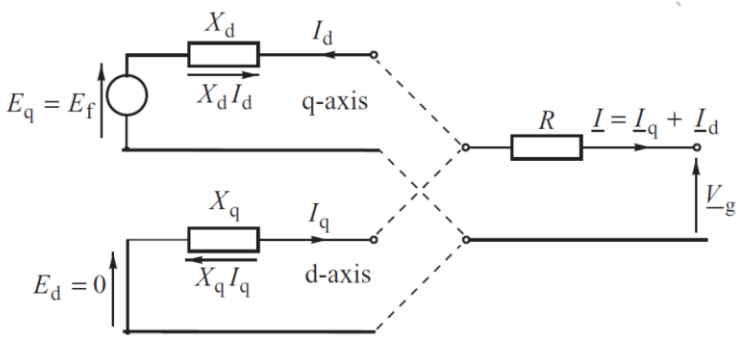

Figure 11: Equivalent d- and q-axis circuit diagram of the salient pole machine [4].

2.5.5 *Torque and power of a salient pole synchronous machine*

The torque developed in a salient-pole generator consists of two components. The first component, proportional to sin δ_{fr}, is termed the synchronous torque. The second component, termed the reluctance torque, arises as the rotor tries to assume a position of minimum magnetic reluctance by moving towards the air-gap mmf. This additional torque is due to the non-uniform air gap and is a direct consequence of the air-gap mmf and flux not being in phase [4].

The torque expression for a single pole pair generator is

$$\tau = \frac{\pi}{2}\phi_f F_r \sin\delta_{fr} + \frac{\pi}{4}F_r^2 \frac{\Re_q - \Re_d}{\Re_q \Re_d} \sin 2\delta_{fr} \tag{2.25}$$

where δ_{fr} is referred to as the torque angle [4].

The active power for a salient pole generator based on the equivalent circuit

$$P = \frac{E_q V}{x_d} \sin \delta_{gt} + \frac{V^2}{2} \frac{x_d - x_q}{x_d x_q} \sin 2\delta_{gt} \tag{2.56}$$

where the first component is dominant and depends on the sine of the angle between the voltage and the generator emf. The second component, referred to as the reluctance power, exists only in salient-pole generators ($x_d > x_q$), and the resistances of the equivalent circuit are neglected [4].

2.5.6 Excitation system

The basic function of an excitation system is to provide magnetizing current to the synchronous machine [6].

The excitation system must be able to perform control and protective functions essential to the satisfactory performance of the power system by controlling the field voltage and field current.

The basic requirement of the excitation system is to supply and automatically adjust the field current of the synchronous machine to maintain the terminal voltage and be able to respond to transient disturbances with the field forcing consistent with the

The excitation system should be able to perform effective control of voltage and enhancement of system stability.

The excitation system should be able to respond rapidly to a disturbance to enhance transient stability, and of modulating the generator field as to enhance small-signal stability.

Figure 12 show the functional block diagram of a typical excitation control system.

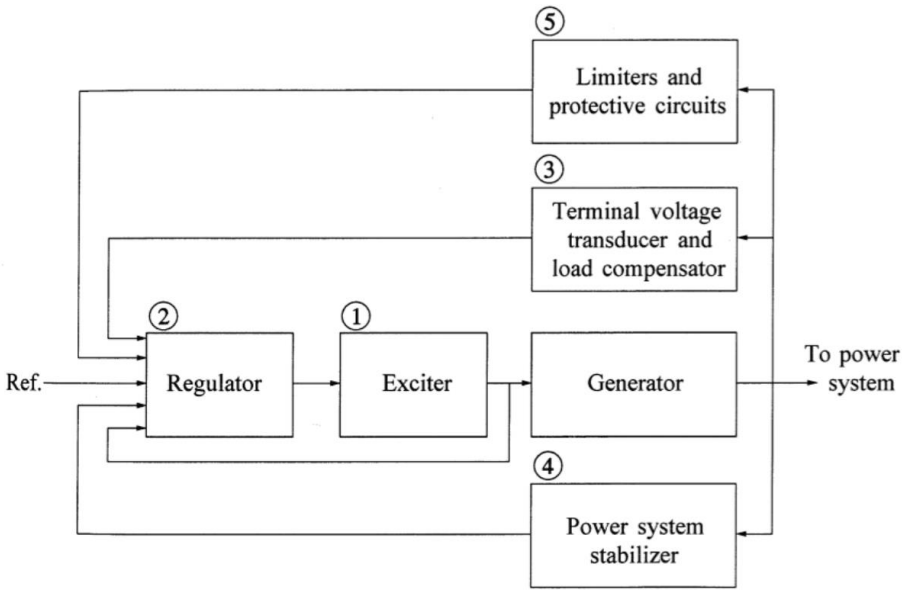

Figure 12: Functional block diagram of a synchronous generator excitation control system [6].

where:

(1) Exciter. Provide DC power to the synchronous machine field winding.
(2) Regulator. Processes and amplifies input control signal to a level and form appropriate for control of the exciter.
(3) Terminal voltage transducer and load compensator. Senses generator terminal voltage, rectifies and filters it to DC quantity, and compares it with a reference that represents the desired terminal voltage. In addition, load compensation may be provided, if it is desired to hold constant voltage at some point electrically remote from the generator terminal.
(4) Power system stabilizer. Provides additional input signal to the regulator to damp power system oscillations.
(5) Limiters and protective circuits. These include a wide array of control and protective functions to ensure the capability limits of the exciter and synchronous generator are not exceeded.

According to Machowski et al. [4], exciters can be classified as either rotating or static. Figure 13 shows some typical systems. In the rotating exciters of Figure 13a– c, the excitation current is supplied either by a DC generator or by an AC generator with rectifiers. Some alternative exciter systems using static thyristor converters are shown in Figure 13d– f. In these exciters, the thyristor rectifiers are controlled directly by a voltage regulator. The main differences between the systems is in the type of supply used [4].

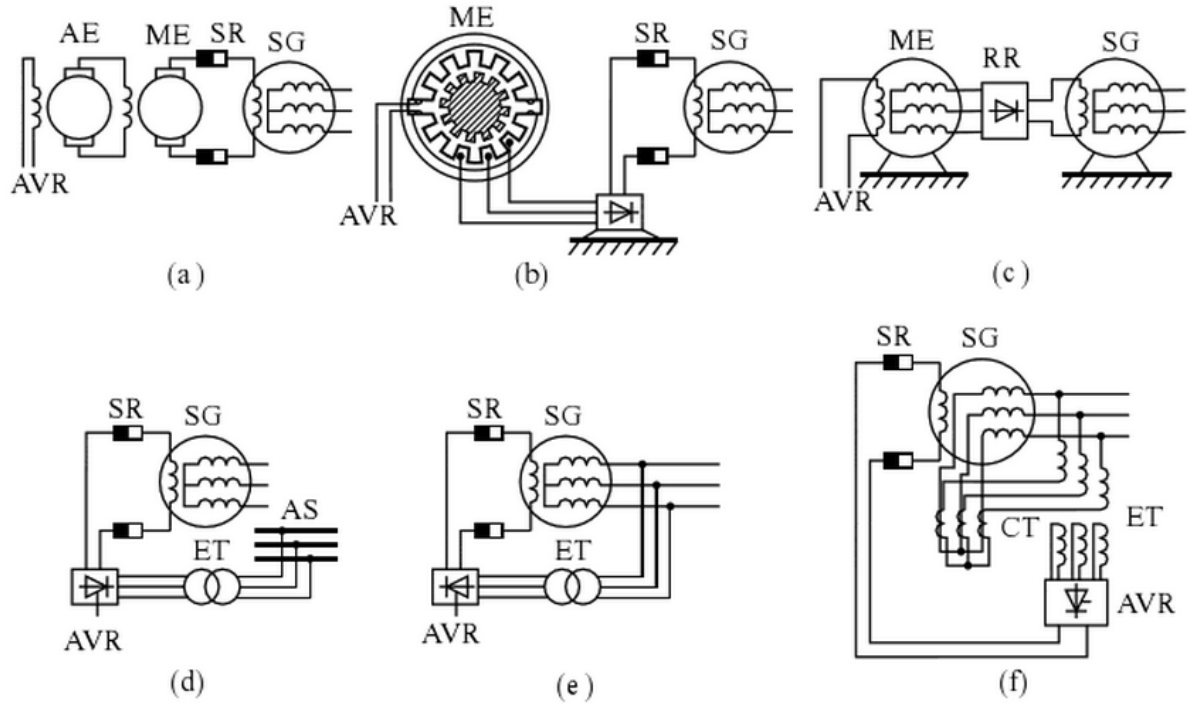

Figure 13: Typical exciter systems: (a) cascaded DC generators; (b) reluctance machine with rectifier; (c) inside-out synchronous generator with rotating rectifier; (d) controlled rectifier fed from the auxiliary supply; (e) controlled rectifier fed from the generator terminals; (f) controlled rectifier fed by the generator's voltage and current. SG, synchronous generator; SR, slip rings; ME, main exciter; AE, auxiliary exciter; RR, rotating rectifier; ET, excitation transformer; AS, auxiliary service busbars; CT, current transformer; AVR, automatic voltage regulator [4].

2.5.7 *Turbine governors*

The basic function of a turbine governor is to control speed and/or load [6]. The primary speed/load control function involves feeding back speed error to control the gate position. In order to ensure satisfactory and stable parallel operation of multiple units, the speed governor is provided with a droop characteristic. The purpose of the droop is to ensure equitable load sharing between generating units [6].

When determining the hydraulic governor settings, there are two important considerations to note [6]:

1. Stable operation during system-islanding conditions or isolated operation.
2. Acceptable speed of response for loading and unloading under normal synchronous operation.

For stable operation under islanding conditions, the optimum choice of the temporary droop R_T and reset time T_R is related to the water starting time T_W and mechanical starting time T_M=2H as follows [6]:

$$R_T = [2{,}3 - (T_W - 1{,}0)0{,}15]\frac{T_W}{T_M}$$
$$T_R = [5{,}0 - (T_W - 1{,}0)0{,}5]T_W \tag{2.27}$$

The above setting ensure good stable performance when the unit is at full load supplying an isolated load. This represents the most severe requirement and ensures stable operation for all situations involving system islanding [6]. For loading and unloading during normal interconnected system operation, the above settings result in too slow response for satisfactory loading rates, the reset time T_R should be less than 1,0, preferably close to 0,5 s [6].

2.6 Rotor angle stability

Rotor angle stability refers to the ability of synchronous machines of an interconnected power system to remain in synchronism after having experienced a disturbance. It depends on the ability to maintain or restore equilibrium between electromagnetic torque and mechanical torque of each synchronous machine in the system. Instability that may result occurs in the form of increasing angular swings of some generators leading to their loss of synchronism with other generators [3].

With electric power systems, the change in electrical torque of a synchronous machine following a disturbance can be resolved into two components:

$$\Delta T_e = T_S \Delta\delta + T_D \Delta\omega \tag{2.28}$$

where

$T_S \Delta\delta$ is the component of the torque change in phase with the rotor angle disturbance $\Delta\delta$ and is referred to as the synchronizing torque component; T_S is the synchronizing torque coefficient.

$T_D\Delta\omega$ is the component of torque in phase with the speed deviation $\Delta\omega$ and is referred to as the damping torque coefficient; T_D is the damping torque coefficient.

System stability depends on the existence of both components of torque for each of the synchronous machines. Lack of sufficient synchronizing torque results in instability through an aperiodic drift in rotor angle, while lack of sufficient damping torque results in oscillatory instability.

2.6.1 The swing equation

The equations of central importance in power system stability analysis are the rotational inertia equations describing the effect of unbalance between the electromagnetic torque and the mechanical torque of the individual machines [6].

Any unbalanced torque acting on the rotor will result in the acceleration or deceleration of the rotor as a complete unit according to Newton's second law

$$J\frac{d_{\omega m}}{dt} + D_d\omega_m = \tau_m - \tau_e \tag{2.29}$$

where J is the total moment of inertia of the turbine and generator rotor (kgm^2), ω_m is the rotor shaft velocity (mechanical rad/s), τ_m is the torque produced by the turbine (Nm), τ_e is the counteracting electromagnetic torque and D_d is the damping-torque coefficient (Nms) and accounts for the mechanical rotational loss due to windage and friction [4].

A normalized per unit inertia constant H in Ws is defined as [4] [6]

$$H = \frac{0.5J\omega_n^2}{S_n} \tag{2.30}$$

where ω_n is the synchronous speed in rad/s, and S_n is the machine rating in MVA. The inertia coefficient M is defined

$$M = \frac{2HS_n}{\omega_s} \tag{2.31}$$

where

$$\omega_s = \frac{\omega_n}{p} \tag{2.32}$$

is the angular speed in electrical rad/s, and p is pole-pairs of the machine [4]. Equation (2.29) can then be expressed as the second order equation

$$M\frac{d^2\delta}{dt^2} = P_m - P_e - P_D = P_{acc} \tag{2.33}$$

where P_{acc} is the net accelerating power, P_m is the net mechanical power, P_e is the electrical power over the air gap and P_D is the damping power. The time derivative of the rotor angle $d\delta/dt = \Delta\omega = \omega - \omega_s$ is the rotor speed deviation in electrical radians per second. Equation (2.32) and (2.33) can be rearranged into two first order equations

$$M\frac{d\Delta\omega}{dt} = P_m - P_e - P_D = P_{acc}$$
$$\frac{d\delta}{dt} = \Delta\omega \tag{2.34}$$

where δ is the power angle in electrical radians [4].

2.6.2 Damping power

The main source of damping in the synchronous generator is provided by the damper or amortisseur windings. During a fault, the additional rotor currents prevent the armature flux from entering the rotor windings, they have the effect of screening the rotor from these changes in armature flux, which is illustrated in Figure 14.

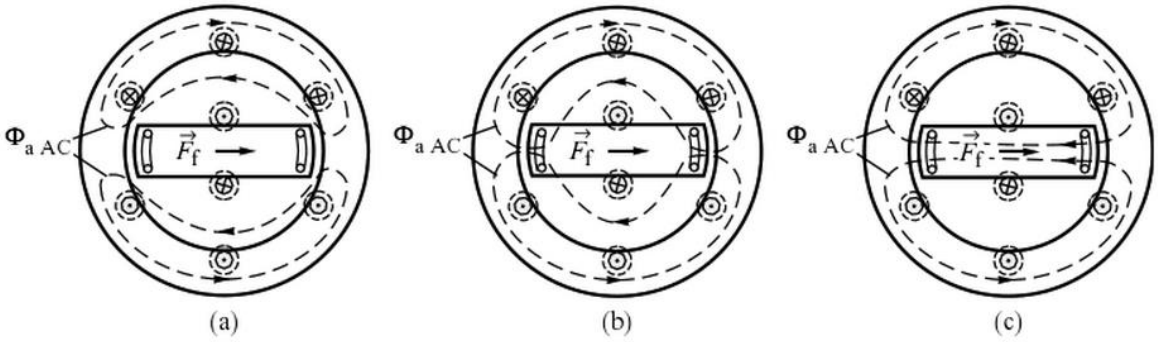

Figure 14: The path of the armature flux in: (a) the subtransient state (screening effect of the damper winding and the field winding); (b) the transient state (screening effect of the field winding only); (c) the steady state. In all three cases the rotor is shown to be in the same position but the actual rotor position corresponding to the three states will be separated by a number of rotations [4].

In the subtransient state these windings act as a perfect screen and the changes in the armature flux cannot penetrate them. In the transient state the air-gap flux, which rotates at the synchronous speed, penetrates the damper windings and induces an emf and current in them whenever the rotor speed ω is different from the synchronous speed ω_s . This induced current produces a damping torque that, according to Lenz's law, tries to restore the synchronous speed of the rotor [4]. As this additional torque only appears when $\omega \neq \omega_s$, it is proportional to $\Delta\omega = d\delta/dt$ and is referred to as the asynchronous torque [4].

The expression for damping power P_D is expressed, as generator - infinite busbar system, when the following assumptions are made [4]:

(i) the resistances of both the armature and the field winding are neglected;
(ii) damping is produced only by the damper windings;
(iii) the leakage reactance of the armature winding can be neglected;
(iv) excitation does not affect the damping torque.

The resultant damping power is in Machowski et al. [4] expressed as

$$P_D = V_S^2 \left[\frac{X'_d - X''_d}{(X + X'_d)^2} \frac{X'_d}{X''_d} \frac{T''_d \Delta\omega}{1 + (T''_d \Delta\omega)} \, sin^2\,\delta + \frac{X'_q - X''_q}{\left(X + X'_q\right)^2} \frac{X'_q}{X''_q} \frac{T''_q \Delta\omega}{1 + \left(T''_q \Delta\omega\right)} cos^2\,\delta \right] \quad (2.35)$$

where V_S is the infinite busbar voltage, X'_d and X''_d is the transient and subtransient reactance in d-axis, X'_q and X''_q is the transient and subtransient reactance in q-axis, and T''_d and T''_q is the subtransient time constants of the d- and q-axis, respectively [4].

The damper power depends on the rotor angle and fluctuates with the rotor speed deviation Δω = dδ/dt. For small speed deviations, the damping power is proportional to speed deviation, while for larger speed deviations it is a nonlinear function of speed deviation. Equation (2.35) then simplifies to

$$P_D = V_S^2 \left[\frac{X'_d - X''_d}{(X + X'_d)^2} \frac{X'_d}{X''_d} T''_d \, sin^2\,\delta + \frac{X'_q - X''_q}{\left(X + X'_q\right)^2} \frac{X'_q}{X''_q} T''_q \, cos^2\,\delta \right] \Delta\omega. \quad (2.36)$$

When δ is large, damping is strongest in the d-axis, and when δ is small, the q-axis damper winding produce the stronger damping. P_D can be expressed

$$P_D = \left[D_d \, sin^2\delta + D_q \, cos^2\delta \right] \Delta\omega = D(\delta)\Delta\omega \quad (2.37)$$

where D_d and D_q are damping coefficients in both axes [4].

2.6.3 Steady state analysis

Figure 15 can be used for steady state analysis of a generator operating on an equilibrium point.

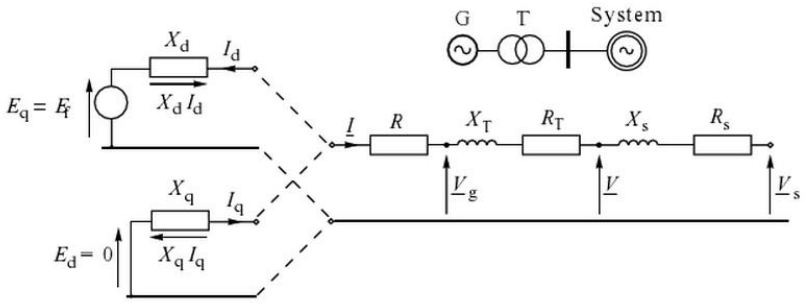

Figure 15: Equivalent circuit of a generator connected to a system through a transformer on an infinite busbar [4].

The infinite busbar is assumed to have constant voltage and frequency, neither of which is influenced by the action of an individual generator. This means that the voltage, V_s, can be used as a reference and the phase angles of all the other voltages and currents in the circuit measured with respect to it.

If the resistance of the generator and the network is neglected (r << Z), P is equal to the real power load on the generator.

$$P_s = P_{sEq} = \frac{E_q V_s}{x_d} \sin\delta + \frac{V_s^2}{2} \frac{x_d - x_q}{x_d x_q} \sin 2\delta \quad (2.38)$$

where $x_d = X_d + X_T + X_s$ and $x_q = X_q + X_T + X_s$. P_{sEq} is valid for the case E_q = constant. Note that P_{sEq} is a function of the power angle δ only. Function P_{sEq} (δ) is referred to as the power– angle characteristic of the generator operating on the infinite busbar and is shown in Figure 16.

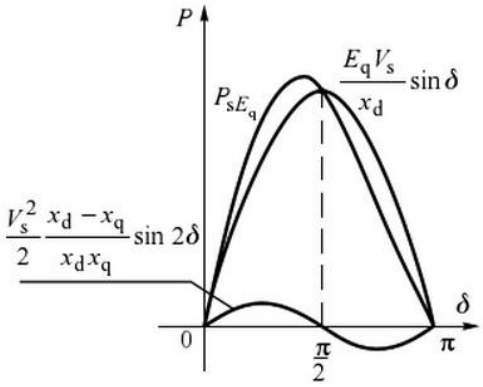

Figure 16: Power–angle characteristic PsEq (δ) for Eq = constant. The reluctance power term deforms the sinusoidal characteristic so that the maximum of PsEq (δ) occur at δ < π/2. For the round-rotor generators the maximum of PsEq (δ) occurs at δ = π/2 [4].

2.6.4 Equilibrium points

To simplify considerations, the round-rotor generator with $x_d = x_q$ is assumed, so that the reluctance part of equation (2.38) disappears. The expression for the air-gap power simplifies to

$$P_e(\delta) = P_{Eq}(\delta) = \frac{E_q V_s}{x_d}\sin\delta \tag{2.39}$$

This characteristic is shown in Figure 17, where the mechanical power in steady state is constant and is drawn as horizontal lines. The intersections between the mechanical power and the electrical power are possible equilibrium points of operation. The maximum value of P_{Eq} (δ) is referred to as the critical power $P_{Eq\,cr}$, and the corresponding value of the rotor angle is referred to as the critical angle δ_{cr}, for a round-rotor generator.

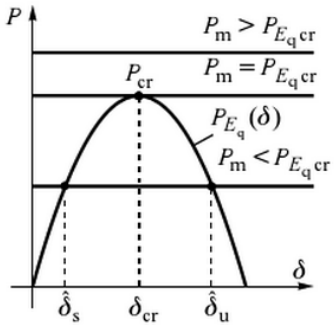

Figure 17: Equilibrium points for various values of mechanical power [4].

In Figure 17, three possible situations are shown:

1. $P_m > P_{Eq\,cr}$. The mechanical power exceeds the electrical power-angle curve, thus no equilibrium points exist and the generator cannot operate at such a condition.

2. $P_m = P_{Eq\,cr}$. There is only one equilibrium point at δ_{cr}.

3. $P_m < P_{Eq\,cr}$. There are two equilibrium points at $\hat{\delta}_s$ and $\hat{\delta}_u$.

If now the mechanical power P_m is slowly increased by a small amount, the electrical power P_e must follow the changes so that a new equilibrium point of $P_m = P_e$ is reached. In other words, the system is steady-state stable if an increase/decrease in mechanical power causes a corresponding increase/-decrease in electrical power. If the system reaction is opposite to this, that is an increase in mechanical power is accompanied by a decrease in electrical power, then no equilibrium point can be reached. These stability considerations are illustrated in Figure 18.

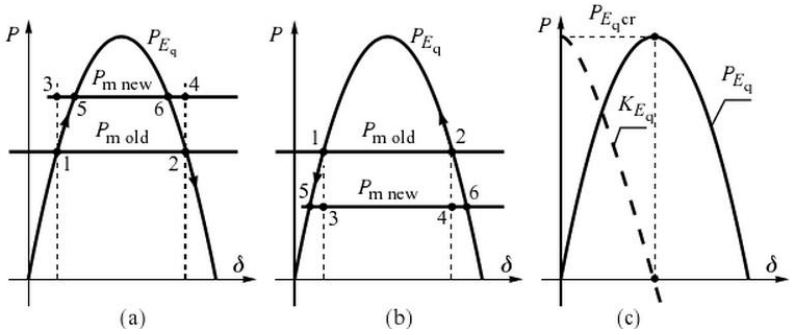

Figure 18; Illustration of the conditions for steady-state stability: (a) increase in mechanical power; (b) decrease in mechanical power; (c) the generator steady-state power and synchronizing power coefficient [4].

A generator - infinite busbar system with constant excitation emf E_f is steady-state stable only on the left hand side of the power– angle characteristic; that is, when the slope K_{Eq} of the characteristic is positive

$$K_{Eq} = \left.\frac{\partial P_{Eq}}{\partial \delta}\right|_{\partial=\hat{\delta}_s} > 0 \tag{2.40}$$

K_{Eq} is referred to as the steady-state synchronizing power coefficient and the critical power $P_{Eq\,cr}$ is often referred to as the pull-out power to emphasize the fact that a larger mechanical power will result in the unregulated generator losing synchronism with the rest of the system. Figure 18c shows the plot of $K_{Eq'}$ (δ) and $P_{Eq\,cr}$.

2.7 Small signal stability

Small-signal stability is the ability of the power system to maintain synchronism under small disturbances. Such disturbances occur continually on the system because of small variations in loads and generation. The disturbances are considered sufficiently small for linearization of system equations to be permissible for purposes of analysis. Instability that may result can be of two forms: (i) steady increase in rotor angle due to lack of sufficient synchronizing torque, or (ii) rotor oscillations of increasing amplitude due to lack of sufficient damping torque [6].

Small-signal analysis using linear techniques provides valuable information about the inherent dynamic characteristics of the power system and, according to Kundur [6], the small-signal

stability problem is usually one of insufficient damping of system oscillations. Figure 19 show the nature of generator response with and without excitation controls [6].

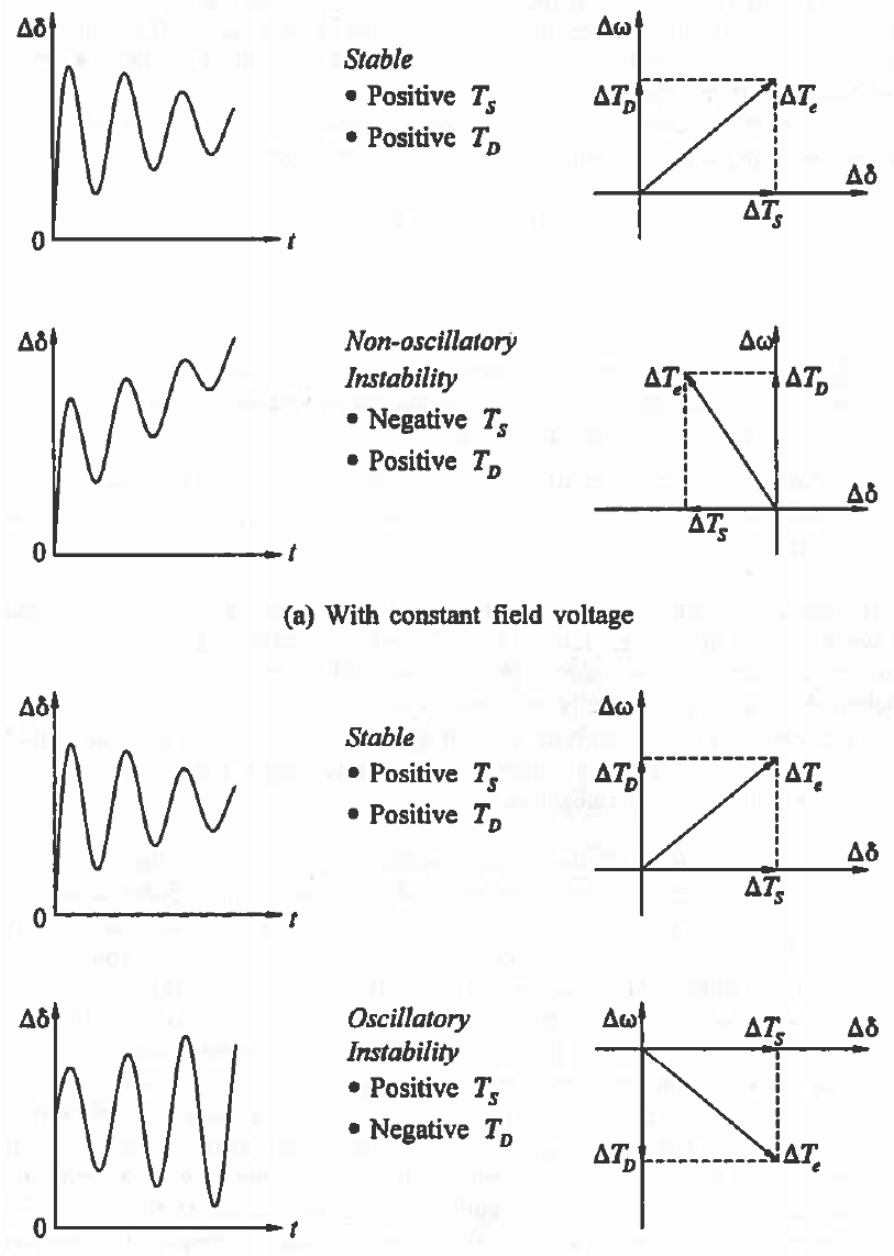

Figure 19: Nature of small-disturbance response [6].

The stability of the following types of oscillations is of concern [6]:

Local modes or machine-system modes are associated with the swinging of units at a generating station with respect to the rest of the power system. The term local is used because the oscillations are localized at one station or a small part of the power system.

Interarea modes are associated with the swinging of many machines in one part of the system against machines in other parts. They are caused by two or more groups of closely coupled machines being interconnected by weak ties.

Control modes are associated with generating units and other controls. Poorly tuned exciters, speed governors, HVDC converters and static VAr compensators are the usual causes of instability of these modes.

Torsional modes are associated with the turbine-generator shaft system rotational components. Instability of torsional modes may be caused by interaction with excitations controls, speed governors, HVDC controls and series-capacitor-compensator lines.

2.8 Transient stability

Transient stability is in [4] [6] defined as the ability of the power system to reach a steady-state operating point following a disturbance. The resulting system response involves large excursions of generator rotor angles and is influenced by the nonlinear power-angle relationship [6]. The stability of the power system depends both the initial operating conditions and the severity of the disturbance [6]. Figure 20 illustrates the behaviour of a synchronous machine for one stable and two unstable situations.

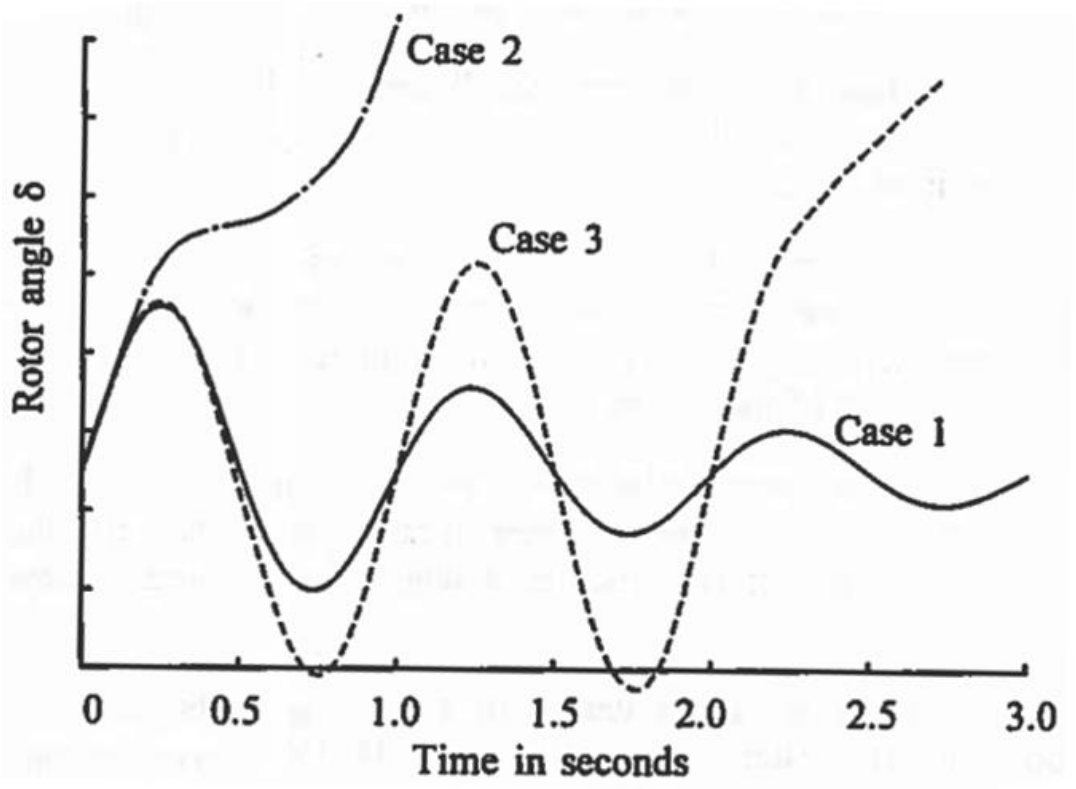

Figure 20: Rotor angle response to a transient disturbance [6].

In the stage case (Case 1), the rotor angle increases to a maximum, then decreases and oscillates with decreasing amplitude until it reaches a steady state. In Case 2, the rotor angle continues to increase until synchronism is lost. This form of instability is referred to as first-swing instability and is caused by insufficient synchronizing torque. In Case 3, the system is stable in the first swing but becomes unstable as a result of growing oscillations as the end state is approached. This form of instability occurs when the postfault steady-state condition itself is “small-signal” unstable, and not necessarily as a result of the transient disturbance [6].

2.9 Linear analysis

2.9.1 State-space representation

The behaviour of a dynamic system, such as a power system, may be described by a set of n first order nonlinear ordinary differential equations of the following form [6]:

$$\dot{x}_i = f_i(x_1, x_2, \dots, x_n; u_1, u_2, \dots, u_r; t) \qquad i = 1,2, \dots, n \tag{2.41}$$

where n is the order of the system and r is the number of inputs. This can be written in the following form by using vector-matrix notation:

$$\dot{x} = f(x, u, t) \tag{2.42}$$

where

$$x = \begin{bmatrix} x_1 \\ x_2 \\ \vdots \\ x_n \end{bmatrix} \qquad u = \begin{bmatrix} u_1 \\ u_2 \\ \vdots \\ u_r \end{bmatrix} \qquad f = \begin{bmatrix} f_1 \\ f_2 \\ \vdots \\ f_n \end{bmatrix} \tag{2.43}$$

The column vector x is referred to as the state vector, and its entries x_i as state variables. The column vector u is the vector of inputs to the system. These are the external signals that influence the performance of the system time is denoted by t, and the derivative of a state variable x with respect to time is denoted by $\dot{x}$.

If the derivatives of the state variables are not explicit functions of time, the system is said to be autonomous [6], and equation (2.42) can then be simplified to

$$\dot{x} = f(x, u) \tag{2.44}$$

2.9.2 Linearization

According to [4] [6], the equations describing the generator behaviour can be linearized in the vicinity of the predisturbance operating point for steady-state stability analysis.

The linearized swing equation can be expressed as

$$M\frac{d^2\Delta\delta}{dt^2} + D\frac{d\Delta\delta}{dt} + K_{E'_q}\Delta\delta = 0 \tag{2.45}$$

The classical generator model is represented by a constant emf E' behind the transient reactance X_d, and equations (2.34) in the linearized form is written as

$$M\Delta\dot{\omega} = P_m - P_e - P_D\Delta\omega \tag{2.46}$$

$$\dot{\delta} = \Delta\omega$$

The linearized system is presented as

$$\Delta\dot{\boldsymbol{x}} = \boldsymbol{A}\Delta\boldsymbol{x} \tag{2.47}$$

where $\Delta\dot{\boldsymbol{x}}$ is the state vector and $\boldsymbol{A}$ is the state matrix

$$\boldsymbol{A} = \begin{bmatrix} \frac{\partial f_1}{\partial x_1} & \frac{\partial f_1}{\partial x_2} \\ \frac{\partial f_2}{\partial x_1} & \frac{\partial f_2}{\partial x_2} \end{bmatrix} = \begin{bmatrix} \frac{\partial f_1}{\partial \delta} & \frac{\partial f_1}{\partial \omega} \\ \frac{\partial f_2}{\partial \delta} & \frac{\partial f_2}{\partial \omega} \end{bmatrix} \tag{2.48}$$

Using the matrix form, the expression becomes

$$\begin{bmatrix} \Delta\dot{\delta} \\ \Delta\dot{\omega} \end{bmatrix} = \begin{bmatrix} 0 & 1 \\ -\frac{K_{E'}}{M} & -\frac{D}{M} \end{bmatrix} \begin{bmatrix} \Delta\delta \\ \Delta\omega \end{bmatrix} \tag{2.49}$$

2.9.3 Eigenvalues

From the linearized system, the eigenvaules can be found. The eigenvalues may be real or complex.

The time dependent characteristic of a mode corresponding to an eigenvalue λ_i is given by $e^{\lambda_i t}$, and the stability of the system is determined by the eigenvalues that follows [6]:

(a) a real eigenvalue corresponds to a non-oscillatory mode. A negative eigenvalue represents a decaying mode. The larger the magnitude, the faster the decay. A positive real eigenvalue represents aperiodic instability.
(b) Complex eigenvalues occur in conjugate pairs, and each pair corresponds to an oscillatory mode.

The eigenvalues of the state matrix may be determined by

$$det(\boldsymbol{A} - \lambda \boldsymbol{I}) = \begin{vmatrix} -\lambda & 1 \\ -\frac{K_{E'}}{M} & -\lambda - \frac{D}{M} \end{vmatrix} = \lambda^2 + \frac{D}{M}\lambda + \frac{K_{E'}}{M} = 0 \tag{2.50}$$

The complex eigenvalues is solved from

$$\lambda_{1,2} = -\frac{D}{2M} \pm j\sqrt{\frac{K_{E'}}{M} - \left(\frac{D}{M}\right)^2}. \tag{2.51}$$

By separating the real and complex parts, where

$$\sigma = \frac{D}{2M} \quad \Omega = \sqrt{\frac{K_{E'}}{M} - \left(\frac{D}{M}\right)^2}, \tag{2.52}$$

where the real component (σ) of the eigenvalues gives the damping, and the imaginary component (Ω) gives the frequency of oscillation. A negative real part represents a damped oscillation whereas a positive real part represents oscillations of increasing amplitude [6]. For a complex pair of eigenvalues

$$\lambda = \sigma \pm j\Omega, \tag{2.53}$$

the damping ratio [4] [6]is given by

$$\zeta = \frac{-\sigma}{\sqrt{\sigma^2 + \Omega^2}}. \tag{2.54}$$

The damping ratio ζ determines the rate of decay of the amplitude of the oscillation [6]. Damping ratio within 0,05 is considered sufficient damping [4].

2.9.4 AVRs influence on transient response

In practice the armature will be connected to the system by a transmission line of finite reactance when the actual time constants involved will depend on the impedance in the armature circuit.

A change in the field winding flux linkage, and hence a change in E_q , can be produced by either a change in the excitation voltage or a change in the armature current. For a salient pole machine when $E' = E'_q$, the transient effect of time varying flux linkage can be expressed as [4]:

$$\Delta E'_q = E'_{q(\Delta\delta)} + E'_{q(\Delta E_f)} \tag{2.55}$$

where

$$E'_{q(\Delta\delta)} = -\frac{AB}{1.BT'_{d0}s}\Delta\delta, \qquad E'_{q(\Delta E_f)} = \frac{B}{1+BT'_{d0}s}\Delta E_f \tag{2.56}$$

and $\Delta\delta = \Delta\delta'$ [4]. These two components are due to the rotor swings and voltage regulation, respectivley. If the generator armature resistance and transmission link resistance are neglected, then

$$A = \frac{1-B}{B}\, V_s\, sin\delta_0 \quad \text{and} \quad B = \frac{X'_d + X_s}{X_d + X_s} = \frac{x'_d}{x_d} \tag{2.57}$$

Machowski et al. [4] shows that a change on the transient emf when the rotor angle $E'_{q(\Delta\delta)}$ changes, will lead the change in rotor angle by π/2. It will be in phase with the speed deviation $\Delta\omega = d\Delta\delta/dt$ and contribute damping torque.

Figure 21 shows how a change in the rotor angle influence $\Delta E'_{q(\Delta E_f)}$.

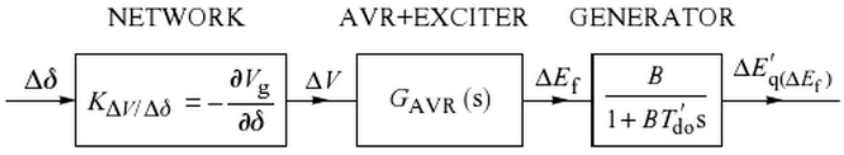

Figure 21: Components determining the phase shift between Δδ and $\Delta E'_{q(\Delta E_f)}$ [4].

The first block in Figure 21 constitutes a proportional element, as an increase in the rotor angle by Δδ causes a decrease in the generator voltage by $V_g \cong (\partial V_g/\partial\delta)\Delta\delta$ so that the following voltage error is $K_{\Delta V/\Delta\delta}\,\Delta\delta$ [4].

$K_{\Delta V/\Delta\delta}$ is expressed at the linearization point defined by δ^0, E'_0 and V_{g0} [4]:

$$\mathrm{K}_{\Delta \mathrm{V}/\Delta\delta} = -\frac{\partial \mathrm{V_g}}{\partial \delta'}\Delta\delta = \frac{\mathrm{X'_d\ X}}{\left(\mathrm{X'_d + X}\right)^2}\frac{\mathrm{E'_0}}{\mathrm{V_{g0}}}\ \mathrm{V_s}\sin\delta'_0 \tag{2.58}$$

$\mathrm{K}_{\Delta \mathrm{V}/\Delta\delta}$ is in other literature (ie. Kundur [6]) referred as the linearizing constant K5. It is to note that $\mathrm{K}_{\Delta \mathrm{V}/\Delta\delta}$ and K5 is defined with different notations. This coefficient is positive over a wide range of angle changes, which means that the voltage regulation error is in phase with the angle changes Δδ.

The second block in Figure 21 introduces a phase shift between ΔE_f and ΔV dependent on the transfer functions of the AVR and exciter. The third block in Figure 21 represents the generator, which introduces a phase shift equal to π/2.

This is shown in Figure 22 which contains two phasor diagrams of increments rotating with the swing frequency Ω (rad/s) drawn for two general types of AVR systems. In both diagrams the phasors of increments Δδ and ΔV are in phase, where the component $\Delta E'_{q(\Delta\delta)}$ leads by Δδ by π/2, while $\Delta E'_{q(\Delta E_f)}$ lags the changes in Δδ by π/2.

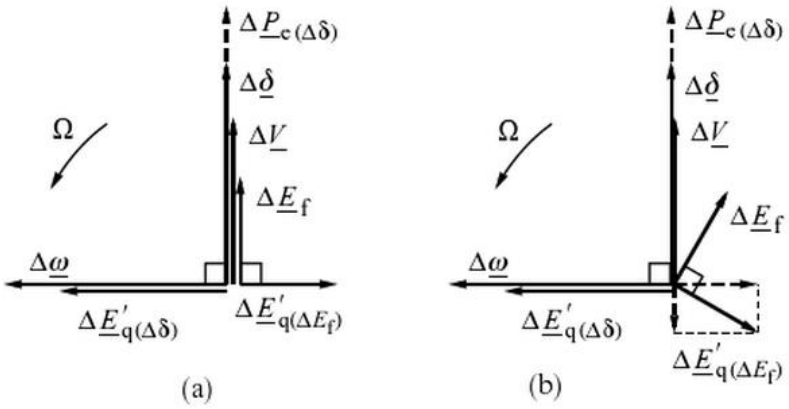

Figure 22: Phasors of increments rotating with the swing frequency Ω for: (a) the AVR proportional system; and (b) the AVR proportional system with inertia [4].

The phasor diagram shown in Figure 22a is valid for a proportional AVR system when $\Delta\underline{E}_f$ and $\Delta\underline{V}$ are almost in phase. The component $\Delta E'_{q(\Delta E_f)}$ lags $\Delta\underline{E}_f$ by π /2 and directly opposes $\Delta E'_{q(\Delta\delta)}$. This diagram shows that voltage regulation, represented by $\Delta E'_{q(\Delta E_f)}$, weakens the damping introduced by the field winding and represented by $\Delta E'_{q(\Delta\delta)}$. If the magnitude of $\Delta E'_{q(\Delta E_f)}$ is greater than that of $\Delta E'_{q(\Delta\delta)}$ then the voltage regulation will introduce a net negative damping into the system. This negative damping is enhanced by:

- Large generator load resulting in a large value of the coefficient $K_{\Delta V/\Delta\delta}$.
- Large gain $|G_{AVR}(s)|$ in the AVR controller determining the magnitude of $\Delta\underline{E}_f$.
- Large network reactance X determining the value of the coefficient $K_{\Delta V/\Delta\delta}$, where max value of $K_{\Delta V/\Delta\delta}$ is obtained for $X = X'_d$. Usually $X \ll X'_d$, assuming the higher the network reactance X, the higher the coefficient $K_{\Delta V/\Delta\delta}$.

2.9.5 AVR effect on the damper windings

A change in the rotor angle δ results in the speed deviation ω. According to Faraday's law, an emf is induced which is proportional to the speed deviation. The current driven by this emf interacts with the air-gap flux to produce a torque referred to as the natural damping torque.

Now consider the influence of the AVR on the damper windings. The d-axis damper winding lies along the path of the excitation flux produced by the field winding. This means that the two windings are magnetically coupled and may be treated as a transformer, Figure 23 (b), supplied by E_f and loaded with the resistance R_D of the damper winding. Consequently, the additional current $\underline{i}_{D(E_f)}$ induced in the damper winding must lag ΔE_f. Figure 23 (c) shows the position of phasors. The horizontal component of $\underline{i}_{D(E_f)}$ directly opposes the horizontal component of $\underline{i}_{D(\Delta\omega)}$. As the former is due to the AVR while the latter is due to speed deviation and is responsible for the natural damping, it may be concluded that voltage regulation weakens the natural damping. This weakening effect is referred to as artificial damping. Artificial damping is stronger for larger $\underline{i}_{D(E_f)}$ currents. This current is, in turn, proportional to the variations in $\Delta\underline{E}_f$ and $\Delta\underline{V}$ caused by $\Delta\underline{\delta}$.

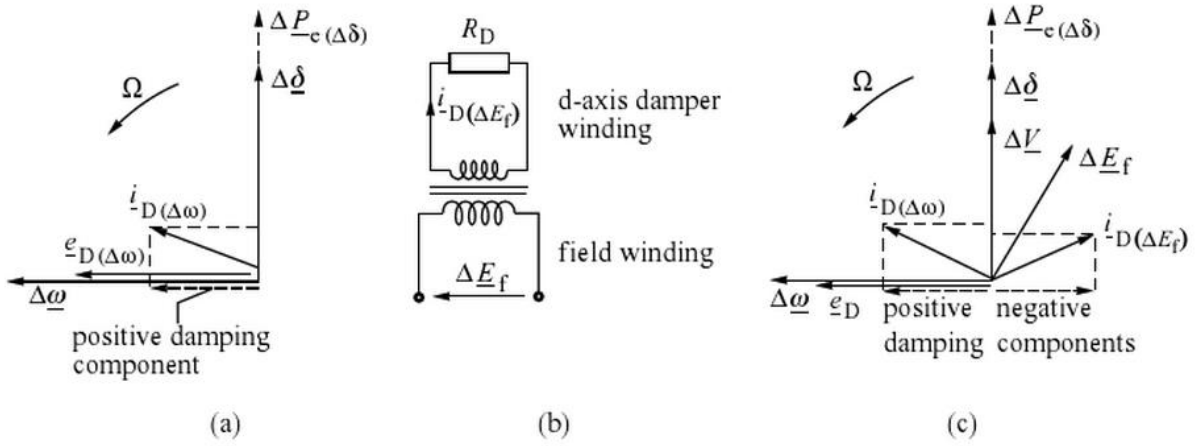

Figure 23: Phasor diagram of increments oscillating with the swing frequency (in rad/s) for the damper windings: (a) natural damping only; (b) field and damper windings as a transformer; (c) natural and artificial damping [4].

2.10 Protective relays

Relaying is the branch of electric power engineering that detects abnormal power system conditions and initiates corrective action as quickly as possible in order to return the power system to its normal state. The quickness of response is an essential element of protective relaying systems – response times of the order of a few milliseconds are often required. The response must be automatic, quick, and should cause a minimum amount of disruption to the power system [8].

2.10.1 CT & VT

The function of CT and VT, or transducers, is to transform power system currents and voltages to lower magnitudes and to provide galvanic isolation between the power network and the relays and other instruments connected to the transducer secondary windings [8].

The transducers must be designed to tolerate higher values for abnormal system conditions. Thus, CTs are designed to withstand fault currents for a few seconds, while VTs are required to withstand power system dynamic overvoltages of the order of 20% above the normal value almost indefinitely, since these types of overvoltage phenomena may last for long durations [8].

CTs are magnetically coupled, multi-winding transformers, while the VTs, in addition to the magnetically coupled VT, may include a capacitive voltage divider for higher system voltages. In the latter case, the device act as a coupling capacitor voltage transformer (CCVT), and when the transformer primary winding is directly connected to the power system is known as a VT. CTs and VTs may be freestanding devices, or they may be built inside the bushing of some power apparatus with a grounded tank [8].

The function of transducers is to provide current and voltage signals to the relays that are accurate reproductions of the corresponding primary quantities [8].

3 Simulation Model

The grid modelled in this report are based on the data provided from NTE in K.Sjøholts [1]. The model is constructed in the power system analysis tools from DIgSILENT PowerFactory. The one-line diagram of the grid is shown in Appendix A.

The purpose of the simulation model is to study the damping properties of the network, when subjected to the open conductor fault that occurred the 7th of March 2008, where the aim is to find the main factors that influence the oscillations that occurred.

3.1 Network topology

The power system grid of question is a 66kV grid in the supply area of NTE which is in Nord-Trøndelag county. The simulation model consists of generation- and load nodes. The external grid is connected to node NamsosT1. The network model is constructed after NTEs real network topology which consists of five hydro power plants, including a total of eight generators, a total number of eight load nodes, two capacitor banks and an external grid which is Namsos. The network topology is shown in Appendix A.

3.2 DIgSILENT PowerFactory

The calculation program PowerFactory by DIgSILENT is a computer aided engineering tool for the analysis of transmission, distribution, and industrial electrical power systems. PowerFactory is designed as an integrated engineering tool to provide a comprehensive suite of power system analysis functions within a single executable program [9].

3.2.1 The DIgSILENT synchronous machine

The Technical Reference Document Synchronous Machine [10] provides a detailed description load flow analysis and transient analysis in PowerFactory, and it describes all the equations implemented in PowerFactory for synchronous machines. The equivalent circuits of the synchronous machine models used in the network model is found in Appendix J. The generator data in the network model can be found in Appendix F to I.

3.2.2 DIgSILENT load modelling

The PowerFactory General Load model is constructed to represent either a complete feeder, or a combination of dynamic and static loads [11]. The load model used in the network model is chosen as a balanced load.

The load models used in the network model found in Appendix J. The load nodes in the network model is modelled as a impedance load for active and reactive power to replicate the real world network.

3.2.3 External grid

The PowerFactory External Grid Element is used to represent external networks. The element is modelled as a voltage source with an internal impedance and the mechanical equations are

as for synchronous machine [12]. The SL type used in the network model. In Appendix J, the different types of external grid models are explained.

The external grid is in the network model chosen as a SL type. This is done to calculate the oscillations that occur during an open conductor fault event. The minimum short circuit capacity of the external gird is set to be 2000 MVA, since it is assumed to represent close the real short circuit capacity based on modified judgement from reference [13], as the short circuit capacity is assumed to be less in the middle of Norway.

3.2.4 *Overhead Lines Systems*

PowerFactory handles both DC and AC lines, including all phase technologies (3ph, 2ph and single phase), with/without neutral conductor and ground wires, for both single circuit and mutually coupled parallel circuits [14].

The document Technical Reference Overhead Line Models [14] provides a detailed description of all available line models for both the steady-state and the transient simulations. The details of the line constant calculation function, is found in Technical Reference Overhead Line Constants [14].

Figure 24 show the equivalent circuit of the three-phase line used in the network model.

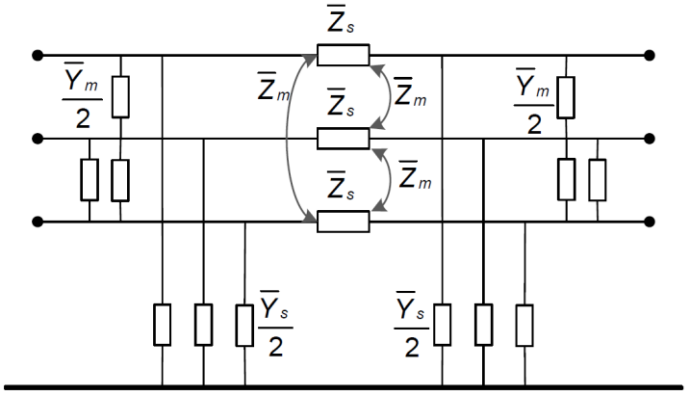

Figure 24: DIgSILENT three-phase line model [13].

The input parameters in the line type are defined in terms of positive and zero sequence impedances and admittances Z1; Y1; Z0 and Y0. The negative sequence is assumed to be equal to the positive sequence [14]. The current limits are chosen base on reference [15].

3.2.5 *The DIgSILENT two-winding transformer*

The DIgSILENT two-winding transformer model is a very detailed model for various kinds of three-phase, two-winding transformers in power systems.

Figure 25 show the positive-sequence model with impedances. It contains the leakage reactances and the winding resistances of the HV and LV side and the magnetization reactance and the iron loss admittance close to the ideal transformer [16].

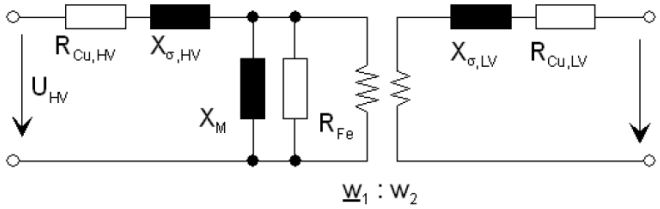

Figure 25: Positive and negative sequence two-winding transformer model [14].

The Technical Reference Document Two-Winding Transformer [16] provides detailed explanation of the two-winding transformer.

3.2.6 Capacitor banks

The capacitor banks in the network model are connected to the 22 kV side of node Saltbotn and Steinkjer. They are both 1 MVAr in size. The Technical Reference Document SVS – Static Var System provides detailed explanation of the capacitor banks [17].

3.2.7 Control systems & regulators

The control regulator modelled for AVR and turbine governor used in the model are modelled after the model in K.Sjøholts [1] thesis, since it is modelled to represent the real world AVR. The block diagram of the AVR and turbine governor in PowerFactory is described in Appendix J. The AVR and turbine governor is implemented on all the connected generators in the network model.

3.3 Load flow analysis

To verify the network model constructed in PowerFactory, load flow analysis was conducted and the result compared to the network model in K.Sjøholts report. As the data input in the model constructed in PowerFactory is the same as the data used in K.Sjøholts [1] model.

The results from the load flow analysis is almost identical to the load flow analysis in K.Sjøholts [1] report. There are some minor differences in reactive and active power flows. It is presumed that the reason is because there are differences between the power system analysis programs calculation methods incorporated in the programs, as discussed in the specialization report [18]. The load flow of the network model in representative of the actual load flow prior to the open conductor fault event that occurred, and the properties on the network model is comparable to the real world network. The power flows can be found in Appendix D.

3.4 Simulation case description

All the open conductor fault events is simulated by opening of phase a in the circuit breaker on the line Skogmo-NFK. This is done to re-enact the event that happened 7th of March 2008 in simulations according to the actual fault and to study the influence different regulator settings have regarding damping. The fault event is triggered at t = 0,5 seconds for all simulation cases. The different cases are listed below.

1 Base Case open conductor fault

2 Open conductor fault with EXAC4 AVR modified settings
3 Open conductor fault with adjusted turbine governor settings
4 Open conductor fault without regulators
5 Symmetrical fault with actual regulators and reclosing of CB
6 Base Case open conductor fault with reclosing of CB
7 Symmetrical fault with modified regulators and reclosing of CB
8 Open conductor fault with modified regulators and reclosing of CB

In case 5 to 8 the CB is reclosed after 100 milliseconds after the fault is triggered. The simulations are done to comparatively analyse different the damping in different fault cases when the network is excited by a fault.

3.4.1 The Base Case dynamic simulation comparison

Simulating the open conductor fault by opening of CB in phase a at node Skogmo66 at t = 1 second and reclosing of CB at t = 14 seconds, to compare and verify the network model to the real network and to the network model in K.Sjøholts report which is representing the actual network. When comparing the plot result of the generator in NFK, Figure 26 show almost identical behaviour of the generator in the two different power system analysis programs, as concluded in the specialization project [18].

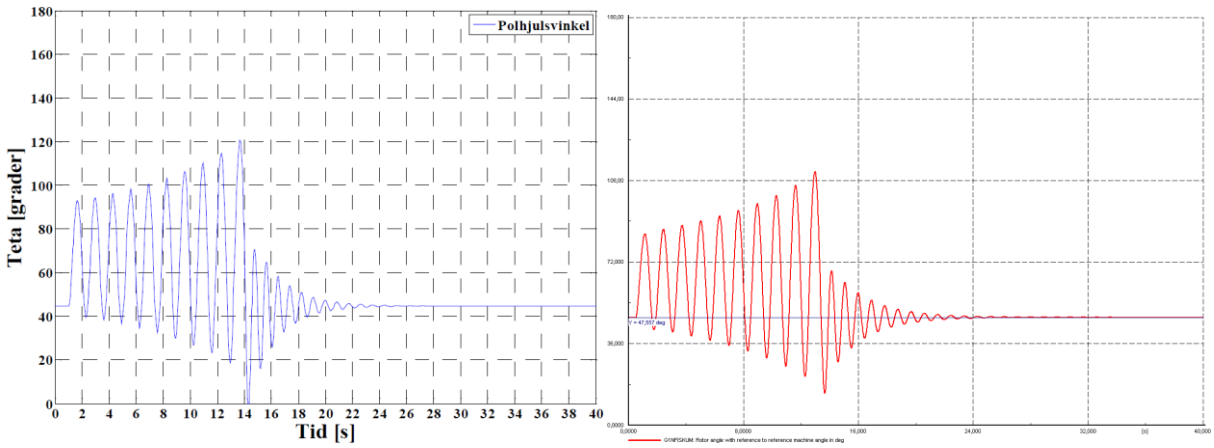

Figure 26: Rotor angle of G1 in NFK from K.Sjøholt [1] to the left and Rotor angle G1NFISKUM to the right.

4 Simulation results

The simulations are based on the event that happened the 7th of March 2008, where a conductor, carrying load suddenly faulted, causing an open-conductor condition. This resulted in uncontrolled speed and power oscillations in the generators in the hydro power plant NFK.

4.1 Base case open conductor fault

The rotor angle and active power plots from the simulation result shows that the generators in NFK start to oscillate with a period of 1,2 seconds after the fault event is triggered. The magnitude of the oscillations are increasing continuously and the generators will after a fault time of 16 seconds start to oscillate uncontrollably.

The simulation result show that it is insufficient damping torque to establish a new operating point of the generators in NFK, and the damping ratio is thus negative. Figure 27 and 28 show G1NFISKUM rotor angle plot and active power plot

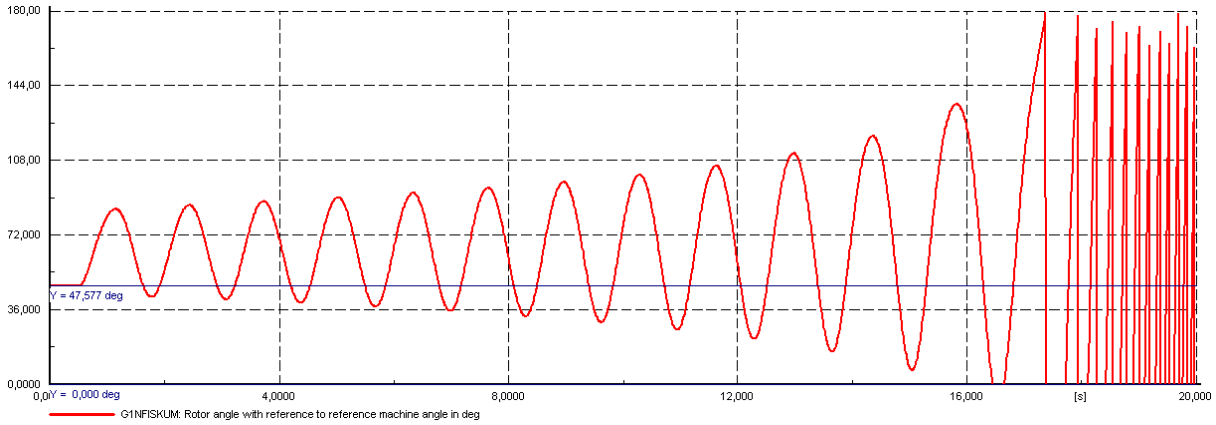

Figure 27: G1NFISKUM rotor angle plot with Base Case regulators.

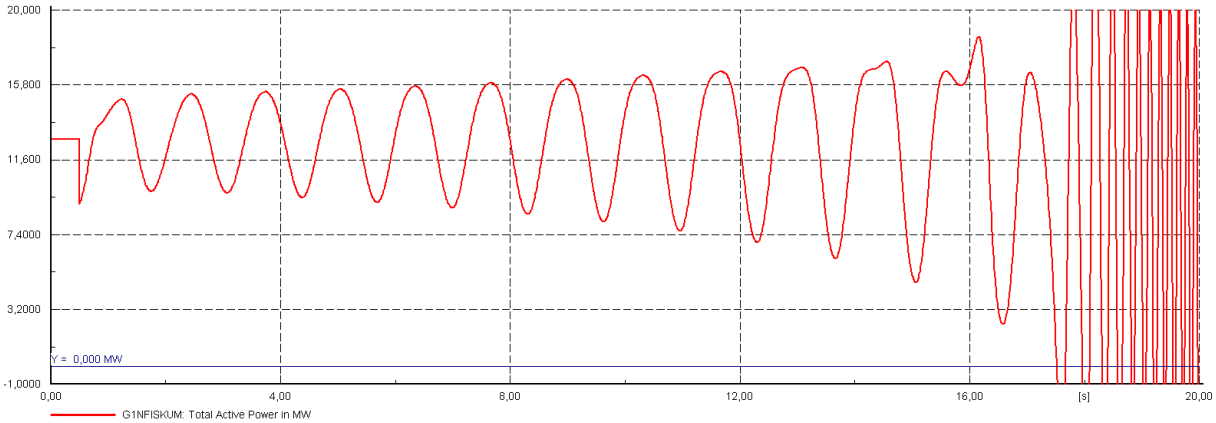

Figure 28: G1NFISKUM active power plot with Base Case regulators.

4.2 Open conductor fault with EXAC4 AVR modified settings

The open conductor fault is simulated with modified settings on the AVR to determine if the network is able to reach a steady state operating point. The parameter modifications is done based on references [6] and [19]. The AVR parameter settings are given in Appedix J.

The AVR parameter settings were chosen after the not so very scientific method of “try and see if this works” method. After a series of different parameter adjustments, a parameter configuration that performed amicable and deemed appropriate was implemented. It is not verified if the applied settings are accessible for modification on the actual regulators.

The simulation result show that the rotor angle oscillations, with a period of 1,27 seconds, during open conductor fault are damped and the oscillations are damped out after 35 seconds. The new operation point is established around 64 degrees relative to the external grid. Figure 29 show the rotor angle oscillations during open conductor fault.

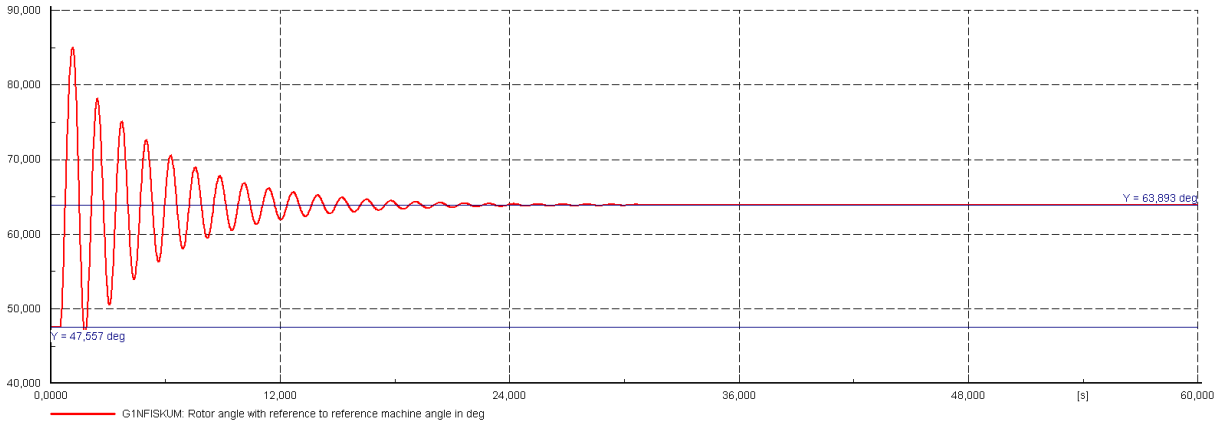

Figure 29: G1NFISKUM rotor angle plot with modified AVR settings and Base Case turbine governor settings.

The rotor oscillations can be expressed as a damped sinusoidal wave, and from Figure 30, the oscillation period

$$\tau_d = 3{,}717 - 2{,}443 = 1{,}274[s].$$

The logarithmic decrement of a damped sinusoidal wave [20] [21]

$$\delta = ln\left(\frac{u_{t1}}{u_{t2}}\right), \tag{4.1}$$

where $u_{t1} = 84{,}045$ and $u_{t2} = 78{,}160$.

$$\delta = ln\left(\frac{84{,}045}{78{,}160}\right) = 0{,}0726$$

The damping ratio

$$\zeta = \frac{1}{\sqrt{1 + \left(\frac{2\pi}{\delta}\right)^2}} \tag{4.2}$$

and $\zeta = 1{,}155\,\%$ for the first oscillation period during open conductor fault at node 66Skogmo.

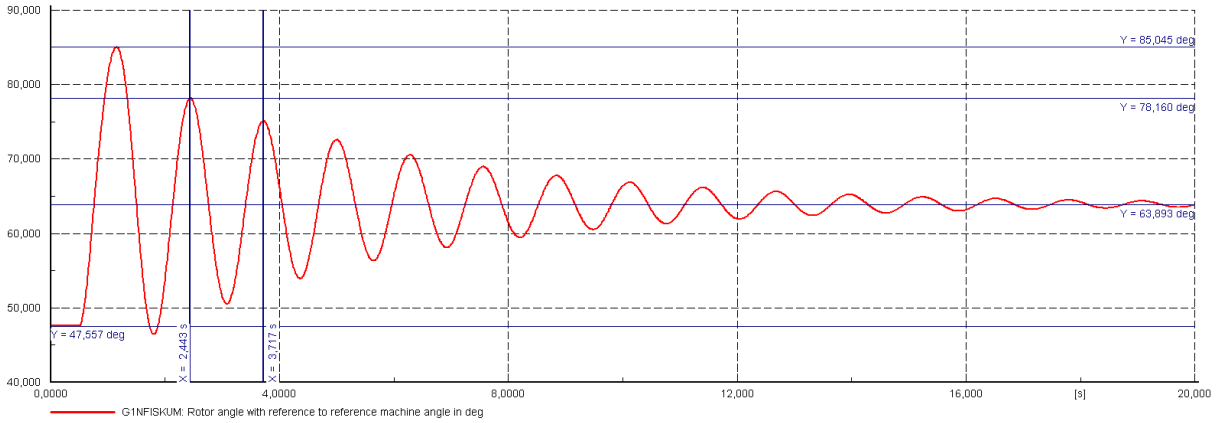

Figure 30: G1NFISKUM rotor angle plot with modified AVR settings and base case turbine governor settings.

Although simulation result show that the rotor oscillations are damped, it is not verified if the implemented settings are exact, since the voltage regulators implemented on the actual generators are old and are modelled after generator performance and behaviour.

4.3 Open conductor fault with adjusted turbine governor settings

The open conductor fault is simulated with tuned settings on the turbine governor to determine whether it can provide net positive damping torque. The parameter modifications is studied and adjusted based on references [24] to [32]. The chosen turbine governor parameter settings is found in Appendix J.

The parameter settings was again chosen after the not so very scientific method of “try and see if this works” method. After a series of different parameter adjustments, a parameter configuration that was deemed appropriate was implemented. It is not verified if the applied settings are accessible for modification on the actual regulators.

The result show that the rotor angle oscillations during open conductor fault base case AVR implemented have a negative damping ratio. The frequency and magnitude of oscillations are almost identical to the simulation result of the network model with the base case turbine governor. Figure 31 show the rotor angle oscillations during open conductor fault.

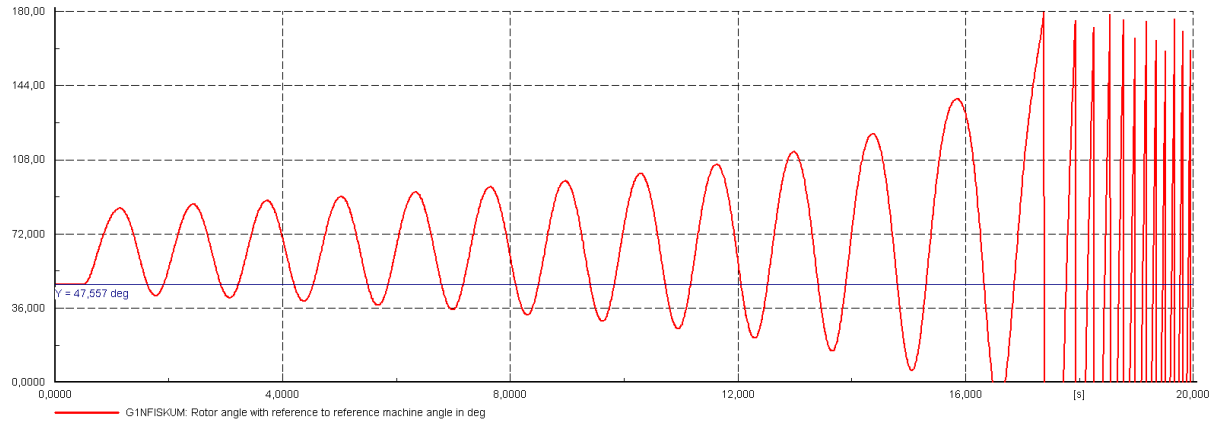

Figure 31: G1NFISKUM rotor angle plot with modified turbine governor settings and Base Case AVR settings.

4.4 Open conductor fault with adjusted turbine governor and AVR settings

Figure 32 show that the rotor angle oscillations during open conductor fault with modified AVR settings, where it has a positive damping ratio. The oscillations are completely damped after 35 seconds and the new operation point is established around 64 degrees relative to the external grid. The frequency and magnitude of oscillations are identical or almost identical to the simulation result in chapter 4.2.

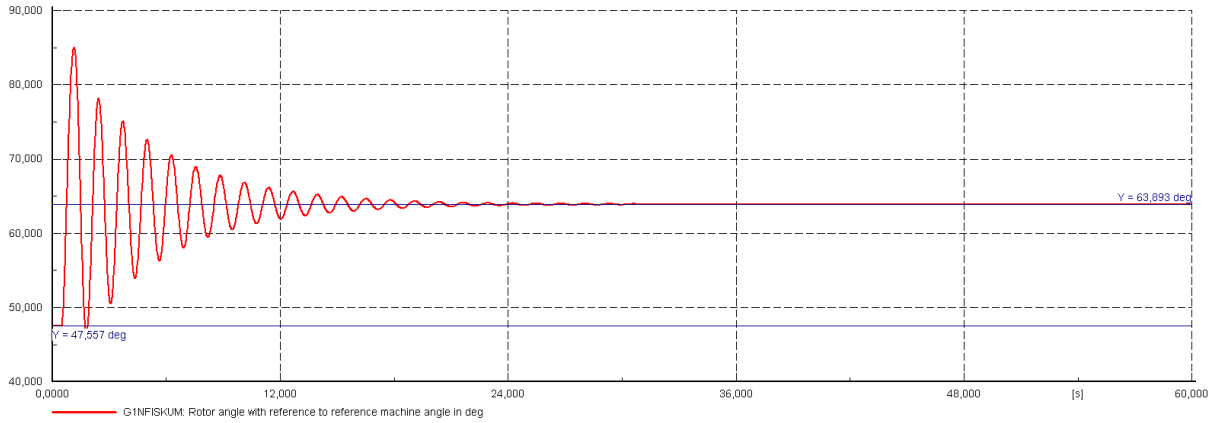

Figure 32: G1NFISKUM rotor angle plot with modified AVR and turbine governor settings.

4.5 Open conductor fault without regulators

The open conductor fault is simulated without any controls to visualise the natural oscillation frequency and damping ratio. The simulation result show that the frequency of oscillations is around 1,4 seconds. The transient oscillations in the network model are damped, but the generator is unable to establish a new steady state operating point, and the rotor angle is continuing to diverge until synchronous operation is lost and the generator starts to oscillate uncontrollably.

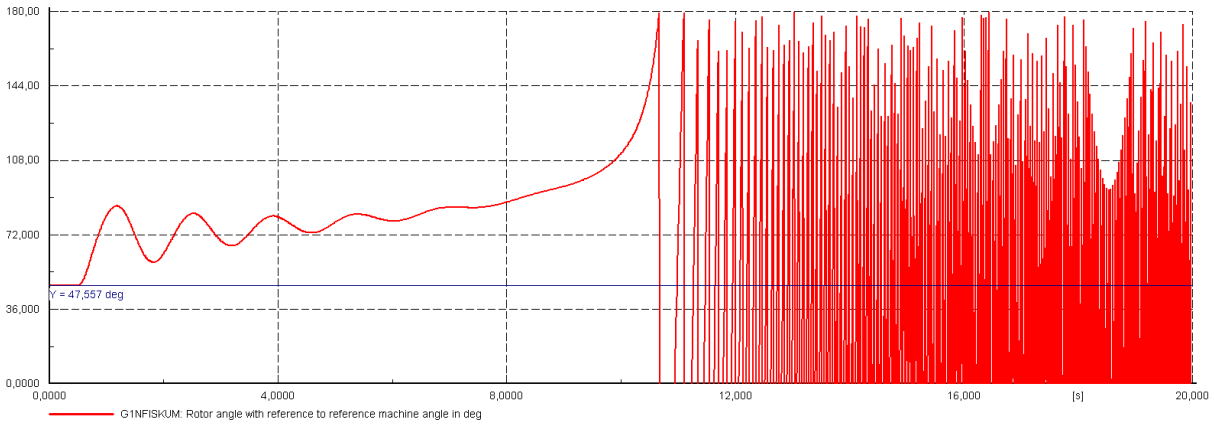

Figure 33: G1NFISKUM rotor angle plot without any regulator incorporated.

4.6 Symmetrical fault with actual regulators and reclosing of CB

The fault event is triggered at t = 0,5 s. Figure 34 show the simulation result.

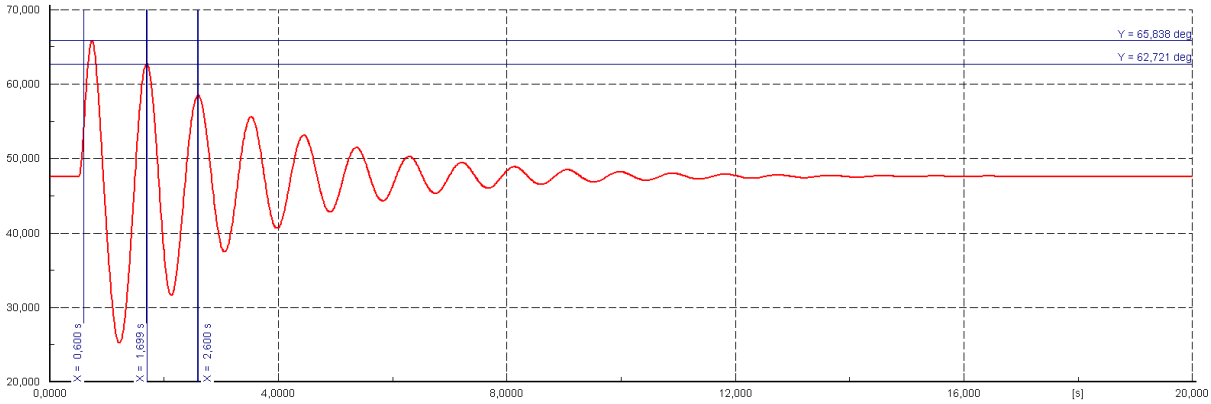

Figure 34:G1NFISKUM rotor angle plot with actual AVR and turbine governor settings.

The rotor oscillations can be expressed as a damped sinusoidal wave, and from Figure 34, the oscillation period

$$\tau_d = 2{,}6 - 1{,}699 = 0{,}901\ [s].$$

$$\delta = ln\left(\frac{65{,}838}{62{,}721}\right) = 0{,}0485$$

and the damping ratio $\zeta = 0{,}772\ \%$ for the first oscillation period after the symmetrical three-phase short circuit fault is reset.

4.7 Base Case open conductor fault with reclosing of CB

The fault event is triggered at t = 0,5 s. Figure 35 show the simulation result.

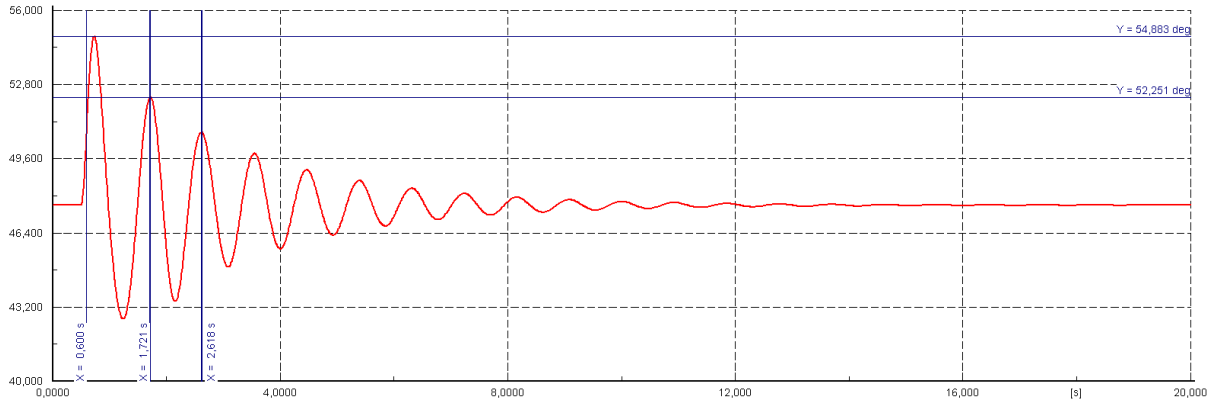

Figure 35: G1NFISKUM rotor angle plot with actual AVR and turbine governor settings.

The rotor oscillations can be expressed as a sinusoidal wave, and from Figure 35, the oscillation period

$$\tau_d = 2{,}618 - 1{,}721 = 0{,}897\ [s].$$

$$\delta = ln\left(\frac{54{,}883}{52{,}241}\right) = 0{,}049$$

and the damping ratio $\zeta = 0{,}782\ \%$ for the first oscillation period after the open conductor fault is reset.

4.8 Symmetrical fault with modified regulators and reclosing of CB

The fault event is triggered at t = 0,5 s. Figure 36 show the simulation result.

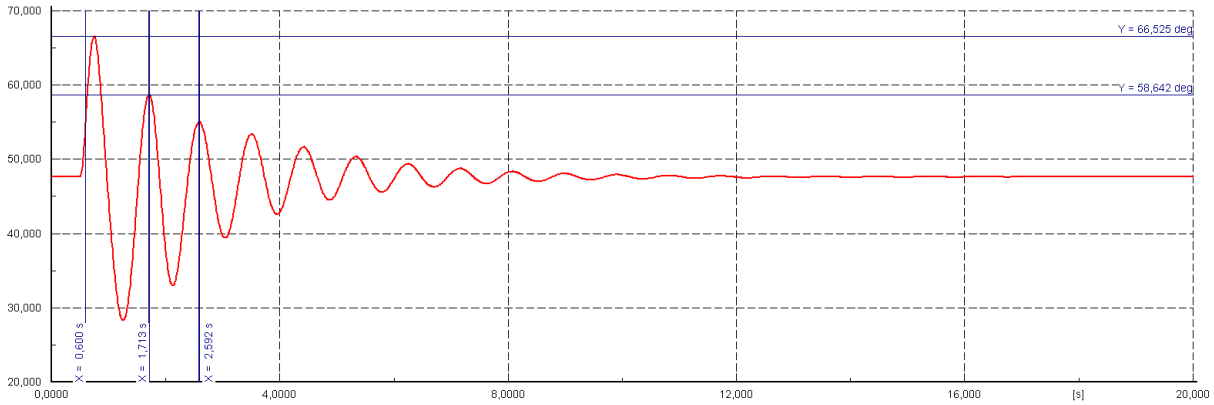

Figure 36: G1NFISKUM rotor angle plot with modified AVR and turbine governor settings.

The rotor oscillations can be expressed as a sinusoidal wave, and from Figure 36, the oscillation period

$$\tau_d = 2{,}592 - 1{,}713 = 0{,}897\ [s].$$

$$\delta = ln\left(\frac{66{,}525}{58{,}642}\right) = 0{,}226$$

and the damping ratio $\zeta = 2\ \%$ for the first oscillation period after the symmetrical three-phase short circuit fault is reset

4.9 Open conductor fault with modified regulators and reclosing of CB

The fault event is triggered at t = 0,5 s. Figure 37 show the simulation result.

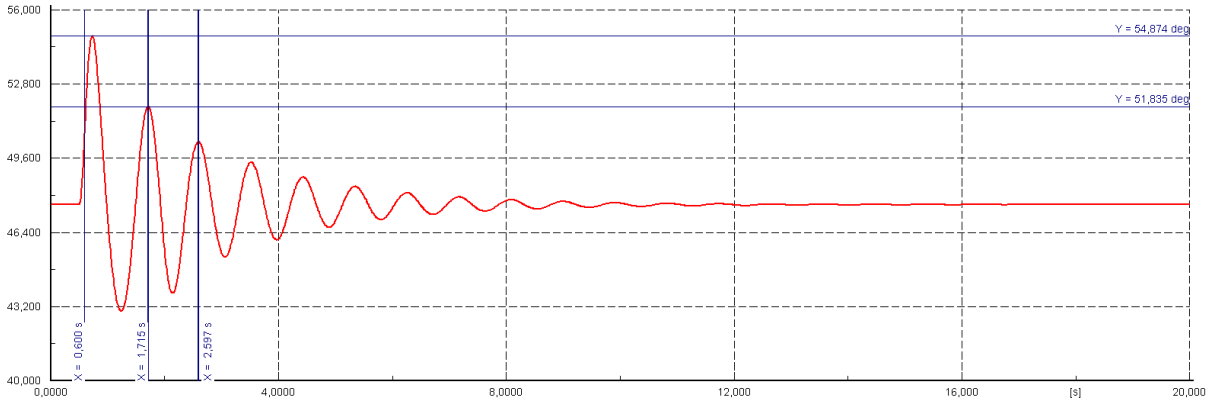

Figure 37: G1NFISKUM rotor angle plot with modified AVR and turbine governor settings.

The rotor oscillations can be expressed as a sinusoidal wave, and from Figure 37, the oscillation period

$$\tau_d = 2{,}597 - 1{,}715 = 0{,}882\ [s].$$

$$\delta = ln\left(\frac{54{,}874}{51{,}835}\right) = 0{,}057$$

and the damping ratio $\zeta = 0{,}91\ \%$ for the first oscillation period after the open conductor fault is reset.

4.10 Discussion of dynamic simulation results

The simulation results show that the network model reproduces the open conductor fault case that occurred in the power system network of NTE. The result from the transient simulation in the base case show that the generators in NFK start to oscillate, and that the oscillations are underdamped.

The base case scenario is simulated again with modified control parameter settings on the AVR and turbine governor to study if the transient response can be improved by adjusting the parameters. The dynamic simulations show that the underdamped oscillations in the Base Case can be “forced” into damped oscillations by adjusting parameter settings in the AVR, and the network is able to maintain operation. The input parameters is not verified to be achievable when compared to the parameters in the actual AVR, and can thus be said to unrealistic if the parameters are not adjustable. The turbine governor is unable to enhance damping by itself when the parameter settings are modified.

It is observed from the transient plots from the base case simulation that the oscillation period is 1,2 seconds, which is in the electromechanical area of oscillations [4] [6]. The same oscillation period is observed when the modified AVR is implemented. The oscillation period without any control regulators is 1,4 seconds.

The dynamic simulation results show that the settings on the AVR and turbine governor have an impact on the network stability when the outcome is whether the network is able to establish a new operating point of operation, or not, after an open conductor fault.

To study the control regulators impact on the generator, a transient simulation without any control regulators is conducted. The simulation result show that the rotor angle is unable to stabilize. The plot result show that the oscillations are damped but lack of synchronizing torque, as presented in Chapter 2.7, is a contributing factor to why the generator is unable to establish steady state operation in the simulation.

Simulations of different fault cases is conducted to compare the damping properties. The oscillation period is observed to be 0,9 seconds when the CB is reclosed. The network is subjected to symmetrical three-phase short circuit and open conductor fault, each for a duration of 100 milliseconds, at node Skogmo. The simulations are don with actual regulators and with modified regulators to compare the different fault types and the influence of the regulators. The simulation in question are Case 5 to 8.

The results show that the damping ratios with actual regulators are similar, were the damping ratios for the first swing during symmetrical short circuit- and open conductor fault are 0,77 %and 0,78 %, respectively. The results show that the damping ratios with modified regulators are different, were the damping ratios for the first swing during symmetrical short circuit- and open conductor fault are 2 %and 0,91 %, respectively.

The actual regulators are implemented in Case 5 and 6, and the results show that it is a marginally difference in damping when comparing the results between symmetrical- and open conductor fault.

The results from Case 7 and 8 show a difference of almost 1,1 % in damping, when comparing the two fault cases, where the symmetrical fault case was better damped compared to the open conductor fault.

The results show improved damping ratio with modifications of the parameter settings on the regulators compared to the actual regulators. This indicates that the regulators, especially the AVR, have significant influence on the network stability.

4.11 Eigenvalue Calculation in PowerFactory

The eigenvalues for the base case network is in PowerFactory calculated by the modal analysis calculation option [9]. PowerFactory modal analysis explanation is given in Appendix J. The modal analysis command calculates the eigenvalues and eigenvectors of a dynamic multi-machine system including all controllers and power plant models. This calculation is conducted at the beginning of a transient simulation and at every time step when the simulation is stopped. Note that sometimes in the literature (ie. Machowski et al. [4], Kundur [6]) modal analysis is referred to as linear analysis or small signal stability.

A modal analysis can be started when a balanced steady-state condition is reached in a dynamic calculation. Normally, such state is reached by a balanced load-flow calculation, followed by a calculation of initial conditions. However, it is also possible to do a balanced RMS simulation and start a modal analysis after the end of a simulation or during a simulation when you have manually stopped it. Although, the modal analysis can be executed at any time in a transient simulation it is not recommended that you do so when the system is not in a quasi-steady state. This is because each modal analysis is only valid for a unique system operating point [9].

4.11.1 Eigenvalue calculation of base case network

The eigenvalues plot show all the different modes inherent in the network. The modal analysis is calculated prior to the open conductor fault event to visualize the expected response of the network when a fault is triggered. The eigenvalues plot is shown in Figure 38.

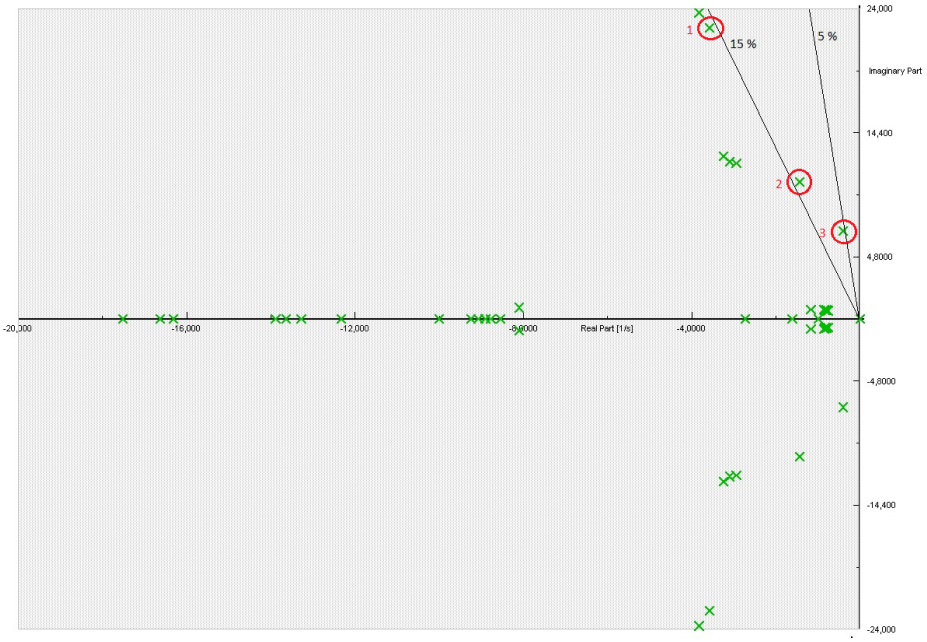

Figure 38: Eigenvalue plot with inserted damping ratio boundaries.

From the plot above, the following eigenvalues are listed:

Mode nr.	Re [1/s]	Im [Hz]	Im [Rad/s]	Damping Ratio
1	-3,5805	3,586432	22,53422	0,1569232
2	-1,438651	1,68863	10,60998	0,1323188
3	-0,3993517	1,108739	6,815615	0,05849332

4.11.2 Eigenvalue calculation of base case network with modified AVR

The eigenvalues plot show all the different modes inherent in the network. The modal analysis is calculated prior to the open conductor fault event to visualize the expected response of the network when a fault is triggered. The eigenvalues plot is shown in Figure 39.

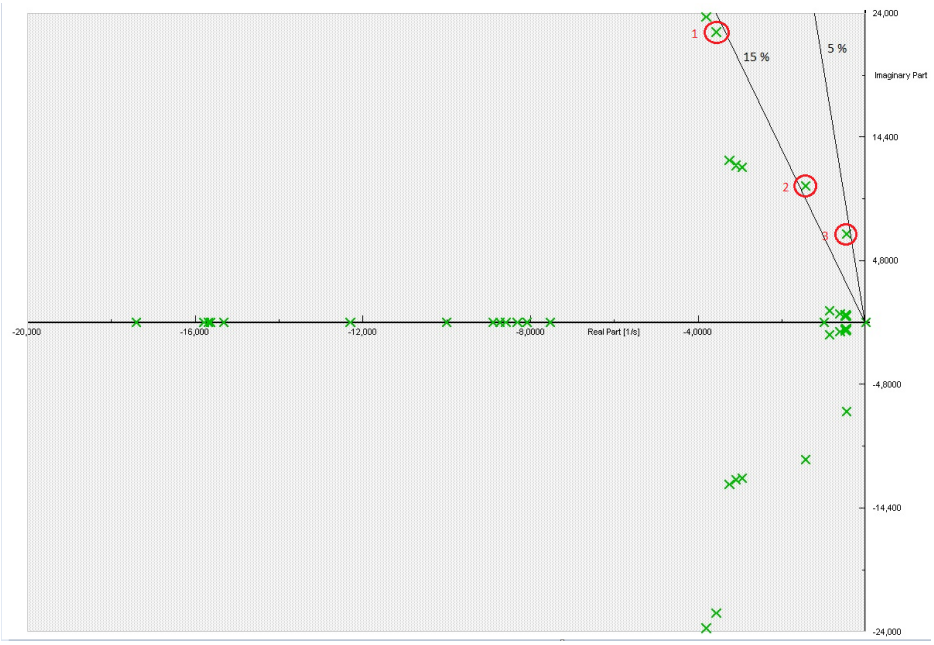

Figure 39: Eigenvalue plot with inserted damping ratio boundaries.

From the plot above, the following eigenvalues are listed:

Mode nr.	Re [1/s]	Im [Hz]	Im [Rad/s]	Damping Ratio
1	-3,568497	3,588442	22,54685	0,1563245
2	-1,43375	1,689921	10,61809	0,1337803
3	-0,4647629	1,095733	6,884691	0,06736343

4.11.3 Eigenvalue calculation of base case network without regulators

The eigenvalues plot show all the different modes inherent in the network. The modal analysis is calculated prior to the open conductor fault event to visualize the expected response of the network when a fault is triggered. The eigenvalues plot is shown in Figure 40.

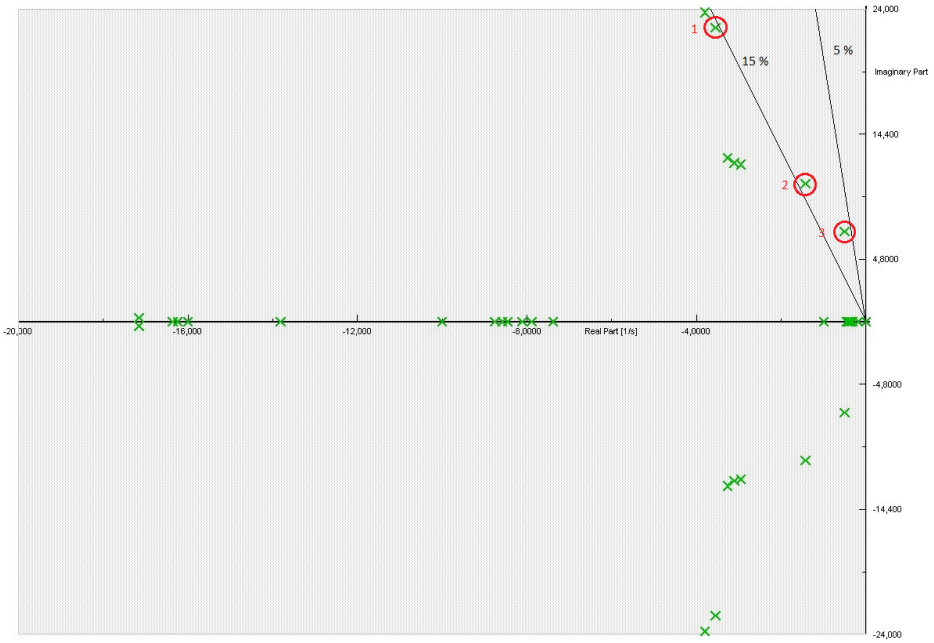

Figure 40: Eigenvalue plot with inserted damping ratio boundaries.

From the plot above, the following eigenvalues are listed:

Mode nr.	Re [1/s]	Im [Hz]	Im [Rad/s]	Damping Ratio
1	-3,556454	3,592739	22,57384	0,1556454
2	-1,429883	1,691383	10,72304	0,1333469
3	-0,5074893	1,1065	6,952342	0,07280175

4.11.4 Discussion of eigenvalue calculations.

From the eigenvalue calculations in PowerFactory at the initial operating conditions, the eigenvalue plot above shows that the least damped oscillation mode for the base case is calculated to have a damping ratio of 5,58% for mode 31 which is the least damped node. The oscillation period is calculated to be 0,9 seconds, which is slightly different compared to the oscillation frequents observed in chapter 4.1, where the oscillation period is observed to be 1,2 seconds.

In the eigenvalue calculation of the network in base case with modified AVR settings, the least damped mode is calculated to have a damping ratio of 6,74%, which is a better result

compared to the actual base case. In the eigenvalue-calculation of the network without any control regulators the least damped node have a damping ratio of 7,28 %. The oscillation period of Mode 3 is 0,9 seconds in the three calculations. This oscillation period is also observed in the dynamic simulation cases 5 to 8.

The initial calculations indicate that the network is supposedly able to establish a steady state operating point after a fault although experience has shown that the network is not able to maintain stable operation after open conductor fault. It is noted that eigenvalue calculation give valid results when the whole network is symmetrical and is calculated at a defined point of operation. When the open conductor fault occurs, the network topology and the operating conditions changes and the eigenvalue calculation prior to the fault is no longer an accurate expression of the state of the network. This is the limitation of the eigenvalue calculation/modal analysis when studying dynamic attributes of a power system.

If the network is unable to establish a stable operating point after the fault, accurate calculation is not possible if the network when it is experiencing transient oscillations as happened to the power system network of NTE. As the network is unable to establish stable operation after the fault, it is not applicable to use eigenvalue calculation/modal analysis on the network for open conductor fault analysis.

PowerFactory are unable to compute the modal analysis of the network when open conductor fault is studied. The inbuilt setup of program requires the simulation to the executed with a balanced load flow, and when studying unbalanced conditions such as a missing phase, the program is unable to provide adequate results that accurately analyse such faults.

It is noted that the excitation systems are observed to have negative influence on stability when conducting modal analysis of Mode 3 when the network is symmetrical. It is not verified that the excitation systems are influencing Mode 3 in open conductor fault conditions since the oscillation period is different, however, it is assumed that it can be a possibility that the oscillation period is changed when the network is subjected to open conductor fault conditions where Mode 3 “shifts” oscillation period, but this is speculations only. Modal analysis is found in Appendix K.

5 Laboratory experiments

The purpose of the laboratory experiments are study the open conductor phenomena and to re-enact the open conductor fault event that happened the 7th March 2008 if possible. This chapter describes the laboratory test setup and the equipment in the laboratory experiments.

5.1 Test setup

The laboratory tests of open conductor fault where performed in the test laboratory at NTNU. The equipment used for the experiments are property of NTNU, and are used for laboratory experiments for employees and students at NTNU. The test setup shown in Figure 41. Pictures of the laboratory setup is found in Appendix L. For simulating an open conductor fault, a separate contactor has been installed to achieve the properties of an open conductor fault. The measurement equipment are provided from SINTEF Energy Research.

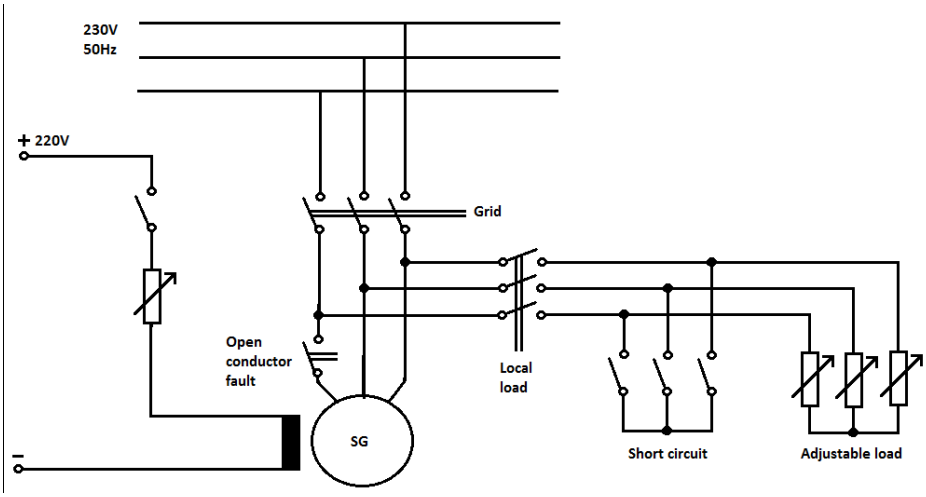

Figure 41: Circuit diagram of laboratory test setup.

The measurement probes for voltage and current are placed as close as practically possible to the synchronous machine. Figure 42 show the schematic placement of the measurement probes used in the laboratory experiments.

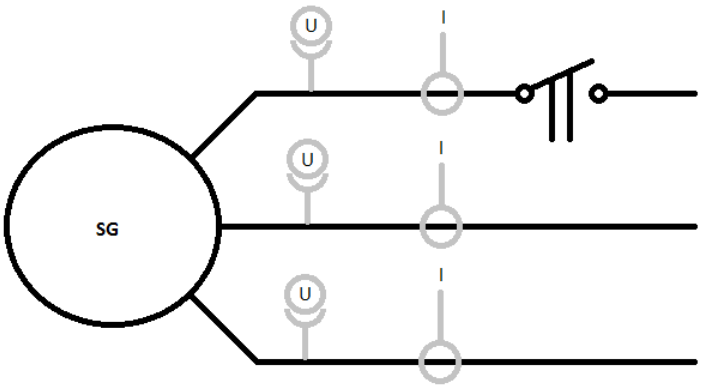

Figure 42: Elspec measurement configuration.

5.1.1 *The Elspec Blackbox*

The G4000 BLACKBOX Power Quality Analyser calculates RMS, harmonics, and all desired values from waveforms in post-processing. The logged data from multiple units are synchronized and displayed on the same time scale with typical 0.1ms resolution [22].

Figure 43 and 44 shows the component identification with physical description and the test setup in laboratory.

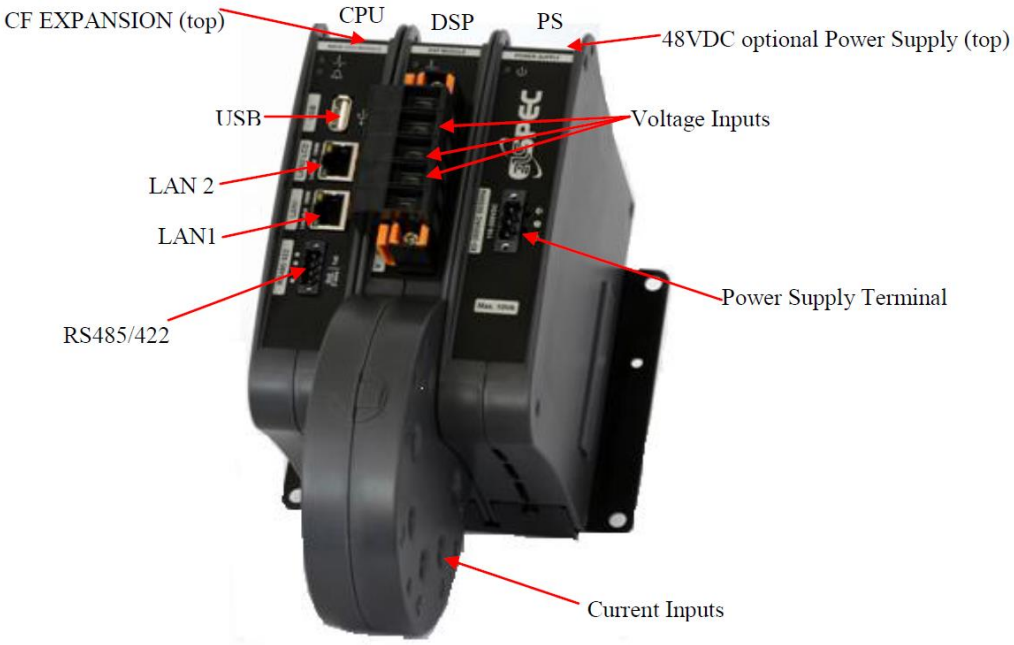

Figure 43: The Blackbox with connection descriptions [22].

Figure 44: The Elspec Blackbox installed in laboratory.

5.1.2 *Wiring configuration*

Connections to a low voltage network require three current transformers. Voltage connections are direct, where overvoltage protection is optional, as shown in Figure 45. The current measurement loops are coupled via current transformers with a 100/5 A ratio. Figure 46 show the CT used in the experiments.

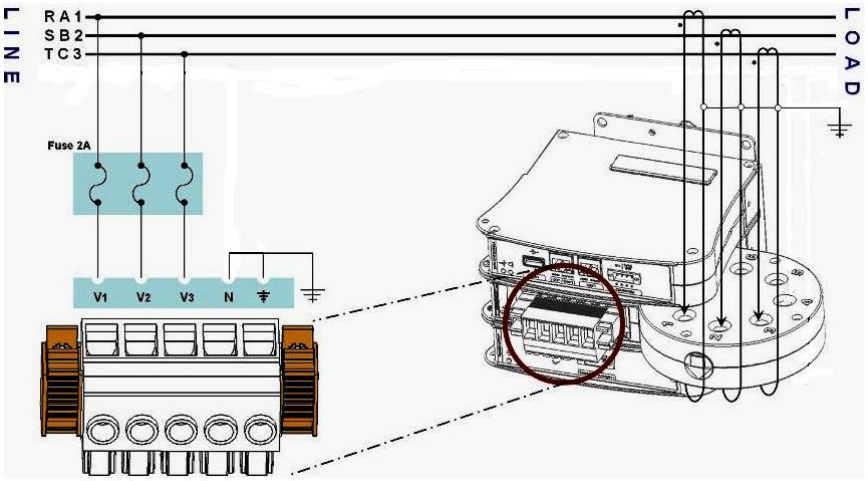

Figure 45: Low voltage 3 wire delta configuration [22].

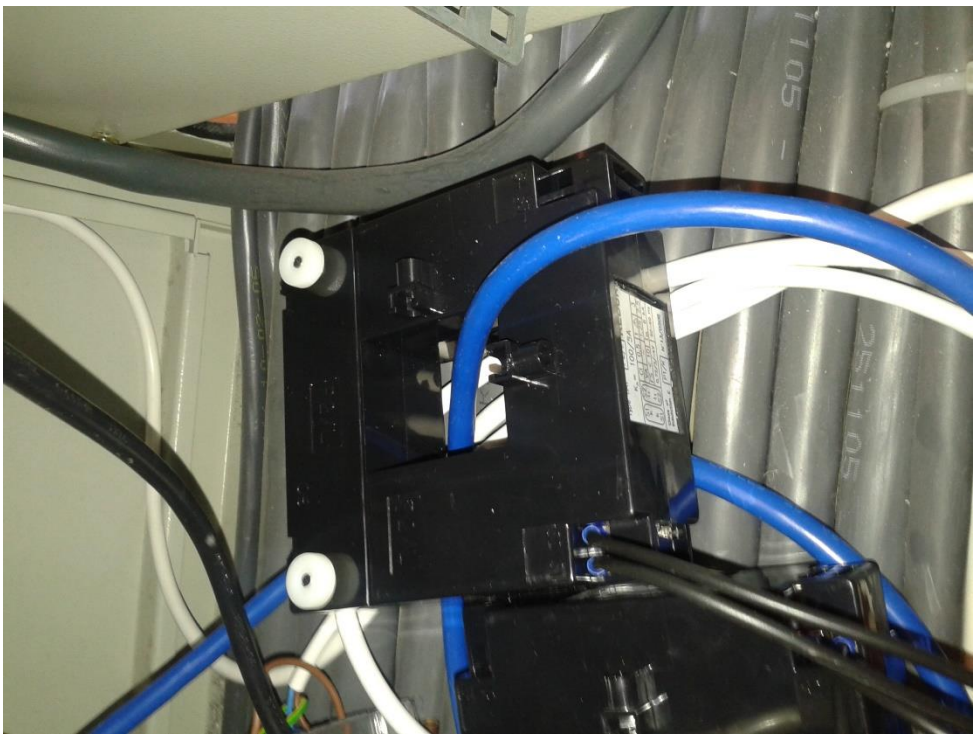

Figure 46: 100/5A current transformer. Property of SINTEF Energy Research.

5.1.3 *The open conductor fault*

The open conductor fault condition was triggered using a contactor as a switch to break the current path to the synchronous machine one of the phases. The requirements for the contactor was that it must be able to break the current at nominal power of the synchronous machine, and that the insulation was able to withstand the rated voltage of the synchronous

machine. A laboratory technician at NTNU installed and tested the contactor setup. Figure 47 shows “the open conductor fault”.

Figure 47: “The open conductor fault”.

5.2 Experiments description

The synchronous machine were driven as a generator, feeding power to the external grid. The generator output is set to a steady state condition before the open conductor fault event is triggered. The measurement instruments on the instrument panel are analog, and is considered to be less than exact in regards of presented measurement value. The generator is considered in a steady state condition when the measurement instruments on the instrument panel have established a stable value, and is not fluctuating by large margins.

The active- and reactive effect adjustments were done manually until stable operation was achieved. The open conductor fault event was triggered by opening of phase a by the installed contactor, and the transient phenomena that followed was logged in the Elspec Blackbox.

To access the logged data from the Blackbox, the measurement device had to be physically brought to Mr. H.Kirkeby at SINTEF Energy Research where the logged data was uploaded to a server from which the measurement data could be accessed.

5.2.1 Experiment 1

The generator is driven up to synchronous speed and connected to the external grid. Stable operation is established and the generator is loaded to nominal active power 7,5 kW, and

reactive power 0,5kVAr. The open conductor fault is triggered by the “open conductor fault” and the generator is subjected to an open conductor fault.

5.2.2 Experiment 2

The generator is driven up to synchronous speed and connected to the external grid. Stable operation is established and the generator is active power is kept at 0,5kW, and reactive power 7,5 kVAr. The open conductor fault is triggered by the “open conductor fault” and the generator is subjected to an open conductor fault.

5.3 Limitations

The experiments is limited to experiments of one open conductor fault. Due to time restrictions and complications with establishing stable operation on local load separated from the external grid, experiments on synchronous machine behaviour in local fault cases was not conducted. Three-phase short circuit experiments are not conducted due to challenges in establishing stable operation on local load. The Elspec measurement equipment is property of Sintef Energy Research and are subjected to confidentiality regarding measurements results and measurements data access. The documentation of the laboratory equipment are old and may not exact, though this is not verified.

6 Laboratory results

The initial experiments yielded some unique harmonic- and sequence voltages and currents results. These results were not expected from the experiments. After some troubleshooting it was discovered that the wiring configuration were erroneous, as the earth-wire had lost the connection to the Blackbox. This error was fixed and the experiment was restarted.

The test results were extracted from the Elspec Investigator software, and the plot results from the laboratory experiments are shown in the following subchapter.

6.1 Experiment 1

The experiment was conducted according to the health and safety regulations for work in laboratory environment at NTNU.

The result from the experiment show that the generator power in the faulty phase drops to zero Watts the instant the open conductor fault is triggered. The power in the two remaining phases increase from 2,5 kW to 4,4 kW in phase L2 and 3,7 kW in phase L3 for a total of 8,1 kW in total during the open conductor fault event. The peak magnitude of the active power following the open conductor fault is measured to 10 kW. That implies that the active power in the two remaining phases peak at 5 kW in each of the phase conductors as the active power in the faulty phase drops to zero Watts. The oscillations of the active power is measured to last for 1,5 second. After that time, there are no active power oscillations recorded and the test setup is in stable operation conditions.

At the moment the faulty phase is reconnected, the measurements plot show that the active power peaks at 3,8 kW in phase L1, and all three phases are establishing a stable operating point that is identical to pre-fault conditions within one second. Large plots of Figure 48 are found in Appendix N.

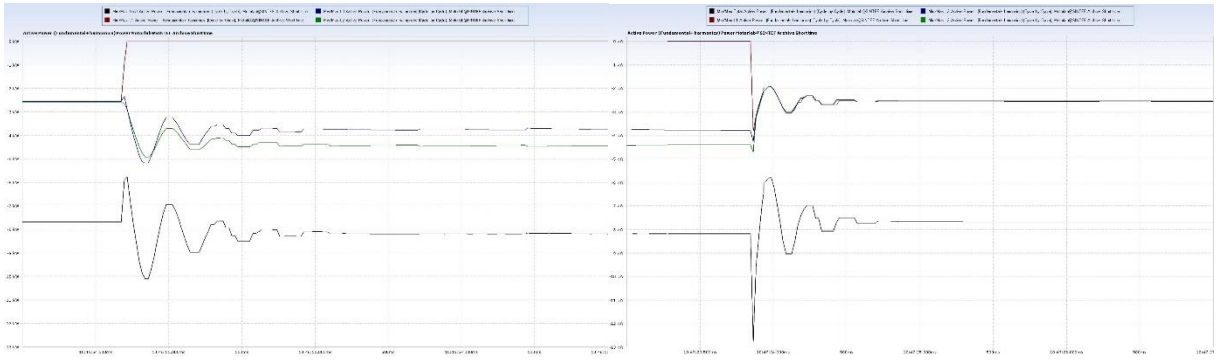

Figure 48: Total- and active phase powers at start and end of open conductor fault experiment, respectively.

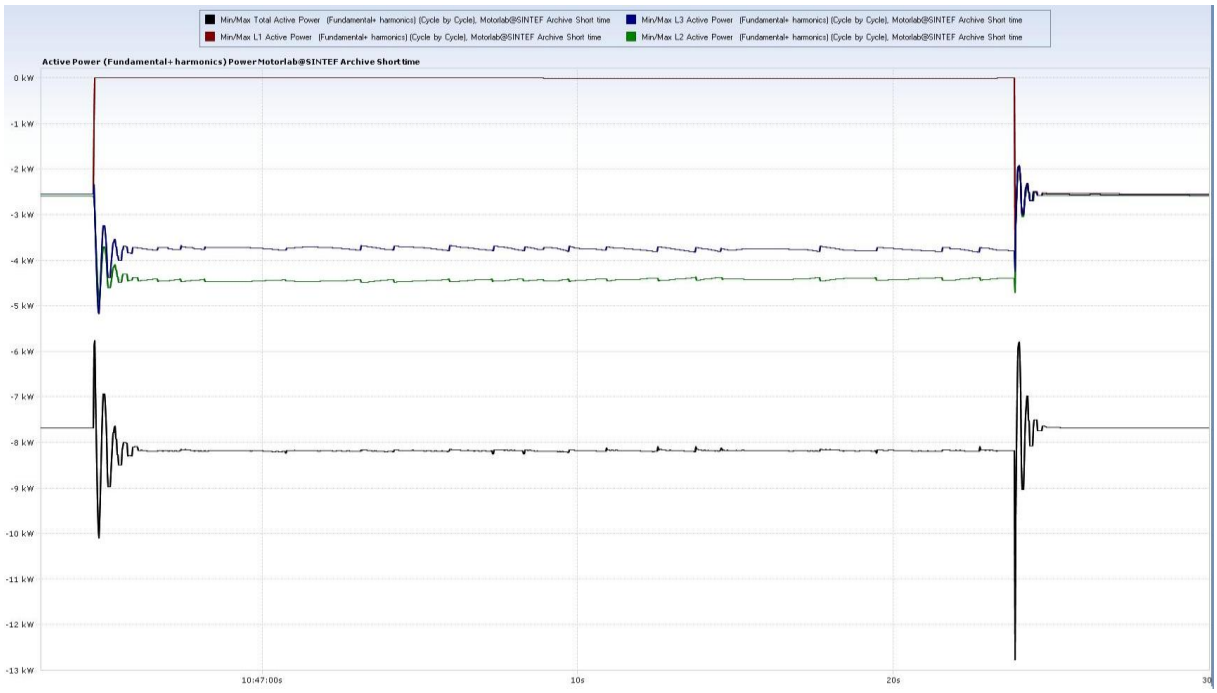

Figure 49: Total- and active phase powers during the open conoductor fault experiment.

6.2 Experiment 2

The experiment were conducted according to the health and safety regulations for work in laboratory environment at NTNU. The result from the experiment show that the reactive power in the faulty phase drops to zero VAr the instant the open conductor fault is triggered. The reactive power in the two remaining phases decrease from 2,5 kVAr to 1,8 kVAr in phase L2 and 2,2 kVAr in phase L3 for a total of 4 kVAr in total during the open conductor fault event. The reactive power generation stabilizes immediately at 4 kVAr following the fault event.

At the moment the faulty phase is reconnected, the measurements plot show that the reactive power establishes a steady state operation point at 2,5 kVAr in phase L1, and all three phases are establishing a stable operating point that is identical to pre-fault conditions immediately with no measured oscillations following the reconnection of the faulty phase.

Figure 50: Reactive phase powers at start and end of open conductor fault experiment, respectivley.

Figure 51: Total- and reactive phase powers during the open conductor fault experiment.

Large plots of Figure 50 are found in Appendix N.

6.3 Discussion of laboratory experiments results

The open conductor fault experiments were carried out without any incidents regarding health and safety. The results from the experiments show that the open conductor fault have an impact on the synchronous generator when it is generating active power and reactive power.

The experiment result of the open conductor fault with the generator loaded at nominal active power shows that the transient oscillations are damped, and the generator establishes a steady operating point during the open conductor fault experiment. The measurements from the experiment show that the RMS current in the two remaining phases increase from 11A to 17A during the open conductor fault, with L2 slightly more loaded compared to L3. The reason why the current in the two conductors are different is not verified, it might occur because of the different phase currents and/or due to unbalances in the loads and/or the external grid. The phase currents are increased during the fault, and if the open conductor fault is present for an extended time length might cause overheating in the generator due to the high currents in the two remaining phases.

The experiment result of the open conductor fault when only reactive power are generated, the current in the two remaining phases drops from 11A to 9,5A, with L2 slightly less loaded compared to L3. The generator establishes a steady state operating point almost immediately after the open conductor fault is triggered.

The objective of the laboratory experiments were to study the impact of the open conductor fault on a synchronous generator, and to recreate the fault conditions of the real world network if possible. The measurement result from the laboratory experiments show that an open conductor fault on a generator operating at nominal rated active power causes the current in the two remaining phases to increase to a high measured value. This might cause the machine to overheat and can lead to breakdown of the machine if the fault is sustained for a prolonged time.

The laboratory test setup did not re-eneact the real world network. To study the laboratory experiments setup characteristic a simulation model in PowerFactory was proposed constructed by supervisor T.Toftevåg. The proposed simulation model were to be constructed after the characteristic of the laboratory experiment setup and equipment, and the aim was to reproduce the measurement results from the laboratory experiments.

7 PowerFactory simulation of laboratory experiment

The laboratory test setup produced results that were different from the simulation results from PowerFactory. A decision was made together with supervisor T.Toftevåg to construct a simulation model for the laboratory test setup in PowerFactroy to determine if the test results from the laboratory experiments could be reproduced in simulations and to study the characteristics of the laboratory setup.

7.1 PowerFactory laboratory experiment setup

The simulation model was constructed as identical as possible to the laboratory test setup. The data on the synchronous machine is given in Appendix M. The data on the machine were incomplete, as there exist no data for the transient reactances and time constants. To compensate for the incomplete data, some considerations had to be made, and the input data for the machine in PowerFactory is chosen based on experienced guesses, with help from table 4.2 in Kundur [6] and Bonfert [23]. The line modelled in PowerFactory is modelled as an ideal lossless line.

The External Grid is in the simulations chosen to have a short circuit current capacity of 1,0 kA, as that is chosen as limit of short circuit current capacity for low voltage systems and is assumed to represent the external grid in the laboratory.

Figure 52 show the laboratory experiment test setup modelled in PowerFactory.

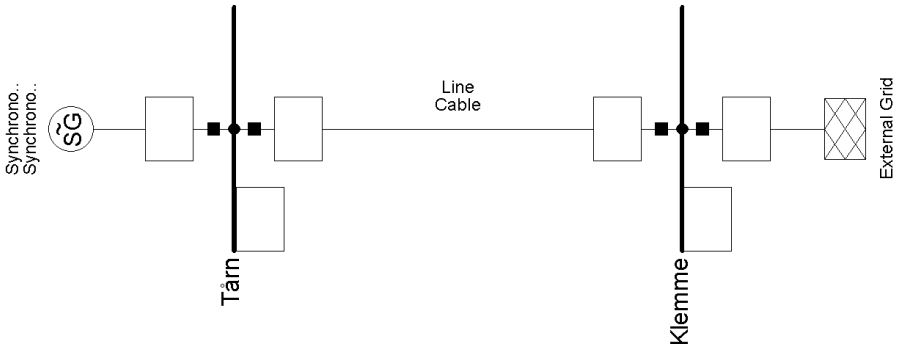

Figure 52: Laboratory simulation model.

7.2 PowerFactory load flow

Load flow analysis is conducted in PowerFactory, and the simulation result is compared to the actual laboratory experiments load flow before the open conductor fault is triggered. The load flow are comparable to the laboratory experiment, and the model is considered to represent the laboratory test setup.

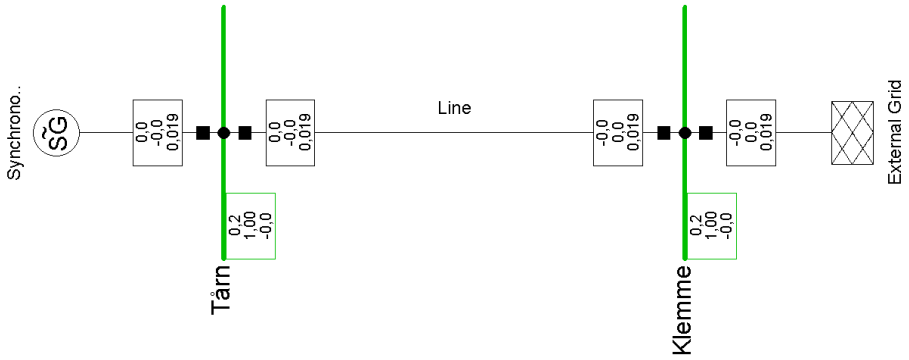

Figure 53: Experiment 1 load flow analysis.

7.3 Limitations

Losses in the test setup are not considered. All resistances are neglected as they are assumed negligible.

The data on the synchronous generator are modelled based on estimations based on values from Table 4.2 in Kundur [6] and Bonfert [23], and may not be completely accurate data for the synchronous generator that was used in the actual laboratory experiments. The simulation results might be different compared to the experiment results because of this.

8 PowerFactory laboratory experiments result

8.1 Experiment 1 result

Figures 54 and 55 shows the result from the simulation where the generator power in the faulty phase drops to zero Watts the instant the open conductor fault is triggered. The power in the two remaining phases increase from 2,5 kW to 3,5 kW in phase B and 4 kW in phase C for a total of 7,5 kW in total during the open conductor fault event. The peak magnitude of the active power following the open conductor fault is 9 kW. The oscillations of the active power are measured to last for one second. After that, the system is in stable operation. The moment the faulty phase is reconnected, the measurements plot show that the active power peaks at 5 kW in phase A, and all three phases are establishing a stable operating point that is identical to pre-fault conditions within one second.

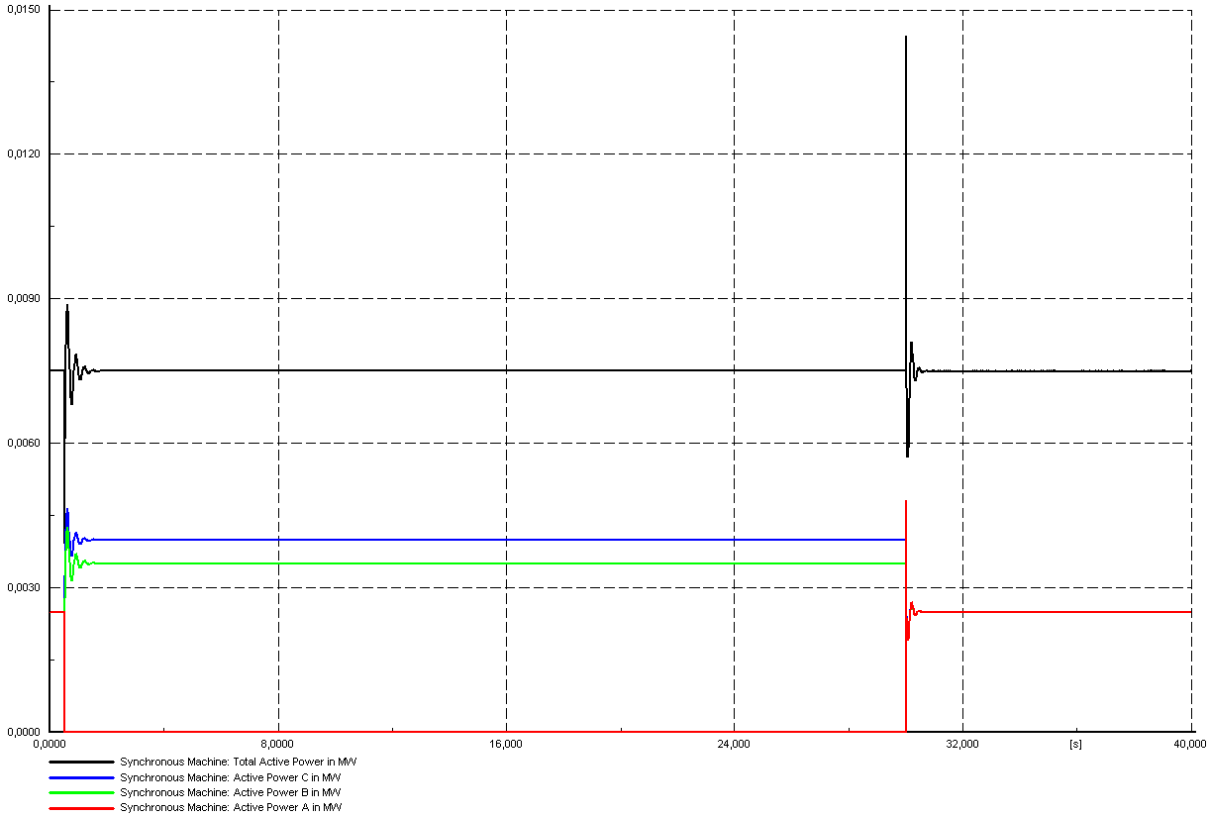

Figure 54: Total- and active phase powers during open conductor fault simulation of Experiment 1.

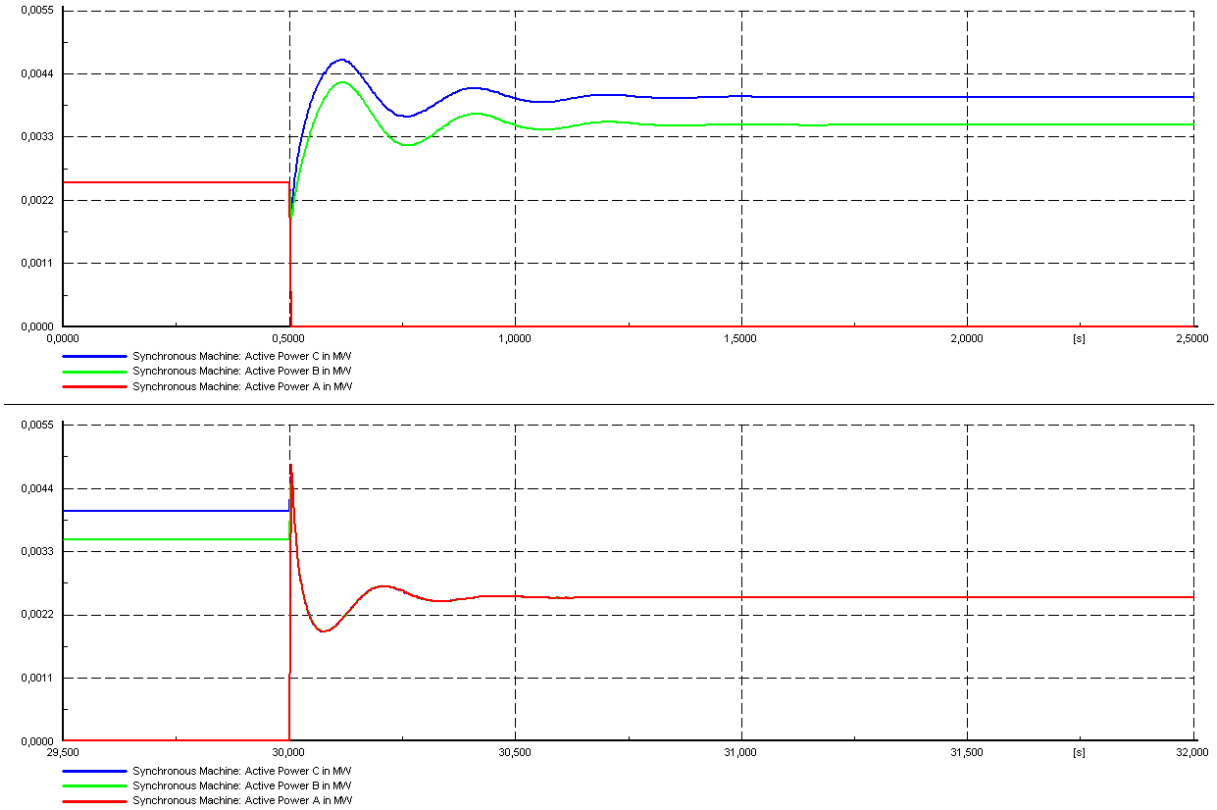

Figure 55: Active phase power at start (upper) and end (lower) of open conductor fault simulation of Experiment 1.

8.2 Experiment 2 result

Figure 56 show the simulation result of the generator behaviour during open conductor fault when the machine is loaded with 7,5 kVAr shows that the phase powers in the two remaining phases establishes a new operating point of 3 kVAr in each of the two remaining phases. This transition happens within one second in the simulation. The moment the faulty phase is reconnected, the simulation plot show the reactive power immediately peak at 4,5kVAr in the three phases.

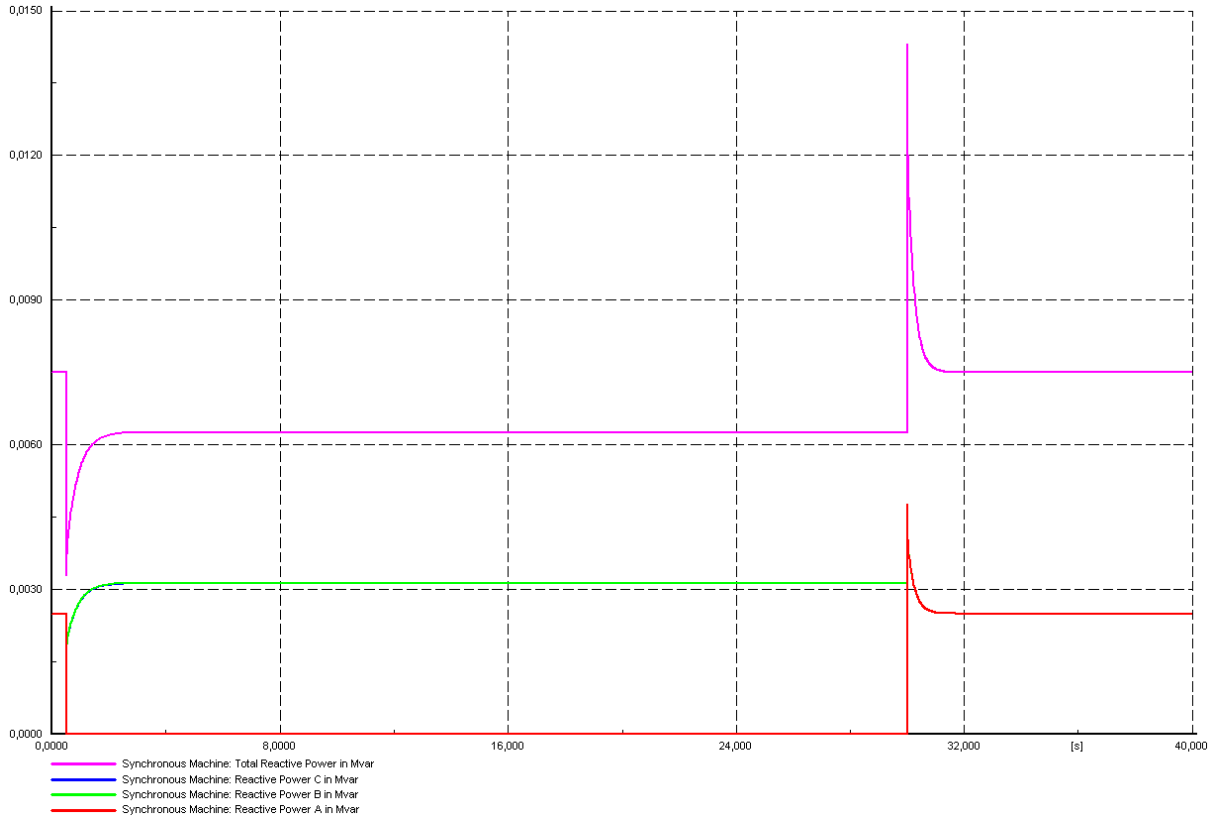

Figure 56: Total- and reactive phase powers during open conductor fault simulation of Experiment 2.

8.3 Discussion of PowerFactory experiments result

The simulation result of Experiment 1 show similar behaviour of the generator compared to the actual experiment. The peak of active power at disconnection is slightly higher in the measurement compared to the simulation result. The peak of active power at reconnection is 1 kW higher in simulation compared to measurement result. The oscillations from the simulation are in the same frequency range and time duration as the measurement result.

The difference in results is not substantial, but from the plot results, it is assumed that the resistance in the circuit may have some influence although this is not verified, and that since the simulation model consists of ideal lossless components, that factor may also influence the results.

The simulation result of Experiment 2 show a peak of reactive power at the moment of disconnection and reconnection of the fault. The generator establishes a new operating point at 6,5 kVAr after the fault, which is 2 kVAr higher compared to the measurement result.

The reactive power peaks in the simulation result differ compared to the measurement result. The generator model consist of estimated reactance values, and the values might be different compared to the real generator.

9 Discussion

Network model topology is based on the real network of NTE, and the validity of the network parameters and accuracy regarding the network model is verified by comparing simulation results to the results is K.Sjøholts report. The accuracy of the model in K.Sjøholts report is confirmed to correlate with the real network, both in load flow analysis and in the Base case scenario during open conductor fault simulation. However, there are some uncertainties regarding the simulations:

- The generator data is incomplete since all the generators are old and there exist no exact documentation. The generators parameters are estimated based on performance and by comparing similar generator data.
- The regulator parameters are estimated based on generator performance since there exist no exact documentation and may not be exact. It is not known if the parameters can be adjusted.
- Saturation characteristics are not incorporated since there exist no data.

The simulations show that the turbine governors are unable maintain operation when underdamped oscillations in the Base Case scenario occurs. The open conductor fault simulation show that G1NFISKUM in NFK was not able to establish a new operating point after the fault, where the damping ratio was negative. The plot result of the transient oscillations of the generator with actual regulators implemented indicates that there was a lack of damping torque injected from the regulators, as presented in chapter 2.7.

The network model is through load flow analysis and dynamic simulations verified to correlate with the real network when comparing results with K.Sjøholts report.

The parameter settings of the regulators on the generators in NFK were modified to see if the network is able to establish and maintain stable operation following the open conductor fault. The result show that the modifications contribute to damping of the oscillations that occur, and that the generators in NFK does not experience underdamped oscillations.

The network response with modified parameter settings provide result that show the generator operation is stabilised as the rotor angle oscillations are damped after the open conductor fault. The result show that the oscillations are damped out after 35 seconds. Although the simulations show that the rotor angle oscillations are damped, the generator is still missing one phase and subjected to unsymmetrical operation and this might cause other harmful effects on the generator.

Simulation of symmetrical fault and open conductor fault was conducted, were the network was exited for 100 milliseconds before the fault was reset, to compare damping. The results show that the damping ratios with actual regulators are similar, were the damping ratios for the first swing during symmetrical short circuit- and open conductor fault are 0,77 %and 0,78 %, respectively. The results show that the damping ratios with modified regulators are different, were the damping ratios for the first swing during symmetrical short circuit- and open conductor fault are 2 %and 0,91 %, respectively. This indicates that the regulators,

especially the AVR, have significant influence on the network stability, as the turbine governor is found to have little contribution to the transient response.

The reason why the damping ratios are different, especially with modified regulator settings, have not been found. It is speculated that the load flow conditions influence the transient response in such way that the generators will start to oscillate more heavily during open conductor faults, compared with three-phase short circuit faults, at node Skogmo. The modified parameter settings may not be appropriate as the transient behaviour of the generators in extreme cases might become “weird” or uncharacteristic compared to expected behaviour. Again, this is speculations that are not verified.

It was proposed to implement protection in the network model. This work proved to be meticulous, and were unable to provide definite results, as the protection settings on the actual network was unavailable and the protection settings in the network model was adjusted toward general recommendations [8].

The eigenvalue calculation of the network model prior to the fault presented results that show a damping ratio for the Mode 3 to be 5,85 % with an oscillation period of 0,9 seconds. The calculated damping ratio is considered sufficient for stability of a power system.

With modifications on the AVR the damping ratio of Mode 3 was calculated to be 6,74 % with an oscillation period of 0,9 seconds, and in the dynamic simulation the network is able to establish and maintain operation after fault. Dynamic simulations of different fault types were conducted and the results show that the AVR influences the damping, were modifications on the parameter settings resulted in improved damping for the network.

The results from the eigenvalue calculations are accurate when the network is intact. However, the moment the fault occurs the network is no longer identical to the prefault network, and it is not possible to linearize the network during transient oscillations. The knowledge gained from the analysis’ are that linear analysis is a powerful tool but must be used in the proper setting, were faults such as a missing phase can influence the network that under special load flow conditions underdamped rotor angle- and power oscillations can cause major disturbances in the power system network. It is speculated that “Mode 3”, which is the least damped mode, is the mode that is excited during the open conductor fault and may be underdamped during the open conductor fault, but this is only speculation since the oscillation period is different compared to the oscillation period observed in the dynamic simulations.

The modal analysis conducted for the symmetrical network of Mode 3 show that the excitations systems have negative influence on stability, both with actual- and modified parameter settings, where the actual parameter settings have the most severe influence on stability.

Modal analysis for the network is not conducted after the open conductor fault, as PowerFactory is unable to calculate the modes for an unbalanced network, and is limiting the basis to say that the regulators is influencing the damping. However, the dynamic simulations of the open conductor fault in the network model show that the response goes from underdamped to damped response when the parameter settings on the AVR is modified. This

points in the direction that the AVR have a significant impact on the damping properties on the generators in the network model without having conducted modal analysis for the network after the open conductor fault.

Laboratory experiments were conducted to study open conductor faults and to recreate the conditions for the actual network if possible.

The measurement results from Experiment 1 show that an open conductor fault on a generator operating at nominal rated active power causes the current in the two remaining phases to increase. This can cause the machine to overheat and can lead to breakdown of the machine if the fault is sustained for a prolonged time.

The measurements from Experiment 2 show that the powers in the remaining phases decreases during the open conductor fault, and the transition from balanced symmetrical condition to missing phase condition is completed almost immediately without oscillations.

When comparing the results, Experiment 1 is a more demanding condition on the generator compared to Experiment 2. If the configuration, conditions etc. are unfavourable, underdamped oscillations can follow open conductor faults, as happened in the power system network of NTE.

To study the laboratory experiments setup characteristic a simulation model in PowerFactory was proposed constructed by supervisor T.Toftevåg, where the aim was to reproduce the measurement results from the laboratory experiments.

The simulation results are not identical compared to the experiments results. Simulation of Experiment 2 results in increase of the phase currents when the generator is generating only reactive power. A guess based on the simulation results is that the generator model might have slightly overestimated reactance values and no resistance values which influences the simulation results for active and reactive powers, but this is just a guess.

10 Conclusions

NTE experienced 7th of March 2008 that the generators in NFK began to oscillate uncontrollably after an open conductor fault. It was observed that G1NFISKUM generator output varied from 0 to 100 % within 2 seconds during the uncontrolled oscillations.

Computer simulations show that the synchronous generator in NFK experience underdamped oscillations with a period of 1,2 seconds during the open conductor fault that occurred the 7th of March 2008.

The linear analysis and eigenvalue calculations indicates that the network is small signal stable. The dynamic analysis of the Base Case network show that the network model experience underdamped oscillations like the open conductor fault that occurred the 7th of March 2008.

The dynamic analysis show that when the settings on the AVR are modified, the response of the generator is damped, and stable operation is established and maintained. Although the modifications on the AVR was successful, it is not verified if the applied settings are accessible for modification on the actual regulators.

Simulation of symmetrical fault and open conductor fault was conducted, were the network was excited for 100 milliseconds before the fault was reset, to compare damping. The results show that the damping ratios with actual regulators are similar, were the damping ratios for the first swing during symmetrical short circuit- and open conductor fault are 0,77 %and 0,78 %, respectively. The results show that the damping ratios with modified regulators are different, were the damping ratios for the first swing during symmetrical short circuit- and open conductor fault are 2 %and 0,91 %, respectively. It is speculated that unfavourable load flow conditions, fault location and/or the modified parameter settings influence the transient response in such way that the generators will start to oscillate more heavily during open conductor faults compared with three-phase short circuit faults at node Skogmo, but this is not verified through simulations, as the modified parameter settings may give an incorrect response of the generators dynamic behaviour.

Laboratory experiments were conducted to study open conductor faults and to re-enact the real network conditions if possible. The experiments were conducted in the laboratory facilities at NTNU.

The laboratory test setup did not re-enact the real world network. However, the results from laboratory experiments show that open conductor faults can cause the generator to oscillate when it is generating active power. If the operating conditions, configurations are unfavourable the generator can start to oscillate and possibly experience underdamped oscillations in extreme cases.

To study the laboratory experiments setup characteristic a simulation model in PowerFactory was constructed, were results show similar behaviour compared to the experiments result. The laboratory experiments and the simulation modelling of the test setup provide basis for further studies of synchronous generator modelling and control parameter tuning during open conductor faults.

Based on literature rewiev, simulations and laboratory experiments the results indicates that the AVR and turbine governor for the generators in NFK were unable to provide sufficient damping torque, in combination with unfavourable load flow conditions at the time of the fault event, which led the power plant to experience severe oscillations during the open conductor fault, and eventually system collapse.

11 Recommendations for further works

The regulators used in the network model are not verified to exactly represent the actual network. Recommendations for further works regarding the regulators are:

- Validly the AVR and turbine governor configuration and parameter settings in NFK by measurements, or by identification of parameters that are adjustable, followed by modification of parameter settings if applicable.
- Study AVR and turbine governor parameter configurations with aim to determine optimal configuration on the generators regarding stability enhancement.
- Study the network by simulations where magnetic saturation is implemented to study the impact of saturation on damping properties.

It is recommended to install permanent measurement equipment in the power system network to detect the oscillations frequencies that may occur if similar events should occur, to detect very low frequent oscillations that may not exceed the thresholds of the protective relays in the network, should there be any.

Simulations of the full network is proposed for further work to study different fault events, fault locations and load flow conditions to determine the networks damping properties under different circumstances.

Laboratory experiments and simulations of a linearized network model is proposed, to study the network under different load flow conditions and fault events.

Cited works

[1] K. Sjøholt, «Ukontrollerte pendlinger i polhjulsvinkel på generatorer i regionalnettet,» Norges teknisk-naturvitenskapelige universitet Institutt for elkraftteknikk, Trondheim, 2010.

[2] S. J. Mabeta, «Open conductor faults and dynamic analysis of a power system,» Department of Electric Power Engineerig, NTNU, Trondheim, 2012.

[3] IEEE/CIGRE joint task force, «Definition and classification of power system stability,» *IEEE Trans.,* nr. Volume 19, Issue 3, 2004.

[4] J. Machowski, J. W. Bialek og J. R. Bumbly, Power System Dymamics Stability and Control, Wiley, 2008.

[5] E. W. Kimbark, Power system stability Volume 3: Synchronous Machines, New York: IEEE Press, 1995.

[6] P. Kundur, Power System Stability and Control, McGraw-Hill, Inc., 1994.

[7] U. Stephen D, Fitzgerald & Kingsley's electric machinery, New York: McGraw-Hill, 2014.

[8] S. H. Horowitz og A. G. Phadke, Power System Relaying, 2014: Wiley, Chichester.

[9] DIgSILENT, PowerFactory Version 15.1 User Manual, Gomaringen: DIgSILENT, 2013.

[10] DIgSILENT, Technical Reference Documentation Synchronous Machine, Gomaringen: DIgSILENT, 2011.

[11] DIgSILENT, Technical Reference Documentation General Load, Gomaringen: DIgSILENT, 2013.

[12] DIgSILENT, Technical Reference Documentation External Grid, Gomaringen: DIgSILENT, 2013.

[13] O.-M. Thu, «Stabilitetsproblemer i regionalnettet i sør-Rogaland,» Institutt for elkraftteknikk NTNU, Trondheim, 2013.

[14] DigSILENT, Technical Reference Documentation Overhead Line Models, Gomaringen: DIgSILENT, 2011.

[15] Nexans, «Kabelboka Håndbok for e-verkskabler,» 2014. [Internett]. Available: https://www.google.no/?gfe_rd=cr&ei=wsltVfanEJKr8weU_YP4CA&gws_rd=ssl#q=nexans+kabelboka. [Funnet 2015].

[16] DIgSILENT, Technical Reference Documentation Two-Winding Transfomer (3-Phase), Gomaringen: DIgSILENT, 2011.

[17] DIgSILENT, Technical Reference Documentation SVS - Static Var System, Gomaringen: DIgSILENT, 2011.

[18] H.O.Roste, «Specialization project - Dynamic behaviour of synchronous machine during open conductor fault,» Norwegian University of Science and Technology, Trondheim, 2014.

[19] IEEE Comimittee Report, «Exitation system models for power system stability studies,» IEEE Trans., 1981.

[20] F. Irgens, Dynamikk, 4. utgave red., Trondheim: Tapir forlag, 1999.

[21] Ø. Nicklasson og I. Østberg, Elektrisitetslære 2 Vekselstrøm, Trondheim: NKI, 1978.

[22] Elspec, Blackbox Full User Guide, Elspec, 2008.

[23] K. Bonfert, Betriebsverhalten der Synchronmaschine : Bedeutung der Kenngrößen für Planung und Betrieb elektrischer Anlagen und Antriebe, Berlin: Springer, 1962.

[24] D. G. Ramey og J. W. Skoglund, «Detailed Hydrogovernor Representation for System Stability Studies,» *IEEE Trans.,* pp. 106-112, januar 1970.

[25] L. N. Hannett, J. W. Feltes og B. Fardanesh, «FIELD TESTS TO VALIDATE HYDRO TURBINE-GOVERNOR MODEL STRUCTURE AND PARAMETERS,» *IEEE Trans.,* pp. 1744-1751, november 1994.

[26] H. Fang, L. Chen, N. Dlakavu og Z. Shen, «Basic Modeling and Simulation Tool for Analysis of Hydraulic Transients in Hydroelectric Power Plants,» *IEEE TRANS.,* pp. 834-841, september 2008.

[27] P.L.Dandeno, P.Kundur og J.P.Bayne, «HYDRAULIC UNIT DYNAMIC PERFORMANCE UNDER NORMAL AND ISLANDING CONDITIONS - ANALYSIS AND VALIDATION,» *IEEE Trans.,* pp. 2134-2143, november/desember 1978.

[28] IEEE, «HYDRAULIC TURBINE AND TURBINE CONTROL MODELS FOR SYSTEM PYNAMIC STUDIES,» *IEEE Trans.,* pp. 167-179, februar 1992.

[29] P.Kundur, D.C.Lee, J.P.Bayne og P.L.Dandeno, «IMPACT OF TURBINE GENERATOR OVERS PEED CONTROLS ON UNIT PERFORMANCE UNDER SYSTEM DISTURBANCE CONDITIONS,» *IEEE Trans.,* pp. 1262-1269, juni 1985.

[30] F.R.Schleif og A.B.Wilbor, «The Coordination of Hydraulic Turbine Governors for Power System Operation,» *IEEE Trans.,* pp. 750-758, juli 1966.

[31] S.Hagihara, H.Yokota, K.Goda og K.Isobe, «STABILITY OF A HYDRAULIC TURBINE GENERATING UNIT CONTROLLE BY P.I.D. GOVERNOR,» *IEEE Trans.,* pp. 2294-2298, november/desember 1979.

[32] J. Nanda, A.Mangala og S.Suri, «Some New Findings on Automatic Generation Control of an Interconnected Hydrothermal System With Conventional Controllers,» *IEEE Trans.,* pp. 187-194, mars 2006.

[33] NTNU, «Instrumentarkiv,» [Internett]. Available: https://tellus.elkraft.ntnu.no/instrumentarkiv/instsokresultat.php.

Appendices

Appendix A – Network topology

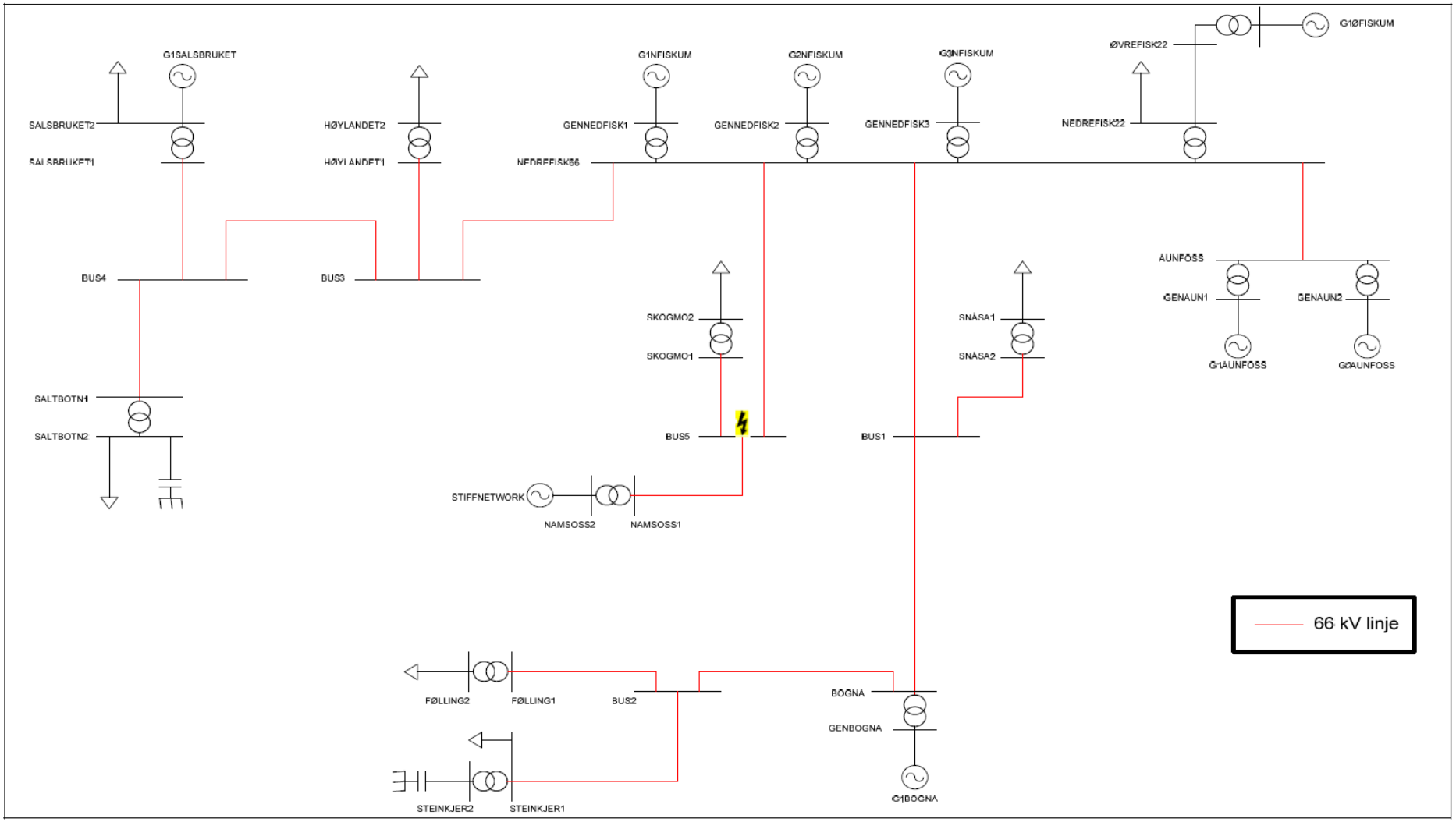

Appendix B – Transformer data

Generator transformer data

Kraftstasjon	Fakta		Kortslutningsimpedans			Merkeytelse	Merkespenning		Koplings-gruppe	Reelle verdier eller ikke?
	Kontakt	Kilde	Z_{K} - ε_k [%]	R_{K} - ε_r [%]	X_{K} - ε_x [%]	S_N [MVA]	Reg. side [kV]	Fix. side [kV]		
ØFK_T1	E. Tønne	NetBas	8.53	0.59	8.51	9	3.2	22	YNd11	Ja
Salsbruket_T1	E. Tønne	NetBas	8.53	0.59	8.51	9	3.2	22	YNd11	Nei
NFK_T1	V. Mygland	Merkeskilt	10.5	0.35	10.49	17	6.6	68	YNd11	Ja
NFK_T2	V. Mygland	Merkeskilt	10.5	0.35	10.49	17	6.6	68	YNd11	Ja
NFK_T3	V. Mygland	Merkeskilt	10.5	0.35	10.49	17	6.6	68	YNd11	Ja
Aunfoss_T1	V. Mygland	Merkeskilt	9.88	0.658	9.858	18	6.3	68	YNd11	Ja
Aunfoss_T2	V. Mygland	Merkeskilt	9.85	0.66	9.828	18	6.3	68	YNd11	Ja
Bogna_T1	V. Mygland	Merkeskilt	8.54	0.281	8.53	60	8.5	70	YNd5	Ja

Grid transformer data

*	Fakta		Kortslutningsimpedans			Merkeytelse	Merkespenning		Koplings-gruppe	Reelle verdier eller ikke?
	Kontakt	Kilde	Z_{K} - ε_k [%]	R_{K} - ε_r [%]	X_{K} - ε_x [%]	S_N [MVA]	Reg. side [kV]	Fix. side [kV]		
66-22	V. Mygland	Merkeskilt	7.8	0.55	7.78	10	66	22	YNyn0	Ja
66-300	E. Tønne	NTE	11.295	0.34	11.29	160	66	300	YNyn0	Ja

Appendix C- Line data

Type	Node		Impedanser		Kapasitanser		Null impedans		Lengde	Spenning	Utforming
	Fra	Til	R [Ω/km]	X [Ω/km]	C_j [nF/km]	C_d [nF/km]	R0 [Ω]	X0 [Ω]	[km]	[kV]	
FEAL 120	NedreFisk66	Aunfoss	0.151	0.387	5.58	9.44	0.297	1.428	10.4	66	Luftledning
FEAL 120	NedreFisk66	BUS1	0.151	0.387	5.58	9.44	0.297	1.428	38.4	66	Luftledning
FEAL 50	NedreFisk22	ØvreFisk22	0.359	0.373	4.85	9.79	0.505	1.457	1.9	22	Luftledning
FEAL 120	BUS1	Snåsa1	0.151	0.387	5.58	9.44	0.297	1.428	0.8	66	Luftledning
FEAL 120	BUS1	Bogna	0.151	0.387	5.58	9.44	0.297	1.428	15.8	66	Luftledning
FEAL 240	Bogna	BUS2	0.076	0.366	5.38	10.03	0.222	1.406	28	66	Luftledning
FEAL 150	BUS2	Følling1	0.121	0.380	5.64	9.61	0.267	1.421	0.18	66	Luftledning
FEAL 240	BUS2	Steinkjer	0.076	0.366	5.38	10.03	0.222	1.406	9.4	66	Luftledning
FEAL 185	NedreFisk66	BUS3	0.089	0.374	5.70	9.79	0.244	1.414	14.2	66	Luftledning
FEAL 50	BUS3	Høylandet1	0.359	0.416	5.34	8.76	0.505	1.457	0.7	66	Luftledning
FEAL 185	BUS3	BUS4	0.089	0.374	5.70	9.79	0.244	1.414	34.8	66	Luftledning
FEAL 185	BUS4	Salsbruket1	0.089	0.374	5.70	9.79	0.244	1.414	0.2	66	Luftledning
FEAL 185	BUS4	Saltbotn1	0.089	0.374	5.70	9.79	0.244	1.414	16.3	66	Luftledning
FEAL 120	NedreFisk66	BUS5	0.151	0.387	5.58	9.44	0.297	1.428	21.5	66	Luftledning
FEAL 120	BUS5	Skogmo1	0.151	0.387	5.58	9.44	0.297	1.428	0.5	66	Luftledning
FEAL 120	BUS5	NamsosS1	0.151	0.387	5.58	9.44	0.297	1.428	12.9	66	Luftledning

Appendix D – Network topology in DIgSILENT PowerFactory with Base Case load flow conditions

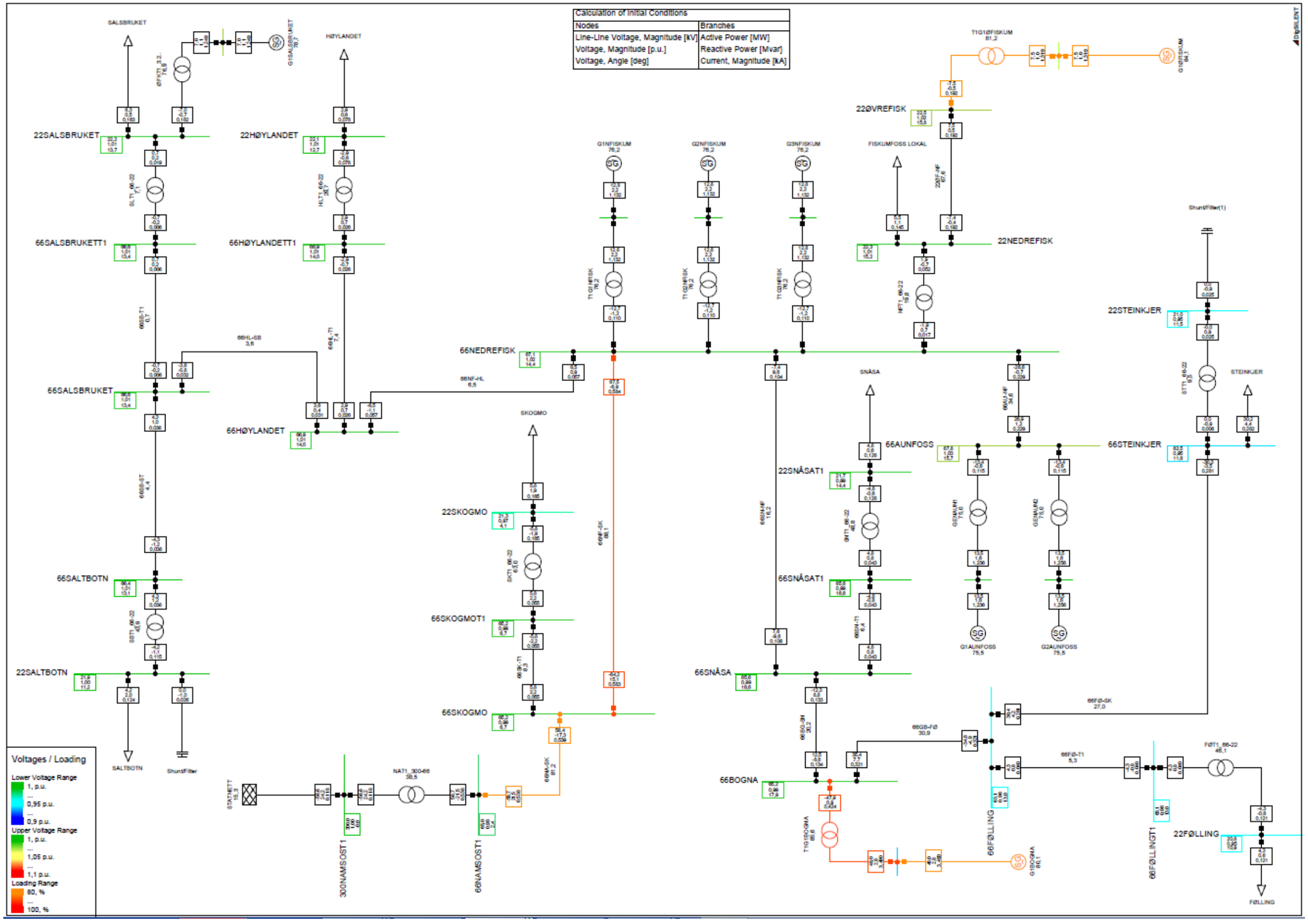

Appendix E - Node load data

Node	P [MW]	Q [MVAr]	Kommentar
Fiksumfoss lokal	5,50	1,08	Erling Tønne i NTE kan bekrefte verdien til P. Den er beregnet i NetBas. Ingen måling av Q, antar samme gjennomsnittsverdi målt 10oktober.
Følling	4,33	0,60	Bruker gjennomsnittsverdier hentet fra målingene (trafo"FING_22T1__PI-CP") av P den 07.mars 2008 (24t). Ingen måling av Q, antar derfor samme gjennomsnittsverdi målt den 10oktober.
Høylandet	2,92	0,63	Bruker gjennomsnittsverdier hentet fra målingene (trafo "HOYL_22T1__PI" og "HOYL_22T1__QI") av lasten den 07.mars 2008 (24t).
Salsbruket	6,28	0,47	Bruker gjennomsnittsverdier hentet fra målingene (trafo "SALS_22T1__PU" og "SALS_22KR1_QU") av lasten den 07.mars 2008 (24t).
Saltbotn	4,24	2,05	Det har ikke vært aktiv- eller reaktivmåling i Saltbotn før 1/7-08. Men ut i fra målingene (trafo "SALT_66A_U" og "SALT_66T2_I-DS") av U og I blir gjennomsnittsverdiene den 07. Mars: P=4.24MW og Q=2.05MVAr.
Skogmo	5,80	1,91	Bruker gjennomsnittsverdier hentet fra målingene (trafo "SKMO_22T1__PI" og "SKMO_22T1__QU") av lasten den 12.mars 2008 (24t). Bruker ikke 07.mars fordi 12.mars er den første dagen det er foretatt P og Q målinger av Skogmo.
Snåsa	4,76	0,65	Bruker gjennomsnittsverdier hentet fra målingene (trafo "SNSA_22T1__PI" og "SNSA_22T1__QI") av lasten den 07.mars 2008 (24t).

Appendix F - Data synchronous generator Aunfoss power station

In the column “Kilde” it is commented were the values are collected from. The values that are not from the machines are from a 20 MVA GAMESA synchronous generator [1].

Beskrivelse av parametrene	Symbol		Størrelse	Kilde
Tilsynelatende merkeeffekt	S_N	$[MVA]$	18	Merkeskilt
Merkespenning	U_N	$[kV]$	6,3	Merkeskilt
Nominell frekvens	f_N	$[Hz]$	50	Merkeskilt
Nominell effektfaktor	$cos\varphi_N$		0,75	Merkeskilt
Nominell rotasjonshastighet	n	$[o/min]$	150	Merkeskilt
Synkron reaktans d-akse	X_d	$[p.u.]$	1,197	GAMESA
Transient synkron reaktans d-akse	X'_d	$[p.u.]$	0,262	GAMESA
Subtransient synkron reaktans d-akse	X''_d	$[p.u.]$	0,163	GAMESA
Synkron reaktans q-akse	X_q	$[p.u.]$	0,746	GAMESA
Transient synkron reaktans q-akse	X'_q	$[p.u.]$		
Subtransient synkron reaktans q-akse	X''_q	$[p.u.]$	0,171	GAMESA
Reaktans i negativ-sekvens	X_2	$[p.u.]$	0,167	GAMESA
Reaktans i null-sekvens	X_0	$[p.u.]$	0,07	GAMESA
Transient tidskonstant d-akse i tomgang	T'_{d0}	$[s]$	5,594	GAMESA
Subtransient tidskonstant d-akse i tomgang	T''_{d0}	$[s]$	0,082	GAMESA
Transient tidskonstant d-akse	T'_d	$[s]$	1,154	GAMESA
Subtransient tidskonstant d-akse	T''_d	$[s]$	0,052	GAMESA
Subtransient tidskonstant q-akse i tomgang	T''_{q0}	$[s]$	0,246	GAMESA
Subtransient tidskonstant q-akse	T''_q	$[s]$	0,049	GAMESA
Tidskonstant for kortsluttet statorvikling	T_a	$[s]$	0,172	GAMESA
Treghetskonstant for hele aggregatet	H	$[s]$	2.69	Beregnet
Treghetsmoment for hele aggregatet	J	$[kgm^2]$	392500	NTE

Appendix G - Synchronous generator data Bogna power station

In the column “Kilde” it is commented were the values are collected from. The values that are not from the machines are from a 65 MVA VSEC synchronous generator [1].

Beskrivelse av parametrene	Symbol		Størrelse	Kilde
Tilsynelatende merkeeffekt	S_N	$[MVA]$	60	Merkeskilt
Merkespenning	U_N	$[kV]$	8.5	Merkeskilt
Nominell frekvens	f_N	$[Hz]$	50	Merkeskilt
Nominell effektfaktor	$cos\varphi_N$		0.83	Merkeskilt
Nominell rotasjonshastighet	n	$[o/min]$	500	Merkeskilt
Synkron reaktans d-akse	X_d	$[p.u.]$	1.18	NTE
Transient synkron reaktans d-akse	X'_d	$[p.u.]$	0.28	NTE
Subtransient synkron reaktans d-akse	X''_d	$[p.u.]$	0.16	NTE
Synkron reaktans q-akse	X_q	$[p.u.]$	0.61	VSEC tpa
Transient synkron reaktans q-akse	X'_q	$[p.u.]$	0.61	VSEC tpa
Subtransient synkron reaktans q-akse	X''_q	$[p.u.]$	0.17	VSEC tpa
Reaktans i negativ-sekvens	X_2	$[p.u.]$	0.18	VSEC tpa
Reaktans i null-sekvens	X_0	$[p.u.]$	0.05	VSEC tpa
Transient tidskonstant d-akse i tomgang	T'_{do}	$[s]$	6.5	NTE
Subtransient tidskonstant d-akse i tomgang	T''_{do}	$[s]$	0.05	VSEC tpa
Transient tidskonstant d-akse	T'_d	$[s]$	1.5	NTE
Subtransient tidskonstant d-akse	T''_d	$[s]$	0.04	NTE
Subtransient tidskonstant q-akse i tomgang	T''_{q0}	$[s]$	0.14	VSEC tpa
Subtransient tidskonstant q-akse	T''_q	$[s]$	0.04	VSEC tpa
Tidskonstant for kortsluttet statorvikling	T_a	$[s]$	0.16	VSEC tpa
Treghetskonstant for hele aggregatet	H	$[s]$	2.28	Beregnet
Treghetsmoment for hele aggregatet	J	$[kgm^2]$	100000	NTE

Appendix H - Synchronous generator data Nedre Fiskum Kraftverk

In the column “Kilde” it is commented were the values are collected from. The values that are not from the machines are from a 20 MVA GAMESA synchronous generator [1].

Beskrivelse av parametrene	Symbol		Størrelse	Kilde
Tilsynelatende merkeeffekt	S_N	$[MVA]$	17	Merkeskilt
Merkespenning	U_N	$[kV]$	6.6	Merkeskilt
Nominell frekvens	f_N	$[Hz]$	50	Merkeskilt
Nominell effektfaktor	$cos\varphi_N$		0.75	Merkeskilt
Nominell rotasjonshastighet	n	$[o/min]$	187	Merkeskilt
Synkron reaktans d-akse	X_d	$[p.u.]$	1.197	GAMESA
Transient synkron reaktans d-akse	X'_d	$[p.u.]$	0.262	GAMESA
Subtransient synkron reaktans d-akse	X''_d	$[p.u.]$	0.163	GAMESA
Synkron reaktans q-akse	X_q	$[p.u.]$	0.746	GAMESA
Transient synkron reaktans q-akse	X'_q	$[p.u.]$		
Subtransient synkron reaktans q-akse	X''_q	$[p.u.]$	0.171	GAMESA
Reaktans i negativ-sekvens	X_2	$[p.u.]$	0,167	GAMESA
Reaktans i null-sekvens	X_0	$[p.u.]$	0,07	GAMESA
Transient tidskonstant d-akse i tomgang	T'_{d0}	$[s]$	5,594	GAMESA
Subtransient tidskonstant d-akse i tomgang	T''_{d0}	$[s]$	0,082	GAMESA
Transient tidskonstant d-akse	T'_d	$[s]$	1,154	GAMESA
Subtransient tidskonstant d-akse	T''_d	$[s]$	0,052	GAMESA
Subtransient tidskonstant q-akse i tomgang	T''_{q0}	$[s]$	0,246	GAMESA
Subtransient tidskonstant q-akse	T''_q	$[s]$	0,049	GAMESA
Tidskonstant for kortsluttet statorvikling	T_a	$[s]$	0,172	GAMESA
Treghetskonstant for hele aggregatet	H	$[s]$	2,76	Beregnet
Treghetsmoment for hele aggregatet	J	$[kgm^2]$	245000	NTE

Appendix I - Data Salsbruket and Øvre Fiskumfoss Kraftverk

In the column "Kilde" it is commented were the values are collected from. The values that are not from the machines are from a 12,7 MVA ALCONZA synchronous generator [1].

Beskrivelse av parametrene	Symbol		Størrelse	Kilde
Tilsynelatende merkeeffekt	S_N	$[MVA]$	9	Merkeskilt
Merkespenning	U_N	$[kV]$	3,2	Merkeskilt
Nominell frekvens	f_N	$[Hz]$	50	Merkeskilt
Nominell effektfaktor	$cos\varphi_N$		0,92	Merkeskilt
Nominell rotasjonshastighet	n	$[o/min]$	107	Merkeskilt
Synkron reaktans d-akse	X_d	$[p.u.]$	1,426	ALCONZA
Transient synkron reaktans d-akse	X'_d	$[p.u.]$	0,322	ALCONZA
Subtransient synkron reaktans d-akse	X''_d	$[p.u.]$	0,180	ALCONZA
Synkron reaktans q-akse	X_q	$[p.u.]$	0,975	ALCONZA
Transient synkron reaktans q-akse	X'_q	$[p.u.]$		ALCONZA
Subtransient synkron reaktans q-akse	X''_q	$[p.u.]$	0,173	ALCONZA
Reaktans i negativ-sekvens	X_2	$[p.u.]$	0,177	ALCONZA
Reaktans i null-sekvens	X_0	$[p.u.]$	0,112	ALCONZA
Transient tidskonstant d-akse i tomgang	T'_{d0}	$[s]$	5,3952	ALCONZA
Subtransient tidskonstant d-akse i tomgang	T''_{d0}	$[s]$		ALCONZA
Transient tidskonstant d-akse	T'_d	$[s]$	1,2167	ALCONZA
Subtransient tidskonstant d-akse	T''_d	$[s]$	0,0269	ALCONZA
Subtransient tidskonstant q-akse i tomgang	T''_{q0}	$[s]$	0,247	(antar)
Subtransient tidskonstant q-akse	T''_q	$[s]$	0,0475	ALCONZA
Tidskonstant for kortsluttet statorvikling	T_a	$[s]$	0,0475	ALCONZA
Treghetskonstant for hele aggregatet	H	$[s]$	0,69	Beregnet
Treghetsmoment for hele aggregatet	J	$[kgm^2]$	99000	NTE

Appendix J PowerFactcory

The DIgSILENTsynchronous machine

Figures A-1 and A-2 show the equivalent circuit diagrams of the PowerFactory synchronous machine models, which are represented in a rotor-oriented reference system [10].

The d-axis is always modelled by 2 rotor loops representing the damping and the excitation winding. For the q-axis, PowerFactory supports two models, a model with one rotor loop (for Salient Pole machines) and a model with two rotor loops (for Round Rotor Machines). In the simulation model, only the salient pole machine is modelled, since the network model consists of salient pole machines only [10].

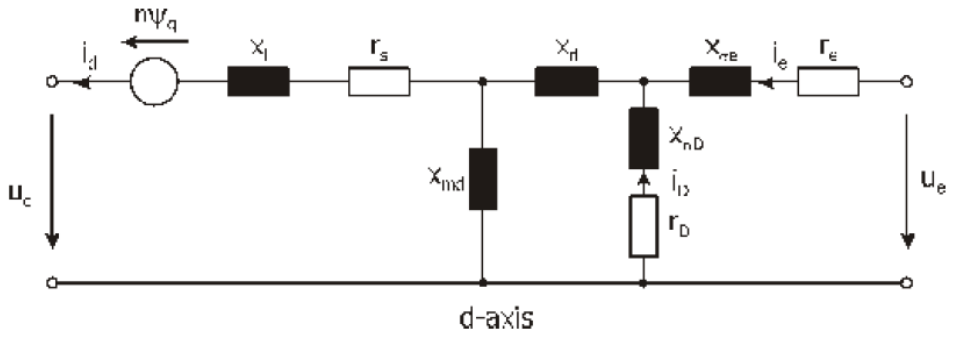

Figure A-1: PowerFactory d-axis equivalent circuit for the synchronous machine representation [9].

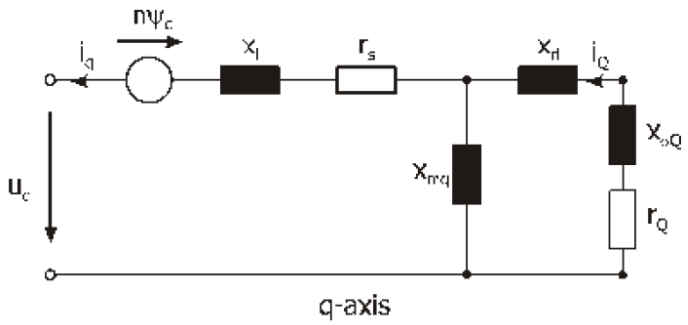

Figure A-2: PowerFactory q-axis equivalent circuit for the synchronous machine representation (salient rotor) [9].

DIgSILENT load modelling

Figure A-3 shows the load model used for balanced load flow analysis, where only P0 and Q0 are required to be specified. All loads specified as 2-phase or 1-phase loads are only considered in unbalanced load flow calculations. They are ignored when a balanced load flow is performed [11].

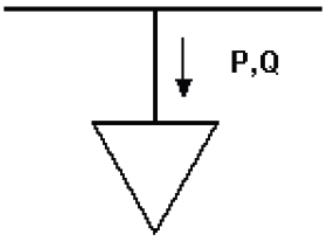

Figure A-3: Load model used for balanced load-flow analysis [10]

The voltage dependency of loads in PowerFactory is modelled using three polynomial terms expressed by equations (A.1) and (A.2) instead of only one polynomial term.

$$P = P_0\left(aP \cdot \left(\frac{v}{v_o}\right)^{e\_aP} + bP \cdot \left(\frac{v}{v_o}\right)^{e\_bP} + (1 - aP - bP) \cdot \left(\frac{v}{v_o}\right)^{e\_cP}\right) \quad \text{(A.6)}$$

where P_0 is the initial active power flow, $1 - aP - bP = cP$, and v is the busbar voltage [p.u.] [11].

$$Q = Q_0\left(aQ \cdot \left(\frac{v}{v_o}\right)^{e\_aQ} + bQ \cdot \left(\frac{v}{v_o}\right)^{e\_bQ} + (1 - aQ - bQ) \cdot \left(\frac{v}{v_o}\right)^{e\_cQ}\right) \quad (7)$$

where Q_0 is the initial reactive power flow, $1 - aQ - bQ = cQ$, and v is the busbar voltage [p.u.] [11]. Table A.1 shows the values required for the exponents in order to model constant power, constant current and constant impedance. The relative proportion of each coefficient can be freely defined using the coefficients aP, bP, cP and aQ, bQ, cQ in PowerFactory [11].

Table A.1. Selection of exponent value for different load model behaviour.

Exponent	Constant
0	Power
1	Current
2	Impedance

DIgSILENT external grid type description

SL type

By default, the external grid controls the voltage, the angle and the frequency of the busbar to which it is connected. If a reference busbar is selected, the voltage and the angle of this reference busbar are controlled. In such cases, the user must define the voltage set point (in p.u.) and the reference angle (in degrees) [12].

PV type

The external grid infeeds a constant active power (for P > 0) and by default controls the voltage of the busbar to which it is connected. Alternatively, the user may select a reference busbar for voltage control. The voltage setpoint is defined in p.u. of the busbar voltage. Only one external grid may control the voltage at any given busbar. It is not possible to execute calculations with two external grid elements (both using option PV) connected to the same busbar [12].

PQ type

The external grid is modelled as a constant P (active power) and constant Q (reactive power) infeed. A positive value for P is considered to be a generated active power and a negative value is considered to be a consumed active power. Optionally, the input values for P and Q may be entered as: P, cos(phi); S, cos(phi); S, Q; or S, P [12].

AVR

An excitation control system includes control, limiting and protective functions which assist in fulfilling the performance requirements described in chapter 2.5.6.

The AVR used in the network model is described as an uncontrolled thyristor controlled voltage regulator with limiters, which is applicable to the block diagram for the AVR used in the network model [19]. The system utilizes a full thyristor bridge in the exciter output circuit to gain high initial response. The voltage regulator controls the firing of thyristor bridges. The exciter alternator uses an independent voltage regulator to control its output voltage to a constant value.

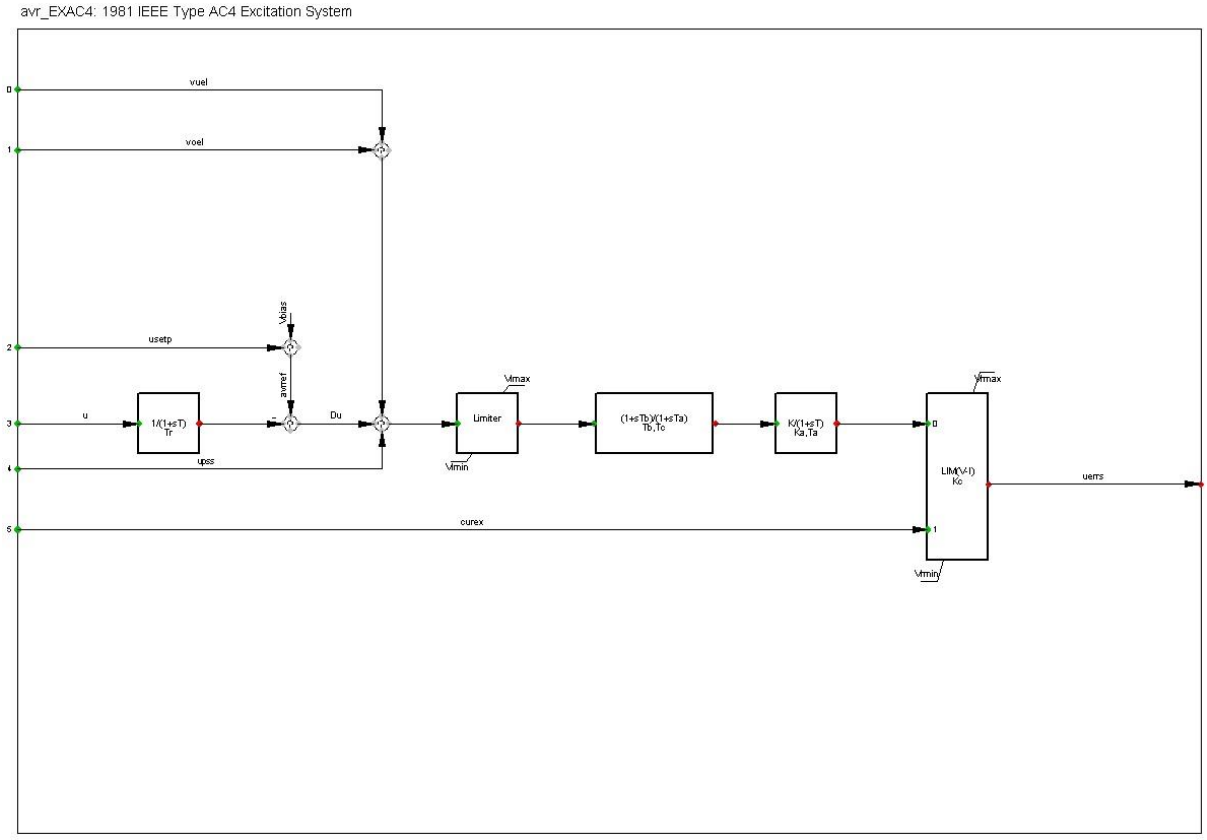

Figure A-4: DIgSILENT Type AC4 Excitation System

EXAC4 parameters list

Table A.2. EXAC4 actual parameters

Parameter	Setting	Unit	Description
Tr	0,05	[s]	Measurement delay
Tb	5,0	[s]	Filter delay time
Tc	1,0	[s]	Filter derivative time constant
Ka	100,0	[p.u.]	Controller gain
Ta	0,004	[s]	Controller time constant
Kc	0	[p.u.]	Exciter current compensation factor
Vimin	-1,0	[p.u.]	Controller minimum input
Vrmin	-3,4	[p.u.]	Exciter minimum output
Vimax	1,0	[p.u.]	Controller maximum input
Vrmax	4,0	[p.u.]	Exciter maximum output

Table A.3. EXAC4 PowerFactory modified parameters

Parameter	Setting	Unit	Description
Tr	0,02	[s]	Measurement delay
Tb	14,0	[s]	Filter delay time
Tc	1,0	[s]	Filter derivative time constant
Ka	140,0	[p.u.]	Controller gain
Ta	0,02	[s]	Controller time constant
Kc	0,2	[p.u.]	Exciter current compensation factor
Vimin	-0,5	[p.u.]	Controller minimum input
Vrmin	-3,4	[p.u.]	Exciter minimum output
Vimax	0,5	[p.u.]	Controller maximum input
Vrmax	4,0	[p.u.]	Exciter maximum output

Turbine governor system

The turbine governor system used in the network model is chosen, based on the turbine and regulator used in K.Sjøholts [1] report, in PowerFactory as the IEEE type 3 speed governing model from the inbuilt library as the description and parameter inputs are identical between the two power system analysis programs. The turbine parameters is modelled as an ideal lossless hydraulic turbine based on sec. 9.1 in Kundur [6], and may not exactly correlate with the actual turbine systems in the network. The turbine governor parameters are set identical as in K.Shøholts report [1]. Detailed explanation of the turbine governing system and determination of parameter settings are found in Kundur [6] and reference [24] to [31].

Block diagram of the speed-governing system used in Power Factory is shown in Figure A-5.

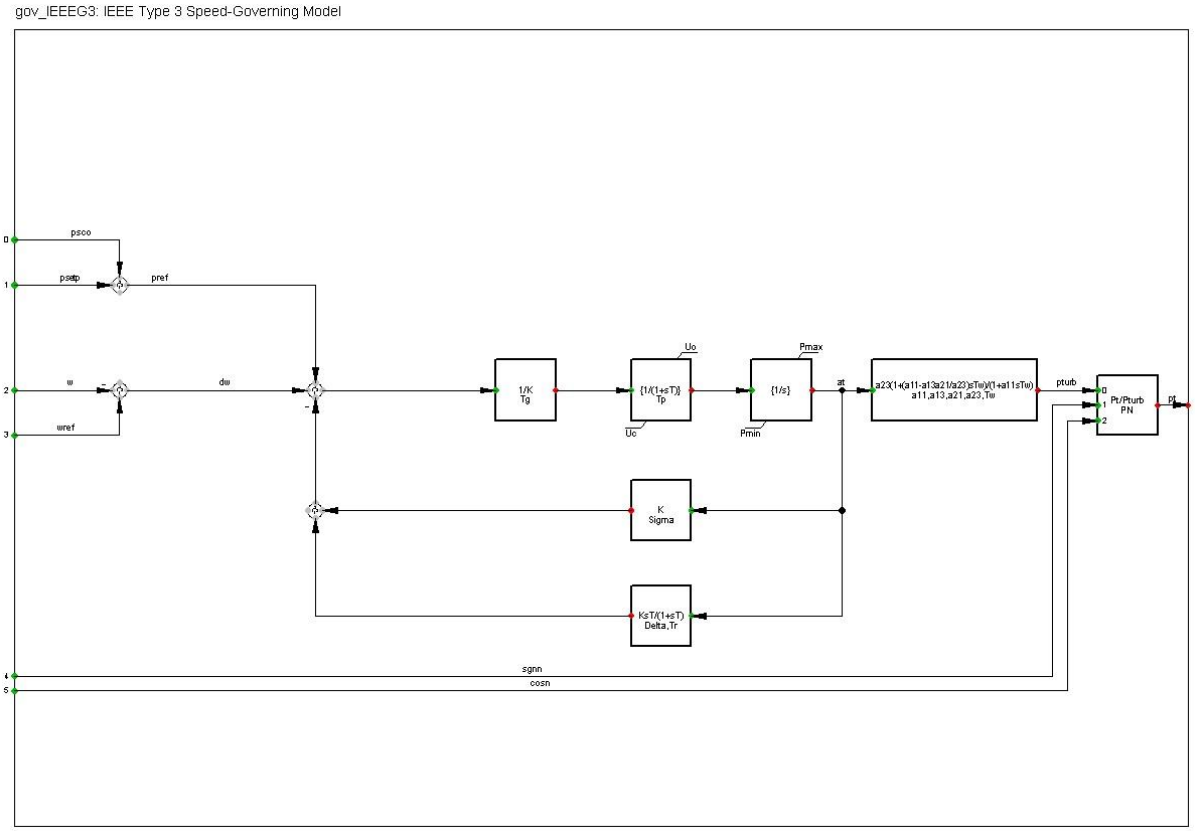

Figure A-5: DIgSILENT IEEE Type 3 Speed-Governing Model.

IEEE3 parameters list

Table A.4. Actual governor settings

Parameter	Setting	Unit	Description
Tg	0,02	[s]	Gate servomotor time constant
Tp	0,04	[s]	Pilot valve time constant
Sigma	0,04	[p.u.]	Permanent droop
Delta	0,4	[p.u.]	Temporary droop
Tr	8,0	[s]	Governor time constant
a11	0,5	[p.u.]	Waterhammer 1st factor
a12	1,0	[p.u.]	Watehammer 2nd factor
a21	1,5	[p.u.]	Waterhammer 3rd factor
a23	1,0	[p.u.]	Waterhammer 4th factor
Tw	1,0	[s]	Water starting time
PN	0	[p.u./s]	Turbine rated power (=0⇒PN=Pgnn [MW]
Pmin	-0,2	[p.u.]	Valve closing time
Uo	0,2	[p.u./s]	Valve opening time
Pmax	1,0	[p.u.]	Maximum gate limit

Table A.5. Adjusted parameters

Parameter	Setting	Unit	Description
Tg	0,05	[s]	Gate servomotor time constant
Tp	0,04	[s]	Pilot valve time constant
Sigma	0,04	[p.u.]	Permanent droop
Delta	0,2	[p.u.]	Temporary droop
Tr	10	[s]	Governor time constant
a11	0,5	[p.u.]	Waterhammer 1st factor
a12	1,0	[p.u.]	Watehammer 2nd factor
a21	1,5	[p.u.]	Waterhammer 3rd factor
a23	1,0	[p.u.]	Waterhammer 4th factor
Tw	0,75	[s]	Water starting time
PN	0	[p.u./s]	Turbine rated power (=0⇒PN=Pgnn [MW]
Pmin	-0,1	[p.u.]	Valve closing time
Uo	0,1	[p.u./s]	Valve opening time
Pmax	1,0	[p.u.]	Maximum gate limit

Modal analysis in PowerFactory

The calculation of eigenvalues and eigenvectors is the most powerful tool for oscillatory stability studies. When doing such a study, it is highly recommended to first compute the “natural" system oscillation modes. These are the oscillation modes of the system when all controller and power plant models are deactivated so every synchronous machine will have constant turbine power and constant excitation voltage. After determining these ’natural’ modes, the effects of controllers (structure, gain, time constants etc.) and other models can be investigated.

After the initial conditions have been calculated successfully, which means that all time derivatives of the state variables should be zero (the system is in steady state), or the simulation has been stopped at a point in time, the modal analysis calculates the complete system A-matrix using numerical, iterative algorithms. The representation of the electrodynamic network model is equivalent to the representation used for the balanced RMS simulation, except for the general load model, for which the frequency dependencies are neglected.
The computation time for the Modal Analysis is approximately proportional to the number of state space variables to the power of three. Considering, that most power system objects and models will contain several (perhaps up to a dozen or more for some complex controllers), the calculation time can rapidly increase as the size of the system being considered increases. For this reason, alternative methods for calculating the system eigenvalues and eigenvectors must be used when the system grows very large [9].

PowerFactory supports two types of analysis methods, they are:

- QR/QZ-Method; This method is the ’classical’ method for calculating all of the system eigenvalues.
- Selective Modal Analysis (Arnoldi/Lanczos); This method only calculates a subset of the system eigenvalues around a particular reference point. Often this method is used in

very large systems when using the QR-method could be very time consuming. It is especially useful if the user knows the target area of interest for the eigenvalues.

A multi-machine system exhibits oscillatory stability if all conjugate complex eigenvalues making up the rotor oscillations have negative real parts. This means that they lie in the left complex half-plane. Electro–mechanical oscillations for each generator are then stable. More formally, assuming that one of the conjugate complex pair of eigenvalues is given by:

$$\lambda_i = \sigma_i \pm j\omega_i \tag{A.8}$$

Then the oscillatory mode will be stable, if the real part of the eigenvalue is negative

$$\sigma_i < 0 \tag{A.9}$$

The period and damping of this mode are given by

$$T_i = \frac{2\pi}{\omega_i}$$
$$d_i = -\sigma_i = \frac{1}{T_p} \cdot ln\left(\frac{A_n}{A_{n+1}}\right) \tag{A.10}$$

where A_n and A_{n+1} are amplitude of two consecutive swing maxima or minima respectively.

The absolute contribution of an individual generator to the oscillation mode which has been excited as a result of a disturbance can be calculated by:

$$\vec{\omega(t)} = \sum_{i=1}^{n} c_i \cdot \vec{\phi}_i \cdot e^{\lambda_i \cdot t} \tag{11}$$

where:

$\vec{\omega(t)}$ generator speed vector
λ_i i'th eigenvalue
$\vec{\phi}_i$ i'th right eigenvalue
c_i magnitude of the excitation of the i'th mode of the system (at t = 0)(depending on the disturbance
n number of conjugate complex eigenvalues (i.e. number of generators – 1)

The elements of the eigenvectors Φ_i then represents the mode shape of the eigenvalue i and shows the relative activity of a state variable, when a particular mode is excited. For example, the speed amplitudes of the generators when an eigenfrequency is excited, whereby those generators with opposite signs in Φ_i oscillate in opposite phase.

The right eigenvectors Φ_i can thus be termed the "observability vectors". The left eigenvectors ψ_i measures the activity of a state variable x in the i-th mode, thus the left eigenvectors can be termed the "relative contribution vectors". Normalization is done by assigning the generator with the greatest amplitude contribution the relative contribution factor 1 or -1 respectively. For a n-machine power system, n-1 generator oscillation modes will exist and n-1 conjugate complex pairs of eigenvalues λ_i will be found. The mechanical speed ω of the n generators will then be described by:

$$\begin{bmatrix}\omega_1\\ \omega_2\\ \vdots\\ \omega_n\end{bmatrix} = c_1 \cdot \begin{bmatrix}\phi_{11}\\ \phi_{12}\\ \vdots\\ \phi_{1n}\end{bmatrix} \cdot e^{\lambda_1 t} + c_2 \begin{bmatrix}\phi_{21}\\ \phi_{22}\\ \vdots\\ \phi_{2n}\end{bmatrix} \cdot e^{\lambda_2 t} + \cdots + c_n \begin{bmatrix}\phi_{n1}\\ \phi_{n2}\\ \vdots\\ \phi_{nn}\end{bmatrix} \cdot e^{\lambda_n t} \quad (12)$$

The problem of using the right or left eigenvectors for analyzing the participation of a generator in a particular mode i is the dependency on the scales and units of the vector elements. Hence the eigenvectors Φ_i and ψ_i are combined to a matrix **P** of participation factor by:

$$P_i = \begin{bmatrix}P_{1i}\\ P_{2i}\\ \vdots\\ Pi_n\end{bmatrix} = \begin{bmatrix}\phi_{1i} \cdot \psi_{i1}\\ \phi_{2i} \cdot \psi_{i2}\\ \vdots\\ \phi_{ni} \cdot \psi_{in}\end{bmatrix} \quad (13)$$

The elements of the matrix p_{ij} are called the participation factors. They give a good indication of the general system dynamic oscillation pattern. They can be used to determine the location of eventually needed stabilizing devices to influence the system damping efficiently. Furthermore, the participation factor is normalized so that the sum for any mode is equal to 1. The participation factors can be calculated not only for the generator speed variables, but for all variables listed in Table A.6. Comprehensive explanation of modal analysis in PowerFactory is found in DIgSILENT User Manual [9].

Table A.6. DIgSILENT mode description

Name	**Unit**	**Description**
s:speed	p.u.	Speed
s:phi	rad	Rotor-angle
s:psie	p.u.	Excitation flux
s:psiD	p.u.	Flux in D-winding
s:psix	p.u.	Flux in x-winding
s:psiQ	p.u.	Flux in Q-winding

Appendix K – Modal analysis

Mode 3. Actual regulators

The mode phasor plot show the observability of the excitation control systems. The excitation systems have negative impact on damping as the phasors are on the right side of the phasor diagram. The excitation systems on the generators in NFK have negative influence on stability in symmetrical conditions.

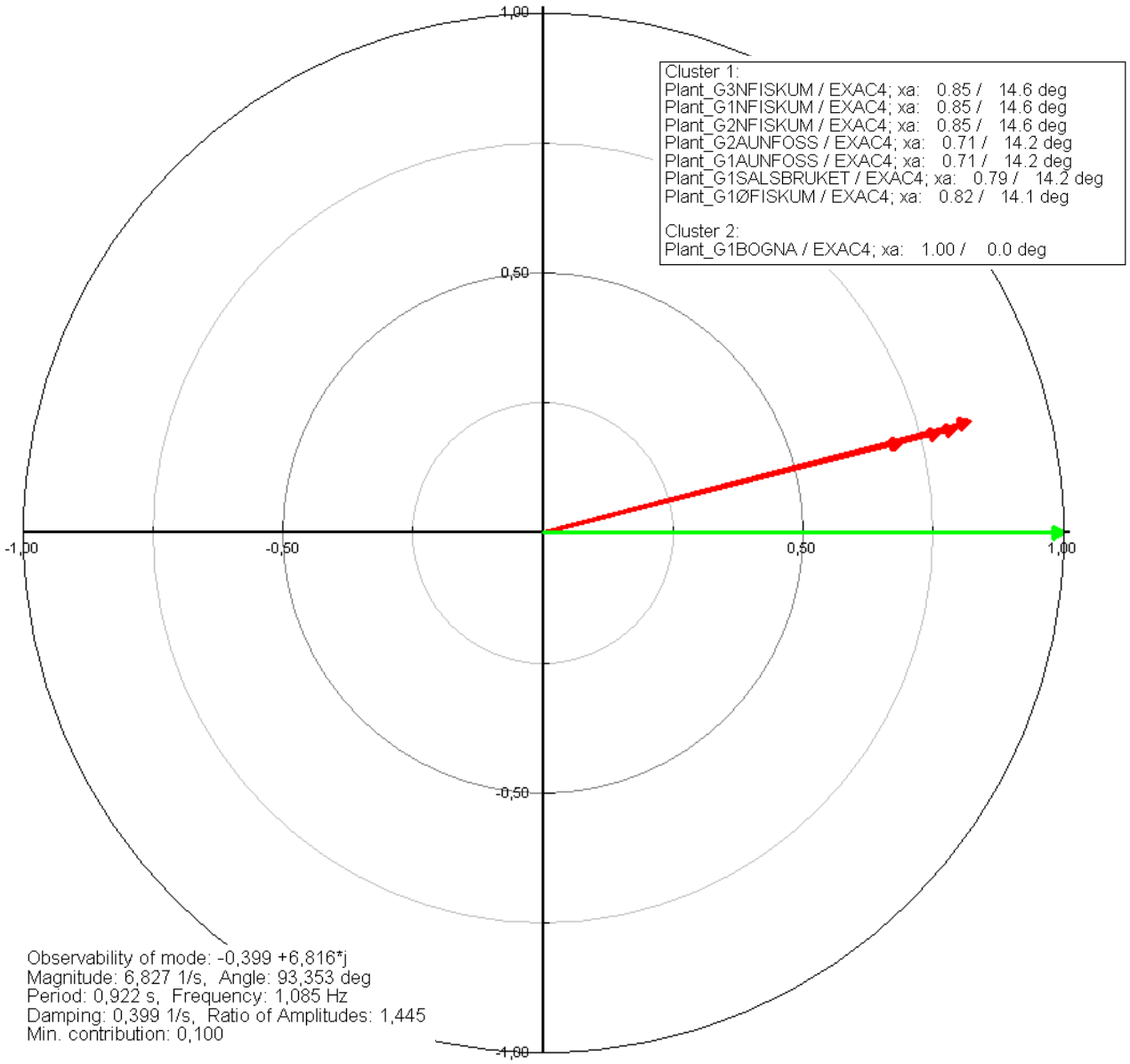

Figure A-6: Mode phasor plot of the actual excitation systems on the generators in the power system network of NTE.

Mode 3. Modified regulators

The mode phasor plot show the observability of the excitation control systems. The excitation systems have negative impact on stability as the phasors are on the right side of the phasor diagram. The excitation systems on the generators in NFK is observed to have less negative influence on stability in terms of phasor magnitude but have still negative influence on stability.

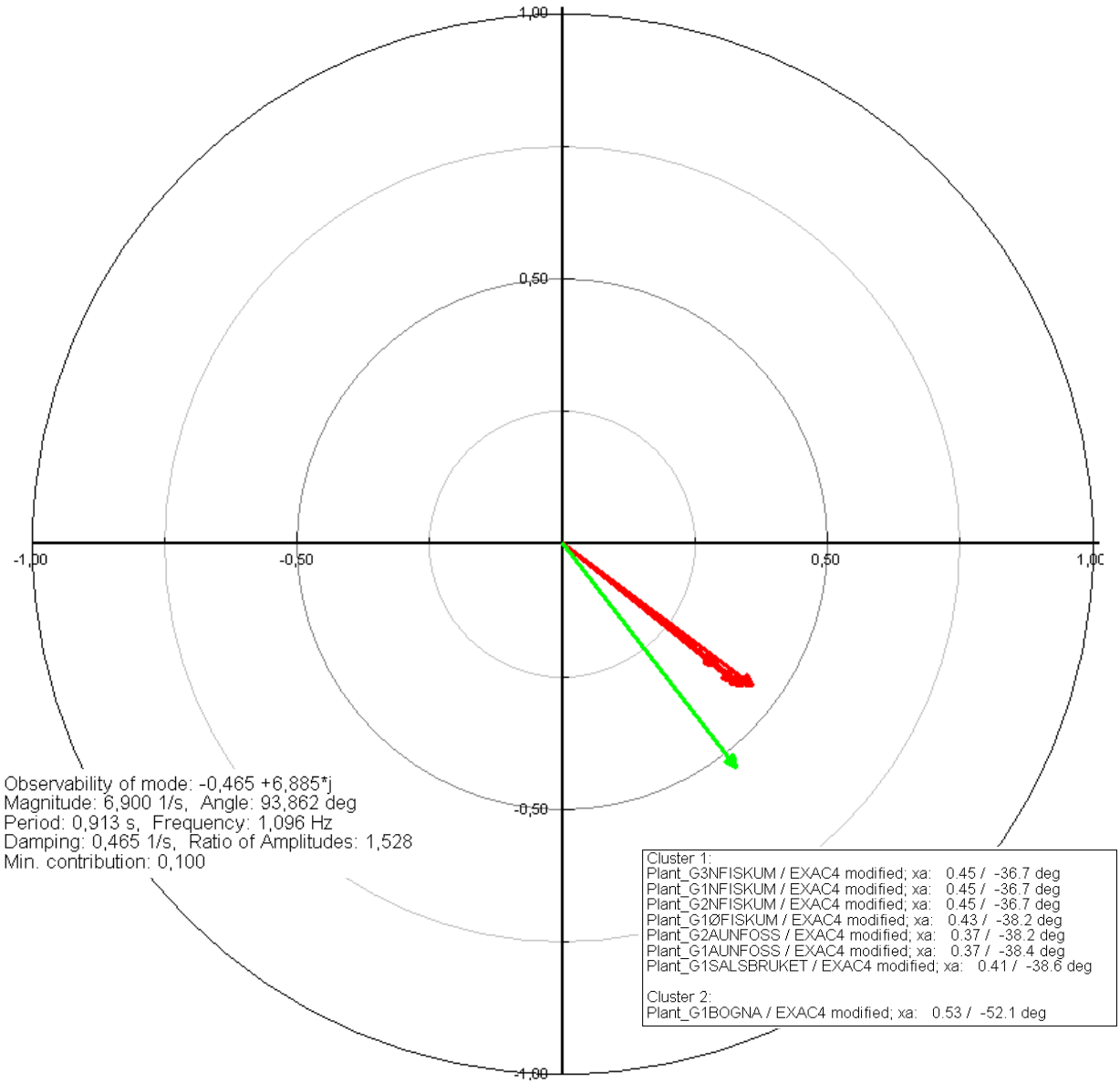

Figure A-7: Mode phasor plot of the modified excitation systems on the generators in the power system network of NTE.

Appendix L - Laboratory pictures

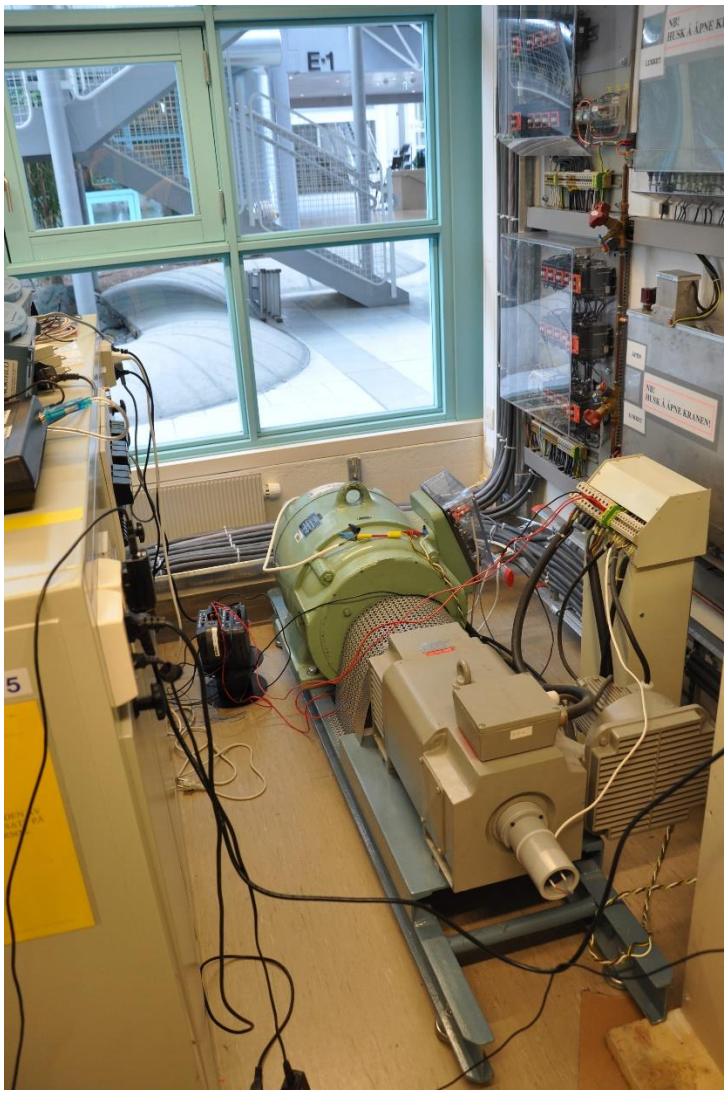

Figure A-8: The laboratory setup.

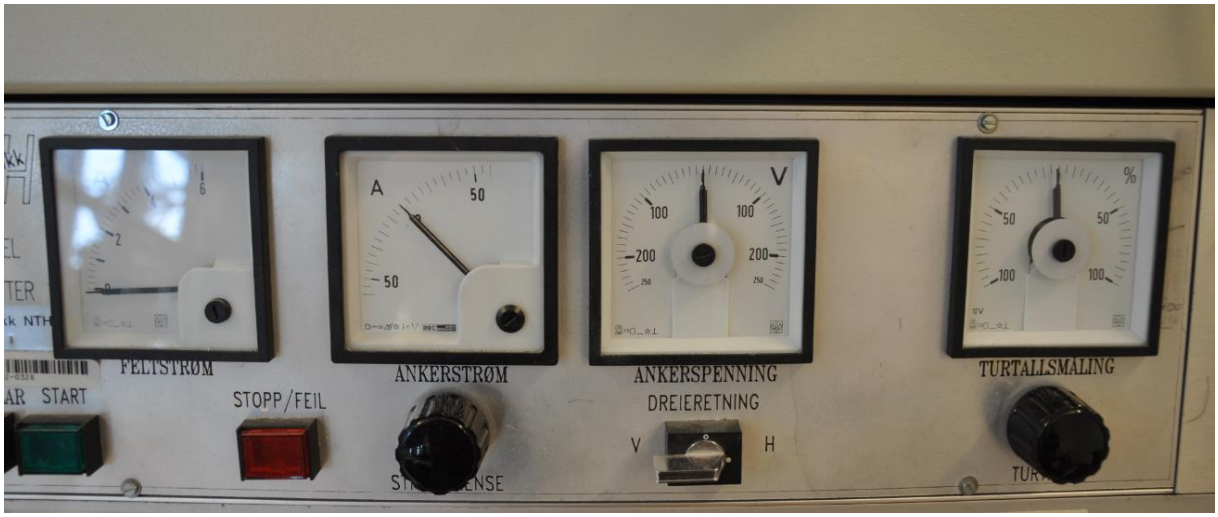

Figure A-9: Instrument panel.

Appendix M – Laboratory synchronous machine data

The machine model in PowerFactory is based on the data that are engraved in the plate fitted on the machine.

Figure A-10: The Synchronous generator identification plate. Also used as basis for the simulation model in PowerFactory as it is the only documentation that exist.

Appendix N – Plots from Elspec Investigator software

Experiment 1

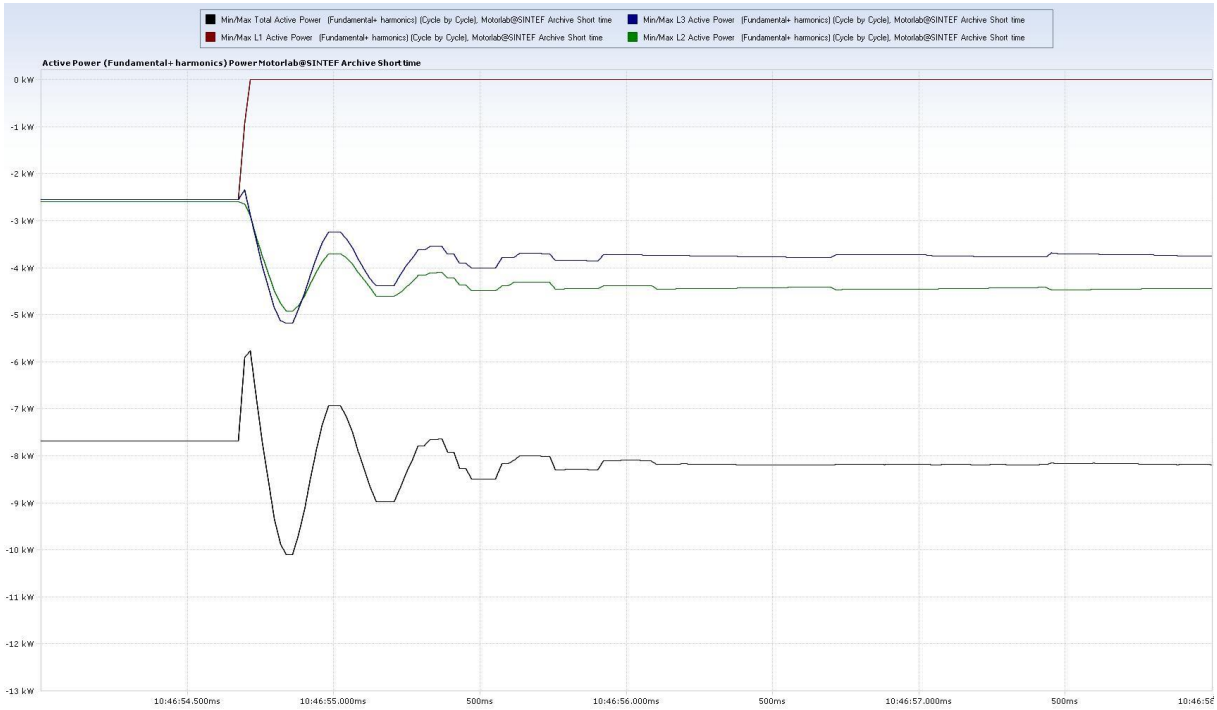

Figure A-11: Experiment 1. Start open conductor fault event. Oscillation period t ≈ 300 ms.

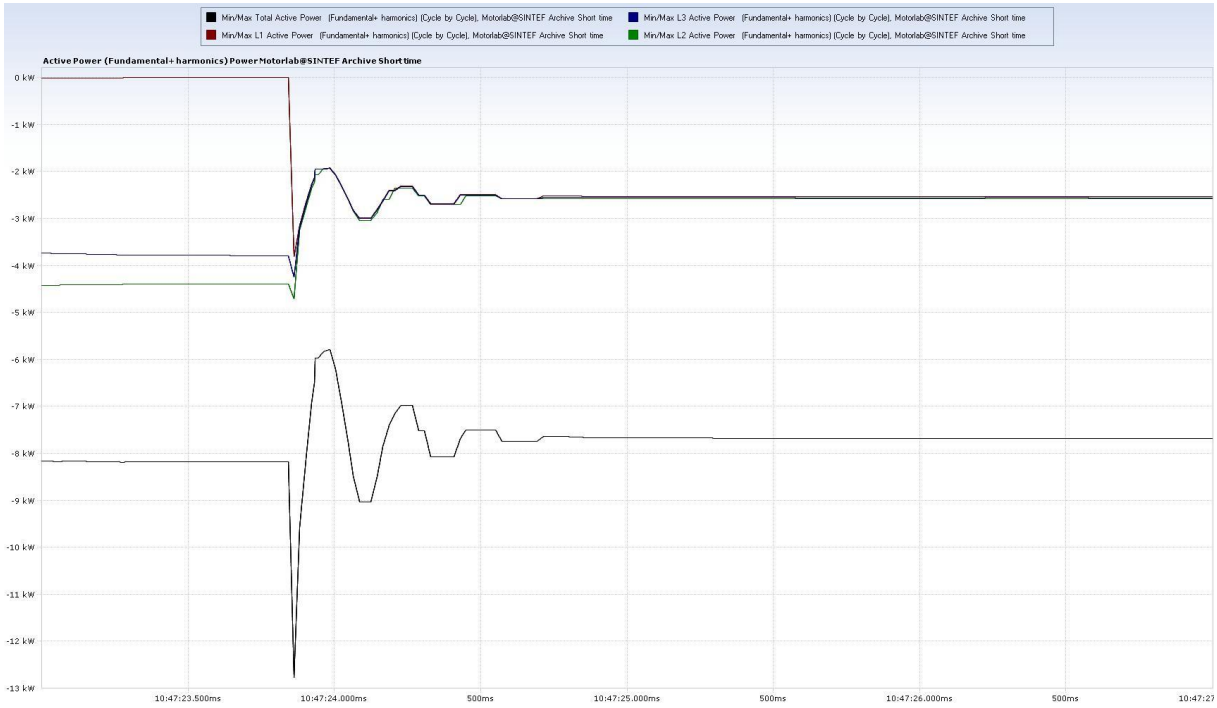

Figure A-12: Experiment 1. End open conductor fault event. Oscillation period t ≈ 300 ms. Peak RMS value 13 kW in total.

Experiment 2

Figure A-13: Experiment 2. Start open conductor fault event.

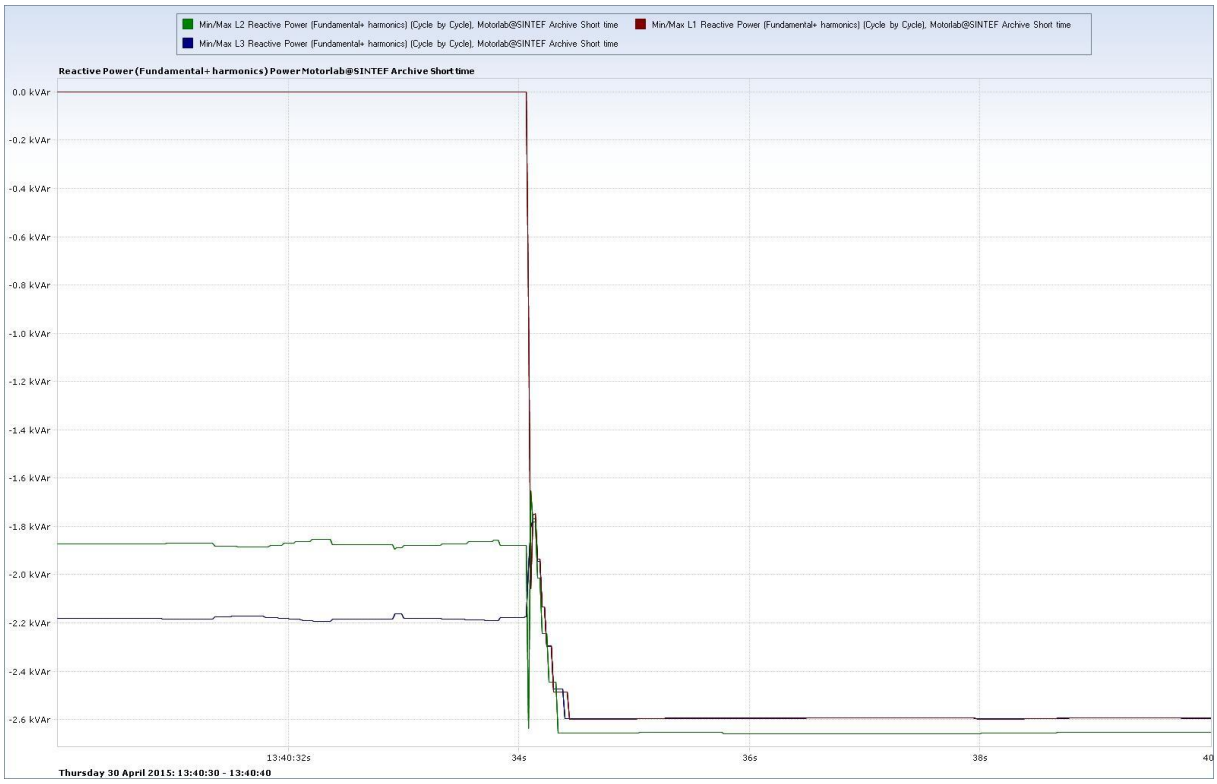

Figure A-14: Experiment 2. End open conductor fault event.

Experiment with active power generation 4 [kW]

Figure A-15: Start open conductor fault experiment. Oscillation period t ≈ 300 ms. Phase powers L2 and L3 changes from 1,5 kW to 2 kW during the fault. The oscillations are damped out after one second.

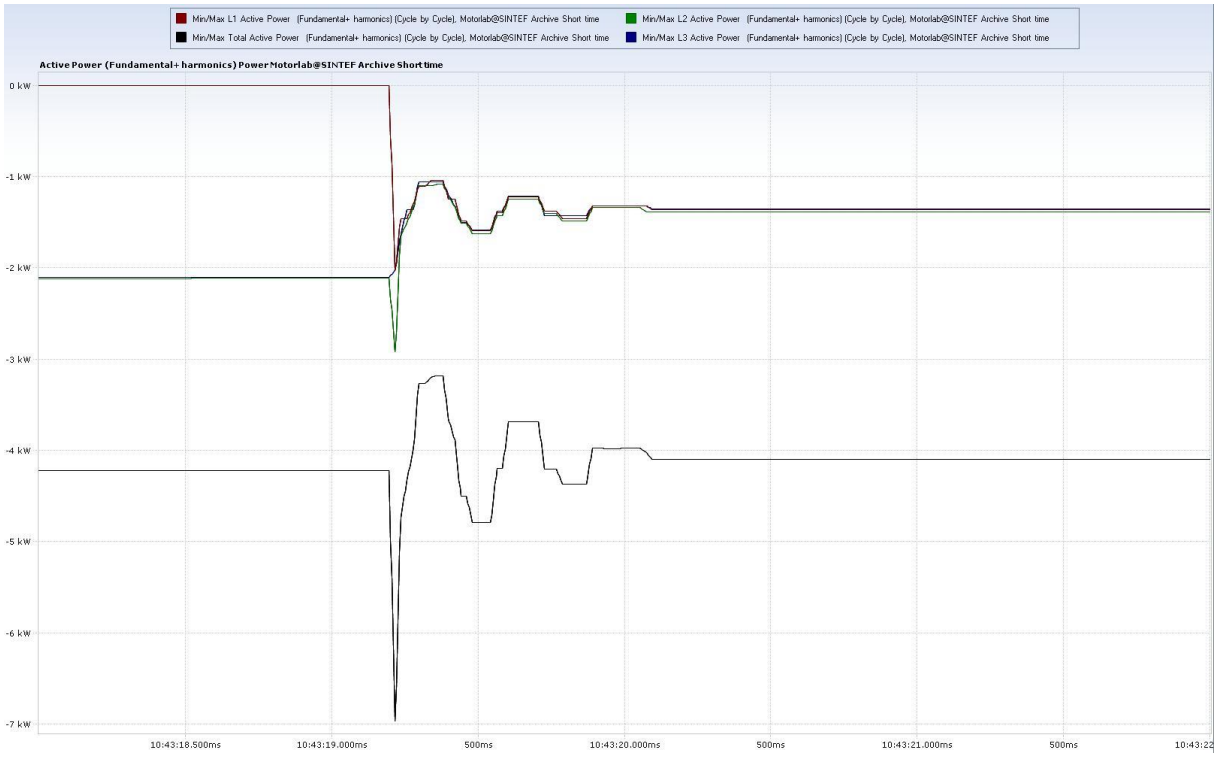

Figure A-16: End open conductor fault experiment. Oscillation period t ≈ 300 ms. Peak RMS value 7 kW in total. The faulty phase is reconnected and the oscillations are damped out after one second.